

**ANALYSIS OF UNSTEADY HYBRID
NANOFLUID FLOW OVER A STRETCHING
SURFACE**

BY

ANISA ASAD



NATIONAL UNIVERSITY OF MODERN LANGUAGES

ISLAMABAD

JUNE, 2024

Analysis of Unsteady Hybrid Nanofluid Flow over a Stretching Surface

BY

ANISA ASAD

MS Mathematics, National University of Modern Languages, Islamabad, 2024

A THESIS SUBMITTED IN PARTIAL FULFILMENT OF
THE REQUIREMENTS FOR THE DEGREE OF

MASTER OF SCIENCE

In Mathematics

To

FACULTY OF ENGINEERING AND COMPUTING



NATIONAL UNIVERSITY OF MODERN LANGUAGES ISLAMABAD

© Anisa Asad, 2024



THESIS AND DEFENSE APPROVAL FORM

The undersigned certify that they have read the following thesis, examined the defense, are satisfied with overall exam performance and recommend the thesis to the Faculty of Engineering and Computing for acceptance.

Thesis Title: Analysis of Unsteady Hybrid Nanofluid Flow over a Stretching Surface

Submitted By: Anisa Asad

Registration #: 28 MS/Math/S21

Master of Science in Mathematics (MS Math)
Title of the Degree

Mathematics
Name of Discipline

Dr. Anum Naseem
Name of Research Supervisor

Signature of Research Supervisor

Dr. Sadia Riaz
Name of HOD (MATH)

Signature of HOD (MATH)

Dr. Noman Malik
Name of Dean (FEC)

Signature of Dean (FEC)

Date: 14 June, 2024

AUTHOR'S DECLARATION

I Anisa Asad

Daughter of Muhammad Idrees

Registration # 28 MS/Math/S21

Discipline Mathematics

Candidate of **Master of Science in Mathematic (MS Math)** at the National University of Modern Languages do hereby declare that the thesis **Analysis of Unsteady Hybrid Nanofluid Flow over a Stretching Surface** submitted by me in partial fulfillment of MS Math degree, is my original work, and has not been submitted or published earlier. I also solemnly declare that it shall not, in future, be submitted by me for obtaining any other degree from this or any other university or institution. I also understand that if evidence of plagiarism is found in my thesis/dissertation at any stage, even after the award of a degree, the work may be cancelled and the degree revoked.

Signature of Candidate

Anisa Asad

Name of Candidate

14th June, 2024

Date

ABSTRACT

Title: Analysis of Unsteady Hybrid Nanofluid Flow over a Stretching Surface

The goal of the current analysis is to investigate the fluid flow and heat transfer of a recently introduced category of fluids known as hybrid nanofluid. This study is focused on the flow of a viscous, unsteady and three dimensional flow of hybrid nanofluid. The fluid is flowing over an exponentially stretching and rotating surface. The phenomenon of mixed convection and slip velocity is considered in the current model. CuO and TiO_2 are taken as a nanoparticles and the base fluid is a mixture of ethylene glycol and water (50%-50%). The system of partial differential equations are reduced into a system of ordinary differential equations by means of suitable similarity transformations. The resulting system is solved numerically with the help of `bvp4c` technique in MATLAB software. The flow analysis is carried out through the graphical presentation of the velocity and temperature profiles. In contrast to simple nanofluids, hybrid nanofluids delivers a superior rating, according to the probe for establishing parameters. The characteristics of essential parameters such as stretching ratio parameter, rotating parameter, mixed convection parameter, velocity slip parameter, temperature exponent parameter and unsteady parameter for the velocity and temperature are evaluated. Moreover the influence of various parameters on friction drag and Nusselt number are also appraised. The comparison tables are also displayed which shows an excellent agreement between the obtained results and already published results.

TABLE OF CONTENTS

CHAPTER	TITLE	PAGE
	AUTHOR'S DECLARATION	iii
	ABSTRACT	iv
	TABLE OF CONTENTS	v
	LIST OF TABLES	viii
	LIST OF FIGURES	ix
	LIST OF ABBREVIATIONS	xii
	LIST OF SYMBOLS	xiii
	ACKNOWLEDGEMENT	xv
	DEDICATION	xvi
1	INTRODUCTION	1
	1.1 Hybrid nanofluid	1
	1.2 Mixed convection	2
	1.3 Velocity slip	4
	1.4 Unsteady Flow	4
	1.5 Stretching surface	5
	1.6 Thesis Organization	6
2	LITERATURE REVIEW	7
	2.1 Hybrid nanofluids	7
	2.2 Mixed convection	8
	2.3 Velocity slip	9
	2.4 Unsteady flow	9
	2.5 Stretching surface	10
	2.6 Summary	11

3	Fundamental Definitions and Concepts	12
3.1	Fluid	12
3.2	Fluid mechanics	12
3.2.1	Fluid statics	13
3.3.2	Fluid dynamics	13
3.3	Nanofluid	13
3.4	Hybrid nanofluid	13
3.5	Flow	14
3.6	Types of fluid flow	14
3.6.1	Steady flow	14
3.6.2	Unsteady flow	15
3.6.3	Viscous flow	15
3.6.4	Non viscous flow	15
3.6.5	Laminar flow	16
3.6.6	Turbulent flow	16
3.6.7	Uniform flow	17
3.6.8	Non uniform flow	17
3.6.9	Compressible flow	17
3.6.10	Incompressible flow	17
3.6.11	Rotation flow	18
3.6.12	Irrotating flow	18
3.6.13	One, two and three dimensional flow	18
3.7	Density	18
3.8	Pressure	19
3.9	Thermal conductivity	19
3.10	Thermal diffusivity	20
3.11	Stress	20
3.11.1	Shear stress	20
3.11.2	Normal stress	20
3.11.3	Strain	21
3.12	Viscosity	21
3.12.1	Dynamic viscosity	21

3.12.2	Kinematic viscosity	21
3.13	Convection	22
3.13.1	Natural convection	22
3.13.2	Force convection	22
3.13.3	Mixed convection	23
3.14	Dimensionless number	23
3.14.1	Reynolds number	23
3.14.2	Prandtl number	24
3.14.3	Skin friction	24
3.14.4	Nusselt number	24
4	A Rotating Flow of Nano Fluid in the Presence of Convective Boundary Condition	26
4.1	Formulation of the problem	27
4.2	Numerical Algorithm	30
4.3	Discussion for the Graphical Results	33
5	The Unsteady Hybrid Nanofluid flow over an Exponentially Stretching Surface in the Presence of Velocity slip parameter	45
5.1	Introduction	45
5.2	Formulation of the problem	46
5.3	Numerical Algorithm	50
5.4	Discussion for the Graphical Results	53
6	Conclusion and Future Projects	70
6.1	Concluding Points	70
6.2	Prospective Project	71
	References	72

LIST OF TABLES

TABLE NO	TITLE	PAGE
4.1	Important thermal feature of TiO ₂ and CuO	31
4.2	Thermo-physical characteristics of nanoparticles and hybrid base fluid.	32
4.3	Comparison with the literature of heat transfer rate for pure fluid with $\alpha = \phi = \gamma = 0$ and $Nc \rightarrow \infty$.	32
5.1	Properties of the hybrid base fluid with nanoparticles in terms of thermo-physical aspects.	51
5.2	Thermo-physical properties of hybrid base fluid with nanoparticles.	51
5.3	Thermo-physical properties of hybrid base fluid and nanoparticles	52
5.4	Comparison with the literature for heat transfer rate with $\alpha = \phi_1 = \phi_2 = \gamma = \lambda = G = A_0 = 0$.	52

LIST OF FIGURES

Figure No	Title	Page No
Figure 1.1	Hybrid Nanofluid.	2
Figure 1.2	Mixed Convection.	3
Figure 3.2	Turbulent flow.	16
Figure 3.3	Thermal Conductivity.	19
Figure 4.1	Geometry of the problem.	27
Figure 4.2	Velocity distribution $p'(\eta)$ for α with CuO–hybrid base fluid.	35
Figure 4.3	Velocity distribution $p'(\eta)$ for α with TiO ₂ –hybrid base fluid.	35
Figure 4.4	Velocity distribution $p'(\eta)$ for γ with CuO–hybrid base fluid.	36
Figure 4.5	Velocity distribution $p'(\eta)$ for γ with TiO ₂ –hybrid base fluid.	36
Figure 4.6	Velocity distribution $q'(\eta)$ for α with CuO–hybrid base fluid.	37
Figure 4.7	Velocity distribution $q'(\eta)$ for α with TiO ₂ –hybrid base fluid.	37
Figure 4.8	Velocity distribution $q'(\eta)$ for γ with CuO–hybrid base fluid.	38
Figure 4.9	Velocity distribution $q'(\eta)$ for γ with TiO ₂ –hybrid base fluid.	38
Figure 4.10	Temperature distribution $\theta(\eta)$ for α with CuO–hybrid base fluid.	39
Figure 4.11	Temperature distribution $\theta(\eta)$ for α with TiO ₂ –hybrid base fluid.	39
Figure 4.12.	Temperature distribution $\theta(\eta)$ for A with CuO–hybrid base fluid.	40
Figure 4.13	Temperature distribution $\theta(\eta)$ for α with TiO ₂ –hybrid base fluid.	40
Figure 4.14	Figure 4.14. Temperature distribution $\theta(\eta)$ for γ with CuO–hybrid base fluid.	41
Figure 4.15	Temperature distribution $\theta(\eta)$ for γ with TiO ₂ –hybrid base fluid.	41

Figure 4.16	Skin friction coefficient along x -axis for α and ϕ with CuO -hybrid base fluid.	42
Figure 4.17	Skin friction coefficient along x -axis for α and ϕ with TiO_2 -hybrid base fluid.	42
Figure 4.18	Skin friction coefficient along y -axis for α and ϕ with CuO -hybrid base fluid.	43
Figure 4.19	Skin friction coefficient along y -axis for α and ϕ with TiO_2 -hybrid base fluid.	43
Figure 4.20	Nusselt number for α and ϕ with CuO -hybrid base fluid.	44
Figure 4.21	Nusselt number $\theta'(0)$ for α and ϕ with TiO_2 -hybrid base fluid.	44
Figure 5.1	Geometry of the problem.	46
Figure 5.2	Velocity distribution $p'(\eta)$ for α .	56
Figure 5.3	Velocity distribution $p'(\eta)$ for A .	56
Figure 5.4	Velocity distribution $p'(\eta)$ for G .	57
Figure 5.5	Velocity distribution $p'(\eta)$ for λ .	57
Figure 5.6	Velocity distribution $p'(\eta)$ for A_0 .	58
Figure 5.7	Velocity distribution $p'(\eta)$ for ϕ_1 .	58
Figure 5.8	Velocity distribution $p'(\eta)$ for ϕ_2 .	59
Figure 5.9	Velocity distribution $q'(\eta)$ for α .	59
Figure 5.10	Velocity distribution $q'(\eta)$ for A .	60
Figure 5.11	Velocity distribution $q'(\eta)$ for G .	60
Figure 5.12	Velocity distribution $q'(\eta)$ for λ .	61
Figure 5.13	Velocity distribution $q'(\eta)$ for A_0 .	61
Figure 5.14	Velocity distribution $q'(\eta)$ for ϕ_1 .	62
Figure 5.15	Velocity distribution $q'(\eta)$ for ϕ_2 .	62

Figure 5.16	Temperature distribution $\theta(\eta)$ for α .	63
Figure 5.17	Temperature distribution $\theta(\eta)$ for A .	63
Figure 5.18	Temperature distribution $\theta(\eta)$ for γ .	64
Figure 5.19	Temperature distribution $\theta(\eta)$ for λ .	64
Figure 5.20	Temperature distribution $\theta(\eta)$ for A_0 .	65
Figure 5.21	Temperature distribution $\theta(\eta)$ for ϕ_1 .	65
Figure 5.22	Temperature distribution $\theta(\eta)$ for ϕ_2 .	66
Figure 5.23	Skin friction coefficient along x -axis for G and ϕ_2 .	66
Figure 5.24	Skin friction coefficient along x -axis for A_0 and ϕ_2 .	67
Figure 5.25	Skin friction coefficient along y -axis for G and ϕ_2 .	67
Figure 5.26	Skin friction coefficient along y -axis for A_0 and ϕ_2 .	68
Figure 5.27	Nusselt number for λ and ϕ_2 .	68
Figure 5.28	Nusselt number for A and ϕ_2 .	69

LIST OF ABBREVIATIONS

<i>MHD</i>	Magnetohydrodynamics
<i>PDEs</i>	Partial differential equations
<i>ODEs</i>	Ordinary differential equations
<i>RPF</i>	Reiner-Philipp off fluid
<i>SWCNTs</i>	Single Wall Carbon Nanotubes
<i>MWCNTs</i>	Multi Wall Carbon Nanotubes
<i>Cu</i>	Copper
<i>Al₂O₃</i>	Alumina / Aluminum oxide
<i>MATLAB</i>	Matrix Laboratory
<i>BVP4C</i>	Boundary Value Problem for 4 th Order Collocation
<i>TiO₂</i>	Titanium dioxide
<i>Nu_x</i>	Local Nusselt Number
<i>CuO</i>	Copper oxide
<i>Cf_x, Cf_y</i>	Skin Friction Coefficient
<i>C₂H₆O₂</i>	Ethylene glycol
<i>Ag</i>	Silver
<i>H₂O</i>	Water
<i>NFs</i>	Nanofluids
<i>HNF</i>	Hybrid nanofluid
<i>TPD</i>	Thermo-phoretic particle deposition
<i>E-SS</i>	Exponentially stretching surface

LIST OF SYMBOLS

x, y, z	Cartesian coordinates
u, v, w	Velocity components
T	Temperature
T_w	Temperature of the wall
T_∞	Ambient temperature
ϕ_1	1 st nanoparticle volume fraction
ϕ_2	2 nd nanoparticle volume fraction
s_1	1 st nano-particle
s_2	2 nd nano-particle
ρ	Density of fluid
ρ_{s1}	Density 1 st nano-particle
ρ_{s2}	Density 2 nd nano-particle
ρ_{nf}	Density of nanofluid
ρ_{hnf}	Density of hybrid nanofluid
μ	Dynamic Viscosity
μ_{nf}	Dynamic viscosity nanofluid
μ_{hnf}	Dynamic viscosity hybrid nanofluid
ν	Kinematic viscosity
ν_{nf}	Kinematic viscosity of nanofluid
α_{nf}	Thermal diffusivity
ν_{hnf}	Kinematic viscosity of hybrid nanofluid
k	Thermal conductivity
k_{nf}	Thermal conductivity of nanofluid

k_{hnf}	Thermal conductivity of hybrid nanofluid
c_p	Specific heat
$(\rho C_p)_{nf}$	Heat capacitance of nanofluid
$(\rho C_p)_{hnf}$	Heat capacitance of hybrid nanofluid
β	Thermal expansion
$(\rho\beta)_{s1}$	Thermal expansion of 1 st nano-particle
$(\rho\beta)_{s2}$	Thermal expansion of 2 nd nano-particle
q_w	Wall heat flux
A	Temperature exponent parameter
ρ_{nf}	Density of nanofluid
Nc	Convective parameter
μ	Dynamic Viscosity
α	Stretching ratio parameter
η	Dimensionless space variable
G	Velocity Slip parameter
A_0	Unsteady parameter
u_0, v_0	Rate of stretching
u_w, v_w	Exponentially stretching velocities at the surface
ω	Constant angular velocity

ACKNOWLEDGEMENT

All my thanks and gratitude's are for Almighty Allah for His countless blessings.

Thanks to Allah and His Prophet Hazrat Muhammad (PBUH).

I offer my sincere acknowledgement to the most respected teacher Dr. Anum Naseem for the concept of the subject and moral encouragement. I sincerely thank Dr. Anum Naseem for her valuable guidance and inspirational efforts throughout my research work. I am so grateful to have such a wonderful individual as my supervisor. My sincere appreciation goes to my respected supervisor, whose assistance helped me reach the pinnacle of my academic career.

My deepest thanks go out to my parents and my beloved siblings, who have always been my support and have showered me with their unwavering love, and care throughout my life. My family's unwavering support, encouragement, and humble prayers are always much appreciated.

(Anisa Asad)

DEDICATION

This thesis is dedicated to my parents, family and teachers, who always supported me for achieving this goal. At times of despair and dissatisfaction they have all served as a source of inspiration and fortitude.

Chapter 1

Introduction

1.1 Hybrid nanofluids

Due to the widespread categorization of fluids (materials) in engineering and industry, analyst's interest in thermal properties of the fluids has lately grown. Heat transmission is limited by the low thermal conductivity of common fluids such as water, fuel oil, kerosene, ethylene and motor oil. Particles that are nano-scale in size, ranging from 1 to 100 nm, can be added to ordinary fluids to boost their thermal conductivity. In 1995, Choi [1] at the Argonne National Laboratory in the United States offered the first suggestion for nanofluid. This fluid has unique properties that are very useful in many applications involving heat transfer phenomena. Nanofluids, a novel class of fluids, may be produced by dispersing nanoparticles or nanotubes in base fluids. Due to their special qualities, nanofluids have the potential to be helpful in a variety of heat transfer applications, including fuel cells, domestic refrigerators, microelectronics, engine cooling and vehicle thermal dissipation. A hybrid nanofluid is an advanced form of nanofluid that is created by blending two different number of nanoparticles containing a base liquid. A hybrid nanofluid combines the physical and thermal characteristics of many materials during the precise same moment. The main goal of hybrid nanofluids is to have enhanced thermal efficiency than isolated ones. Because of their many benefits which include reduction in pressure, superior thermal conductivity, reduced losses due to friction and increased generating force, they are intended to replace nanofluids. Numerous applications,

such as optoelectronic thermal uses and solar collectors, electronic thermal control of components, engine utilizes, vehicle cooling and plenty others, have been researched for hybrid nanofluids. Sarkar *et al.* [2] highlighted the applications of hybrid nanofluids by considering recent researches. Al-Kouz *et al.* [3] used an entropy generation combination with a hybrid nanofluid for thermal applications. They discovered that these nanocomposites improve the thermal behavior of the base liquid significantly and more effectively. Nayak *et al.* [4] highlighted the numerical results of the Cattaneo-Christov model for Oldroyd B hybrid nanofluid flow under the impacts of inclined magnetic field, thermal radiation and viscous dissipation. The Darcy-Forchheimer hybrid nanofluid flow over spinning disc was investigated by Zubair *et al.* [5] in the presence of thermal radiation.

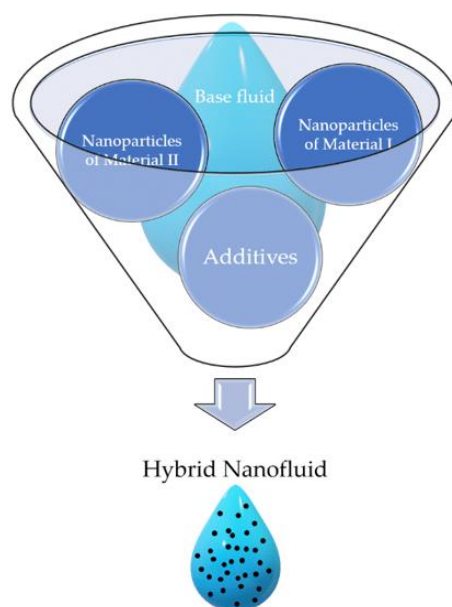


Figure 1.1. Hybrid nanofluid

1.2 Mixed convection

In the current context, mixed convection flow refers to the combination of forced convection and free or spontaneous convection. Mixed convection flow occurs when buoyant force significantly affects forced convection or forced flow. Large temperature differentials and sluggish forced flow velocities make this sort of flow more readily apparent. This particular

form of flow is also important and may be found in many industrial processes, including paper production, continuous casting, wire drawing, polymer extraction, paper manufacturing, steel protrusion, and the condensing operation etc. Applications for mixed convection flow include cooling systems, the boundary layers of the atmosphere, solar and nuclear recycling facilities and many more. Keeping in view of these applications, the influence of thermal radiation and mixed convection, the magnetohydrodynamic flow of nanofluid containing carbon nanotubes (CNTs) was investigated by Maraj *et al.* [6] and found the precise closed form solutions. In another study on hybrid nanofluid that was done by Zainal *et al.* [7], the stagnation point flow over a vertical stretching surface was explored. In an analysis performed by Bouslimii *et al.* [8], the Soret effect was examined for a mixed convective flow of nanofluid flowing across a surface which is subjected to non-linear stretching. In the presence of mixed convection, Varun *et al.* [9] demonstrated the effect of Arrhenius activation energy on the nanofluidic flow flowing due to a stretching surface in the presence of mixed convection.

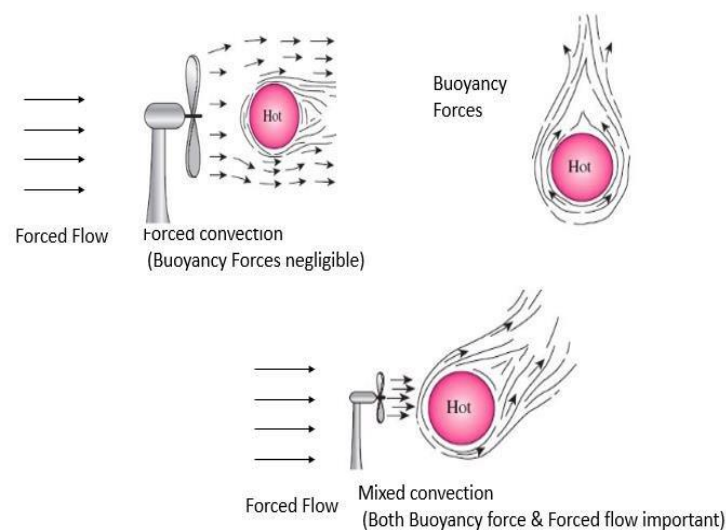


Figure 1.2. Mixed convection

1.3 Velocity slip

One of the characteristics that is heavily acknowledged by scholars and is essential to the fluid flow is based on the involvement of slip conditions. This condition develops when the velocity of the fluid flow deviates from the boundary velocity. Slip conditions are widely employed in the manufacturing of internal cavities, artificial heart valves, micro heat exchangers, medication delivery systems and microelectronic cooling systems etc. The primary benefit of slip occurring may be the reduction in flow resistance in microchannels and the enhancement of the efficiency of nanoscale viscous pumps. In particular, it is important to address the suitable degree of slip for applications that are related in other relevant elements. The velocity slip phenomenon is widely accepted in the field of nano and micro channels and it has several advantages at the solid barrier. Due to this, an extensive study was done on the velocity slip for a variety of physical foundational elements in viscous nanofluids [10]. The slip flow of a mixed convective and magnetohydrodynamic hybrid nanofluidic flow via an expanding sheet was examined by Ramzan *et al.* [11]. A study conducted by Sajid *et al.* [12] regarding a non-Newtonian nanofluid flow over an extended sheet was conducted at the Smoluchowski temperature and Maxwell velocity slip conditions. They used the Tiwari and Das theory to the Reiner-Philipp off liquid (RPF) model using blood as the base fluid. Nandi *et al.* [13] analyzed the effects of velocity slip as well as viscous dissipation on a time dependent MHD, hybrid nanofluid, free convective and stagnation point flow towards an exponentially stretchable surface fixed in a uniform porous medium.

1.4 Unsteady Flow

Unsteady flow discusses a fluid flow where the pressure, velocity, and other properties of the fluid alter with respect to space and time. Recently, a lot of research has been done on the properties and behavior of the unsteady flow for commercial applications and has attracted significant interest of scientists and researchers. Some applications or systems that are related to unsteady fluid flow include turbo machines, maritime propellers, helicopter rotor blades, hydrofoil flutter and many others. The unsteady flow of a hybrid nanofluid due to an exponentially expanding surface in the presence of magnetohydrodynamics and stagnation point was examined via Zainal *et al.* [14] numerically. Ahmad *et al.* [15] observed an unsteady

hybridized nanofluidic flow over a vertical stretching surface which maintains the flow. This research work was carried out with the consideration of stratification, Cattaneo-Christov heat flux and in addition, activation energy. Rehman *et al.* [16] examined non-Newtonian hybrid nanofluid's two-dimensional, unsteady and incompressible flow across a stretched surface. The unsteady and free convection flow within an inclined porous enclosure incorporating hybrid nanofluid which contains a square obstacle was investigated by Nabwey *et al.* [17] with the effects of heat generation/absorption and thermal radiation. Kashi'ie *et al.* [18] investigated the unsteady flow over a Riga plate under the impact of stagnation point and electromagnetohydrodynamic (EMHD) conditions with the occurrence of heat generation/absorption.

1.5 Stretching surface

There are various real-world applications for the study of boundary layer flow with energy transfer over on stretched sheet, including the aerodynamic expulsion of polymers and the condensation of metals. During the fabrication of these slabs, the molten liquid emerges through a slit and is subsequently expanded to the desired thickness. The desirable qualities of the final products are significantly influenced by the ratio of stretching, the rate of freezing throughout the operation, and the method of stretching regarding energy and the transmission of flow. Using the Brownian effect, Arshad *et al.* [19] described the heat transfer for the MHD nanofluid flow over an exponentially stretching surface. Hussain *et al.* [20] investigated three-dimensional rotating nanofluid flow across a stretched surface in the presence of a magnetic field. Mabood *et al.* [21] examined the stability of a viscous hybrid nanofluid flowing across a stretched surface when radiation and a uniform magnetic influences are present. The MHD fluid flow across an exponentially expanding surface in the presence of homogeneous-heterogeneous reactions was investigated by Khan *et al.* [22]. The enormous variety of applications for flow problems across an exponentially extending surface in several disciplines, including geophysics and engineering, has attracted the commendable attention of scholars. These forms of fluid flow have several uses in fluid dynamics, the study of naturally occurring flow, most notably on the crust of the planet.

1.6 Thesis Organization

This section provides a comprehensive summary of our six chaptered study.

Chapter. 1 provides an introduction to various concepts, focusing on their foundations.

Chapter. 2 presents a comprehensive and extensive analysis of the literature based on recent published research.

Chapter. 3 contains all the basic terms and concepts needed for the analysis of the recommended work.

In **Chapter. 4**, the presence of convective boundary conditions for hybrid nanofluid flow on a rotating plate is explored. The problem is described as a system of partial differential equations, which are then subjected to similarity transformations to become a system of ordinary differential equations. The bvp4c methodology, a numerical method, helps to solve these resulting equations. Plots are used to analyze temperature, velocity, Nusselt number and skin friction coefficient.

Chapter. 5 examined the unsteady mixed convection flow of hybrid nanofluid across an exponentially extending and rotating surface. The fluid problem is modelled as partial differential equations which are transformed using similarity transformations. The system of obtained ordinary differential equations is then solved using the bvp4c approach. A visual analysis is done to examine the effects of different parameters on temperature, skin friction coefficient, Nusselt number and velocity.

The **last chapter. 6** summarizes the findings of the study that was done and provides a list of some proposed investigations.

Chapter 2

Literature Review

2.1 Hybrid nanofluids

Hybrid nanofluids are a specific class of nanofluids that possess a greater thermal conductivity as compared to mono nanofluids. In recent years, Hameed *et al.* [23] investigated two dimensional flow of hybrid nanofluid over a nonlinear stretching surface in the presence of an electromagnetic field, heat generation and viscous dissipation. This study's major purpose is to enhance the heat transfer of the fluid, which is in great demand in the industrial and engineering fields. Yasir *et al.* [24] inspected the hybrid nanofluid flow instigated by a stretching permeable surface and the results were concluded using MATLAB software. In the presence of an alternating magnetic field, Rauf *et al.* [25] analyzed the rate of heat exchange in a hybrid nanofluid boundary layer flow flowing over a rotating, non linearly stretched surface. The flow of a hybrid nanofluid across an irregularly rotating surface was examined by Alhowaity *et al.* [26]. Nanda *et al.* [27] examined a three dimensional hybrid nanofluid (containing aluminum alloys) flowing over a nonlinear/linear stretching surface with Joule heating and thermal radiation impact. In the nonlinear stretching surface case, the rate of heat transfer is twice as high as in the linear stretching situation. Ramesh *et al.* [28] explored the rotating flow of hybrid nanofluid on a stretched surface that undergoes stretching both linearly and nonlinearly. Under nonlinear condition of the study, adding nanoparticles increased axial velocity while decreased concentration, and boosted heat transmission in the linear scenario.

Yasir *et al.* [29] in another year investigated the thermal behavior of several nanoparticles including *SWCNT*, *CuO*, *MgO*, *Ag* in *H₂O* and ethylene glycol base fluids. The existence of a magnetic field in the tangent hyperbolic hybrid nanoliquid containing *MgO* and *CuO* nanoparticles was investigated by Sulochana *et al.* [30]. Asghar *et al.* [31] investigated the effects of Joule heating on rotating stretched and shrunk sheets in three-dimensional MHD hybrid nanofluid flow.

2.2 Mixed convection

Mixed convection has so many uses in a variety of scientific and technological domains. In order to investigate the phenomenon of mixed convection flow, Mahmood *et al.* [32] studied the impact of thermal stratification across a porous vertical surface with the existence of magneto hydrodynamics. Khan *et al.* [33] evaluated the effect of mixed convection on the nanofluid flow through a bending sheet in the presence of activation energy, chemical reaction and slip conditions. Waqas *et al.* [34] looked at how a magnetic field affected mixed convection nanofluid flow in the presence of thermal radiation and heat source/sink. Employing the effect of mixed convection, Habib *et al.* [35] analyzed Newtonian heating for the flow caused by stretching surfaces. Verma *et al.* [36] found the results for the two dimensional unsteady nanofluid flow across a stretched sheet in the presence of mixed convection characteristics. They showed that velocity increases in proportion to the helping buoyancy force. The impact of radiation and mixed convection on the heat transfer of a nanofluid in a slip flow through a stretching sheet was assessed by Khan *et al.* [37]. The study involved the influence of activation energy and chemical reaction. The flow rate for both upper and lower branch solutions is slowed down by the inclusion of nanoparticles, according to the results. The mixed convection flow of Casson nanofluid flowing over a nonlinearly stretching porous material with chemical reaction and magnetic influences was investigated by Ashraf *et al.* [38]. In order to examine two dimensional, mixed convective, MHD, unsteady and stagnation point flow of Casson fluid towards a stretching sheet, Mahato *et al.* [39] conducted a study. Zainodin *et al.* [40] investigated the consequences of viscous dissipation, convective boundary conditions, as well as Joule heating on a mixed convective flow across a nonlinearly moving surface near a stagnation-point. Additionally, because of the buoyancy force influencing the flow, the hybrid nanofluid displays an asymmetric flow pattern. Ali *et al.* [41] investigated the heat transfer and the effect of mixed convection on hybrid nanofluid flow over

a disc. The condition of zero mass flux was used. The mixed convection hybrid nanofluid flow with slip conditions and heat generation or absorption was analyzed by Asghar *et al.* [42].

2.3 Slip Velocity

Many heat transfer phenomena, including the cleaning of mechanical heart valves, inner cavity polishing, and micro heat exchangers, are significantly influenced by the presence of slip conditions. A unique framework for hybrid nano fluidic, three-dimensional flow past an uneven stretching surface with the impact of MHD and slip conditions was examined by Tlili *et al.* [43]. The effect of velocity slip conditions on a dusty hybrid nanofluid flow past a deformable surface was studied numerically by Anuar *et al.* [44]. Usafzai *et al.* [45] looked at the several options for increasing the heat transfer of the nanofluid flowing over a stretching surface with velocity slip and temperature jump impacts and found out multiple solutions for the problem. The heat transfer and hybrid nanofluid flow over an exponentially stretching porous surface was examined by Eid and Nafe [46]. Manigandan *et al.* [47] investigated mixed convection hybrid nanofluid flow over an exponentially stretching surface with slip boundary conditions. The study was performed in the presence thermal radiation and heat generation/absorption. They examined a magneto hydrodynamic flow with slip velocity. Nasir *et al.* [48] examined the impact of MHD with velocity slip condition on a hybrid nanofluid composed by adding carbon nanotubes and its flow on a surface that is gradually stretching. By using the Xue modified theoretical model, the nanofluid flow was examined with the existence of viscous dissipation, thermal radiations, and Ohmic heat impacts. The wall jet problem for a hybrid nanofluid flowing over a porous stretching surface and involving convective boundary conditions, velocity slip, thermal radiation and MHD was examined by Aly *et al.* [49].

2.4 Unsteady flow

The study of unsteady boundary layer flow is of immense importance in various fields.

The unsteady laminar flow along a nonlinearly porous stretching sheet with heat and mass transfer for an incompressible and hydromagnetic hybrid nanofluid was studied by Kumbhakar *et al.* [50]. A rotating hybrid nanofluid flow, combined with an unsteady, three dimensional boundary layer flow caused by a stretched sheet was examined by Sohut *et al.* [51]. In consideration of convective boundary conditions and taking thermal radiations into account, Lone *et al.* [52] described the time-dependent hybrid nanofluid flow with nanoparticles dispersed in an engine oil. They explained that greater thermal Biot numbers, nanoparticle volume fractions, and radiation parameters lead to growing temperature. With a focus on convective heat transfer, Mohana *et al.* [53] investigated an unsteady hybrid nanofluid flow over a bidirectionally stretched sheet in the presence of Darcy-Forchheimer effects. Their work aimed to research the flow properties and heat transmission of graphite and cadmium telluride nano particles, including the impacts of viscous dissipation and Joule heating. Nadeem *et al.* [54] carefully examined the impact of fuzzy tangent hyperbolic hybrid nanofluid flow towards an exponentially stretched surface in the presence of magnetohydrodynamics. The study was based on unsteady flow characteristics of the fluid model. Blood based unsteady hybrid nanofluid flow between two stretching disks which were also rotating was studied by Qayyum *et al.* [55] with the existence of magnetohydrodynamics, chemical reaction and convective boundary conditions. Triveni *et al.* [56] analyzed the heat transfer resulting from an unsteady hybrid nanofluid flow across a stretching/shrinking sheet with the consideration of magnetohydrodynamics. Yasir *et al.* [57] examined the unsteady boundary layer flow and thermal transportation analysis of an incompressible Oldroyd-B nanofluid driven by a stretched cylinder using an analytical method. Chu *et al.* [58] investigated the effects of magnetohydrodynamics on an irregular viscous squeezing flow in a channel with particle shape factors. Mathews *et al.* [59] looked at the heat transfer analysis of an unsteady free convection flow of a hybrid nanofluid with the existence of stagnation point and magnetohydrodynamics.

2.5 Stretching surface

A lot of research has been performed on the fluid flow over stretching surfaces due to its importance in enormous fields. The analysis was performed with MHD and Darcy-Forchheimer effects. The study of the effects of activation energy on a hybrid nanofluid flow over a curved stretching surface was proposed by Kumar *et al.* [60]. Sahu *et al.* [61] looked at

the thermal control of a Cross hybrid nanofluid flow caused by a vertically stretched cylinder. The effect of the Arrhenius activation energy on the flow of a continuous, electrically conducting hybrid nanofluid over an impermeable, thin, elastic sheet was the subject of Elattar *et al.* [62] study. Thermophoreses and diffusion affects, thermal radiation, heat generation/absorption, viscous dissipation and velocity slip conditions were all examined in their study. Several researchers had shown their interest on the concept of heat transfer and fluid flow over stretched surfaces because of its usefulness [63-65]. The velocity, temperature profiles and entropy generation of the hybrid nanofluid flowing over a stretching sheet was investigated by Farooq *et al.* [66] utilizing thermal radiation effect. They were able to come up with a better approach, which uses highly non-linear PDEs to design the fluid flow across the geometric features. The influence of surface movement and geometry on fluid velocity and temperature distribution was also highlighted in the study. The variation in heat and mass transfer arising from the flow of a hybrid Casson nanofluid along a stretching sheet was investigated by Alqahtani *et al.* [67]. The heat and mass transfer resulting from the flow of a hybrid Casson nanofluid created by an exponentially stretched sheet was investigated by Alqahtani *et al.* [68].

Inspired by the aforementioned research and keeping in view from the above literature that no work has been done on the investigation of the problem on an unsteady, three dimensional, rotating hybrid nanofluid flow across an exponentially stretching surface using velocity slip condition. CuO & TiO_2 , two distinct nanoparticles are suspended in ethylene glycol and water to create hybrid nanofluid. Using a similarity transformation, the governing equations with boundary conditions are converted into a system of simple ordinary differential equations. The boundary value problem solver (bvp4c) in MATLAB software is then used to solve the system of equations numerically. A graphical illustration of the flow impacts of various parameters is provided. It is assumed that the results obtained from the considered work will be helpful for the researchers in the future.

Chapter 3

Fundamental Definitions and Concepts

This chapter deals with the basic definitions and concepts related to the field of fluid mechanics. The understanding of these definitions play an essential role in the fluid problem modeling.

3.1 Fluid

Substances that are constantly deforming due to external forces are called fluids. They are incapable of resisting the shear force which is the force that modifies a material's shape applied to them. Molten lava, toothpaste, water, air etc. are few examples of fluids. [69]

3.2 Fluid mechanics

It is the branch of physics that involves the study of behavior of fluids (liquids, gases, and plasmas) either at rest or in motion. It comprehends the analysis of how fluid flows and the forces acting on them. [69]

3.2.1 Fluid statics

The study of fluid behavior at rest is referred to as fluid statics in the academic area of fluid mechanics. It entails investigating the pressures and strains that fluids experience while they are at rest. [69]

3.2.2 Fluid dynamic

The study of fluids in motion is focused on the subfield of fluid mechanics known as fluid dynamics. Moreover, hydrodynamics and aerodynamics are two subfields of fluid dynamics. The computations of different fluid parameters as functions of place and time, including flow velocity, pressure, density and temperature, is performed in fluid dynamics. [69]

3.3 Nanofluid

A nanofluid [69] is a fluid that has nanoparticles in it. These fluids are made with the intention of incorporating colloidal nanoparticle suspensions into base liquid. Nanofluids often contain oxides, metallic substances, carbide particles, or carbon nanotubes. Common base fluids include oil, ethylene glycol and water. It has been demonstrated that conventional fluids have lower thermal conductivity than nanofluids.

3.4 Hybrid nanofluid

A hybrid, the most sophisticated type of nanofluid, is produced by combining two nanoparticles with the suitable base fluid. Hybrid nanofluids improve the thermal conductivity of conventional fluids and even of the simple nanofluids. Heat pipes, refrigeration and automobile cooling systems are just a few of the many applications for hybrid nanofluids in heat transmission. [70]

3.5 Flow

Fluid flow is an expression used for referring to the movement of a fluid under the impact of many uneven forces. Until it is exposed to numerous forces that are not balanced, the fluid continues to flow. [71]

3.6 Types of fluid flow

According to variations in their density and velocity, for instance, fluids can be categorized into many classes. Different types of flows refer to different analytical techniques in fluid mechanics. [71]

3.6.1 Steady flow

When a fluid's velocity, pressure and all relevant numerical characteristics (including density and viscosity) are constant with respect to time across the flow field, the fluid is said to be flowing steadily. In theory, only an equilibrium situation (stationary state) allows for a steady flow. The following are the characteristics that relate to steady flow. [71]

$$\frac{\partial P}{\partial t} = 0, \quad (3.1)$$

$$\frac{\partial \mathbf{v}}{\partial t} = 0, \quad (3.2)$$

$$\frac{\partial \rho}{\partial t} = 0. \quad (3.3)$$

3.6.2 Unsteady flow

Unsteady fluid [71] flow is characterized as a flow that occurs when the fluid's parameters, such as velocity, pressure or cross-sectional area, fluctuate over time at any point in the flow. This type of flow corresponds to the following properties

$$\frac{\partial P}{\partial t} \neq 0, \quad (3.4)$$

$$\frac{\partial \mathbf{v}}{\partial t} \neq 0, \quad (3.5)$$

$$\frac{\partial \rho}{\partial t} \neq 0. \quad (3.6)$$

3.6.3 Viscous flow

Viscous flow [71] is a type of fluid flow categorized with the existence of viscosity that in fluids is basically the internal resistance of a fluid to the deforming shear stress. In viscous flow, nearby fluid layers travel with dissimilar velocities, and this velocity gradient leads to the generation of shear stress within the fluid.

3.6.4 Non viscous flow

Non-viscous fluids are regarded as those that indicate zero or no resistance to internal friction. They are commonly used in numerous engineering disciplines, including hydrodynamics, aerodynamics, and fluid mechanics, in which assumptions of non-viscous flow deliver a foundation for understanding essential fluid conduct. [71]

3.6.5 Laminar flow

When there is a smooth fluid flow with consistent pressure and velocity and neighboring layers of fluid flow past each other without noteworthy mixing or disturbance, the flow is referred to as laminar flow. This flow's streamlines are all parallel to one another. This is the only scenario in which low velocity and high viscosity of fluid coexist. [71]

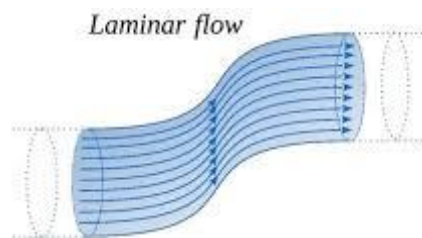


Figure 3.1. Laminar flow

3.6.6 Turbulent flow

A type of flow when the fluid's inertial forces dominate is called turbulent flow. It usually flows at higher velocities and quicker speeds all the time. Pressure and velocity all appear to change erratically. [71]

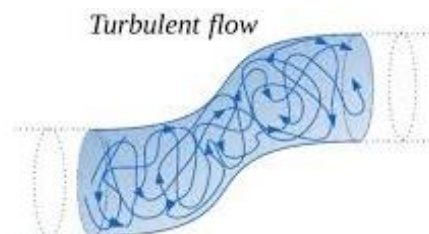


Figure 3.2. Turbulent flow

3.6.7 Uniform flow

A type of fluid flow known as uniform fluid flow [71] occurs when the flow velocity or any other property at any one moment is the same throughout the fluid and has the same magnitude in all directions. The following is a mathematical expression for a uniform flow.

$$\frac{\partial \mathbf{v}}{\partial x} = 0, \quad \frac{\partial \rho}{\partial x} = 0, \quad \frac{\partial P}{\partial x} = 0. \quad (3.7)$$

3.6.8 Non Uniform flow

The fluid's velocity, pressure or any other property varies constantly for every moment in non-uniform fluid flow [71]. Pressure, velocity, and speed are examples of fluid parameters that are always changing.

$$\frac{\partial \mathbf{v}}{\partial x} \neq 0, \quad \frac{\partial \rho}{\partial x} \neq 0, \quad \frac{\partial P}{\partial x} \neq 0. \quad (3.8)$$

3.6.9 Compressible flow

Compressible flow is a type of flow which corresponds to the variation in density, temperature and pressure and these variations are noteworthy to originate changes in the volume of the fluid. [71]

3.6.10 Incompressible flow

Incompressibility is a feature of fluids that prevents the density of a fluid from changing when subjected to shear forces, and it describes the majority of fluids in nature at normal room temperature. [71]

3.6.11 Rotational Flow

In a fluid flow with rotational motion, the fluid rotates while it is in motion. Flowing water in a bathtub vortex, shows the demonstration of this type of flow. [71]

3.6.12 Irrotational flow

In an irrotational fluid flow, the fluid is not rotating along its own axis. The fluid's constituent can travel at any time and in any direction. [71]

3.6.13 One, two and three Dimensional fluid flow

When the fluid's attributes, such as its velocity, density and pressure, fluctuate in only a single direction, the flow is said to be one-dimensional.

When the fluid's characteristics, such as its velocity, density and pressure, fluctuate across two directions, the flow is said to be two-dimensional.

When the fluid's characteristics such as its velocity, density and pressure vary in three dimensions, the flow is said to be three-dimensional. [71]

3.7 Density

Density [71] is a calculation of an amount or mass per unit volume for a particular substance.

$$\rho = \frac{m}{V}. \quad (3.9)$$

The dimensions are $[ML^{-3}]$ and the density is expressed in SI units of kg/m^3 .

3.8 Pressure

Pressure [71] is characterized as the force to area ratio. The term "pressure" relates to the physical force imposed on a substance and it causes the development of stress.

$$P = \frac{F}{A} \quad (3.10)$$

For pressure, the SI units is N/m^2 .

3.9 Thermal conductivity

The study of a material's ability to transport heat is known as thermal conductivity [71]. More specifically, it is described mathematically as

$$\text{Thermal Conductivity} = \frac{\text{heat} \times \text{distance}}{\text{Area} \times \text{Temperature gradient}} \quad (3.11)$$

So,

$$k = \frac{QL}{A\Delta T}, \quad (3.12)$$

where the cross-sectional area is A , thermal conductivity is k , heat transfer in a time-unit is Q and T is the temperature differential. Its dimensions are $\left[\frac{ML}{T^3\theta}\right]$ and its units are W/mk or $kg.m\backslash s^3K$.



Figure 3.3. Thermal Conductivity

3.10 Thermal diffusivity

Thermal diffusivity [71] is defined as the ratio between thermal conductivity and the product of density and specific heat. In mathematical concepts, it is expressed as

$$\alpha = \frac{\rho}{kc_p}, \quad (3.13)$$

where k stands for thermal conductivity, ρ for density and c_p for heat capacity.

3.11 Stress

Stress [72] is the term used to describe the mean force exerted for each unit of affected body surface area.

$$\text{Stress} = \frac{\text{Force}}{\text{Area}}. \quad (3.14)$$

The SI system expresses stress as Nm^{-2} or $\frac{kg}{ms^2}$ and its dimensions are $\left[\frac{M}{LT^2}\right]$. Two distinct components make up the stress.

3.11.1 Shear stress

Shear stress [72] is a type of stress that arises when nearby layers of a fluid slide past each other in analogous directions.

3.11.2 Normal stress

Normal stress [72] is a type of stress that acts normally to the surface of a body or a material. It characterizes the force per unit area applied normal to the object's surface.

3.11.3 Strain

Strain [72] is an assessment of a material's relative deformation when a force is applied to it. It doesn't have any dimensions.

3.12 Viscosity

Viscosity [72] is related to the internal frictional impact that occurs when neighboring fluid layers move in relation to one another. Viscosity is usually influenced by three factors, temperature, pressure and rate of deformation of the fluid. There are two methods for determining viscosity.

3.12.1 Dynamic viscosity

Absolute viscosity, sometimes called dynamic viscosity [70], is defined as the ratio of shear stress to velocity gradient.

$$\text{Viscosity}(\mu) = \frac{\text{Shear Stress}}{\text{Velocity gradient}}, \quad (3.15)$$

Dynamic viscosity has dimensions of $\left[\frac{M}{LT^2}\right]$ and is measured in SI units of Ns/m^2 or $\frac{\text{kg}}{\text{m}\cdot\text{s}}$.

3.12.2 Kinematic viscosity

The relationship between fluid density and dynamic viscosity determines kinematic viscosity [70]. The aforementioned concept may be presented mathematically as

$$\nu = \frac{\mu}{\rho}. \quad (3.16)$$

Kinematic viscosity has units of m^2/s and is measured in $\frac{L^2}{T}$.

3.13 Convection

The flow of thermal energy through fluids is described by convective heat transfer. The large scale molecular movement inside the liquid, gas or liquid-gas mixture causes convection to form. The process by which matter travels inside fluids to exchange thermal energy is mostly known as convection. [72]

3.13.1 Natural convection

The buoyant forces arising from a density differential caused by temperature variations are what cause this type of convection. The fluid's density decreases when it comes into contact with a hot surface or environment because the molecules are scattered and split. [72]

3.13.2 Forced convection

This happens when an external force, such as a fan, pump or water heater, pushes a fluid across a space. This type of flow improves the heat transfer rate between the object's surface and the fluid, as compared to the natural convection. [72]

3.13.3 Mixed convection

A mixture of forced and free convection is referred to as mixed convection. This particular form of heat transfer happens when a fluid flow has both forced and spontaneous convection. In mixed convection, external forces like fans or pumps act in addition to the buoyant forces that arise from the temperature variations. It is frequently used in real-world engineering applications, such as electronic cooling systems and heat exchangers etc. [72]

3.14 Dimensionless numbers

3.14.1 Reynolds number

According to fluid flow, the most important dimensionless number is the Reynolds number [72]. It's clarified as the relationship between inertial and effective viscous forces. The relationship is presented as follows

$$Re = \frac{\text{Inertial force}}{\text{Viscous force}}, \quad (3.17)$$

$$Re = \frac{\rho v^2 / L}{\mu v^* / L^2} = \frac{vL}{\nu^*}. \quad (3.18)$$

Re indicates the Reynolds number, ρ is the fluid's density, v symbolizes the velocity of the flow. If the calculated Reynolds number is high, that is more than 2000, the flow through the pipe is considered turbulent. Laminar flow is defined as having a low Reynolds number (less than 2000). While laminar and turbulent flows are commonly classified according to a range, these values are acceptable numerically. Below 1100 Reynolds numbers, laminar flow occurs and over 2200, turbulent flow occurs.

3.14.2 Prandtl number

The connection between momentum and also thermal diffusivity is determined by the Prandtl number [72], which has no dimensions. The Prandtl number can be defined mathematically as follows

$$\text{Pr} = \frac{\text{Momentum diffusivity}}{\text{Thermal diffusivity}}, \quad (3.19)$$

$$\text{Pr} = \frac{\nu}{\alpha_f}, \quad (3.20)$$

where ν is symbolized for kinematic viscosity and α_f for thermal diffusivity.

3.14.3 Skin friction

Skin friction [72] refers to the type of friction that results from a fluid flowing in relation to a solid surface. The skin friction coefficient is designated mathematically as

$$C_f = \frac{\tau_w}{\frac{1}{2}\rho_f u^2}, \quad (3.21)$$

where ρ signifies density, u represents velocity and τ_w signifies wall shear stress. It is thought that the frictional drag is either in aerodynamics or even in hydrodynamics. It acts on the subject as a resisting force caused by the fluid flow. It begins as a result of the fluid's viscosity and develops from laminar drag to turbulent drag with the surrounding fluid.

3.14.4 Nusselt number

The interaction between conductive and convective heat transport across the boundary is quantified by the Nusselt number [72], a dimensionless quantity. Addressing mathematically, it is as follows

$$Nu_L = \frac{\text{Convective heat transfer}}{\text{Conductive heat transfer}}, \quad (3.22)$$

or,

$$Nu_L = \frac{hL}{k}, \quad (3.23)$$

where L is the characteristic length, h is the heat transfer coefficient and k is the thermal conductivity. When a high Nusselt number is chosen, efficient convection is experienced, which is evident in turbulent pipe flow.

Chapter 4

The Rotating Flow of Nanofluid in the presence of Convective Boundary Conditions

A modern class of fluids with excellent thermal conductivity includes nanofluids. The effect of convective boundary conditions on the flow of a hybrid base nanofluid across an exponentially stretching sheet is investigated. The fluid model is established as a system of partial differential equations. The use of proper similarity transformation leads to a more simplified system of ordinary differential equations from the governing equations of a considered model. The bvp4c technique is employed to graphically assess temperature and velocity, along with skin friction and Nusselt number [73].

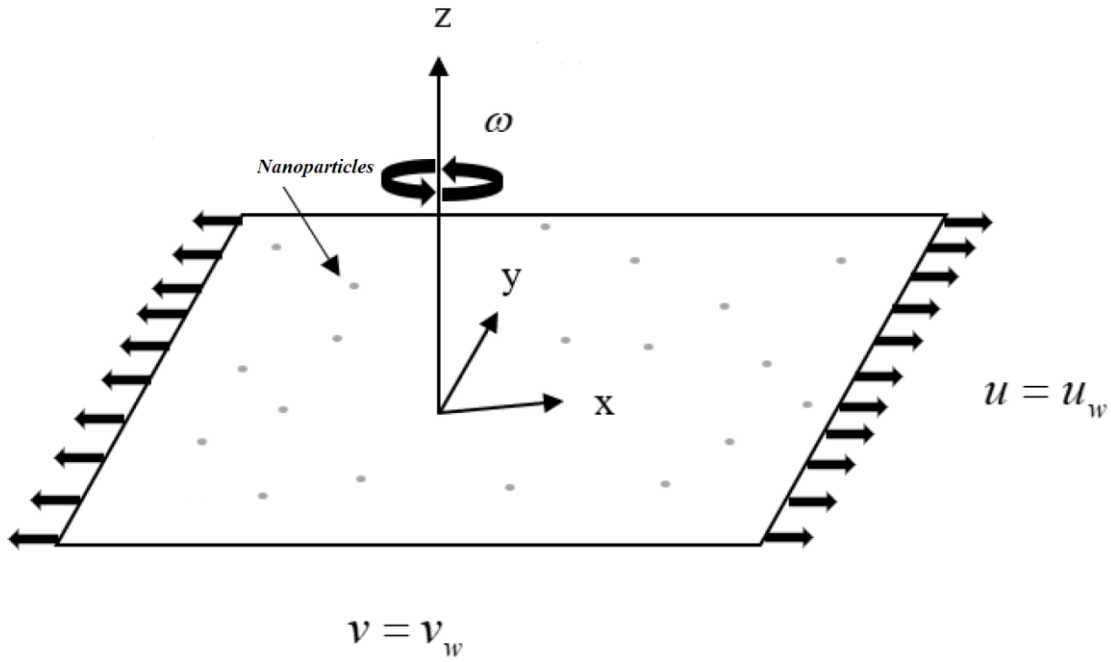


Figure 4.1. Geometry of nanofluid problem.

4.1 Formulation of the Problem

The current model is based on a three-dimensional, continuously rotating, incompressible flow of a viscous nanofluid that is flowing on a stretchy surface within $z \geq 0$ axis. The fluid rotates around the z -axis developing an angular velocity ω . To exponentially extend the wall, it stretches with speed u_w and v_w . CuO and TiO_2 are regarded as nanoparticles with a 50% ethylene glycol and 50% water combination as the base fluid. The governing equations for the fluid flow are stated as:

$$\nabla \cdot (\rho \mathbf{V}) = 0, \quad (4.1)$$

$$(\mathbf{V} \cdot \nabla) \mathbf{V} = \nabla \cdot \boldsymbol{\tau} + \rho \mathbf{b}, \quad (4.2)$$

$$(\mathbf{V} \cdot \nabla) T = \alpha_f \nabla^2 T. \quad (4.3)$$

In the aforementioned equations, ρ denotes the density, \mathbf{V} is the velocity field, ν stand for kinematic viscosity, $\boldsymbol{\tau}$ is represent stress tensor, \mathbf{b} is for body force, T denotes the temperature and α_f is the thermal diffusivity.

Following are the governing four important equations obtained after using the boundary layer approximation

$$\frac{\partial u}{\partial x} + \frac{\partial v}{\partial y} + \frac{\partial w}{\partial z} = 0, \quad (4.4)$$

$$u \frac{\partial u}{\partial x} + v \frac{\partial u}{\partial y} + w \frac{\partial u}{\partial z} - 2\omega v = \frac{\mu_{nf}}{\rho_{nf}} \frac{\partial^2 u}{\partial z^2}, \quad (4.5)$$

$$u \frac{\partial v}{\partial x} + v \frac{\partial v}{\partial y} + w \frac{\partial v}{\partial z} + 2\omega u = \frac{\mu_{nf}}{\rho_{nf}} \frac{\partial^2 v}{\partial z^2}, \quad (4.6)$$

$$u \frac{\partial T}{\partial x} + v \frac{\partial T}{\partial y} + w \frac{\partial T}{\partial z} = \alpha_{nf} \frac{\partial^2 T}{\partial z^2}. \quad (4.7)$$

The above equations are subjected to the conditions

$$\left. \begin{aligned} u = u_w, v = v_w, -k_{nf} \frac{\partial T}{\partial z} = h_f(T_w - T) \text{ at } z = 0 \\ u \rightarrow 0, v \rightarrow 0, T \rightarrow T_\infty \text{ as } z \rightarrow \infty \end{aligned} \right\} \quad (4.8)$$

Due to the stretching of the surface exponentially, the stretching velocities and the wall temperature are seen below:

$$u_w = u_0 e^{\frac{x+y}{L}}, v_w = v_0 e^{\frac{x+y}{L}}, T_w = T_\infty + T_0 e^{\frac{A(x+y)}{2L}}. \quad (4.9)$$

The suitable similarity transformation are

$$\left. \begin{aligned} u = u_0 e^{\frac{x+y}{L}} p'(\eta), v = u_0 e^{\frac{x+y}{L}} q'(\eta), T = T_\infty + T_0 e^{\frac{A(x+y)}{2L}} \theta(\eta), \\ w = -\left(\frac{\nu u_0}{2L}\right)^{1/2} e^{\frac{x+y}{2L}} \{p(\eta) + \eta q'(\eta) + q(\eta) + \eta p'(\eta)\}, \eta = \left(\frac{u_0}{2\nu L}\right)^{1/2} e^{\frac{x+y}{2L}} z \end{aligned} \right\} \quad (4.10)$$

where the similarity space factor is denoted through η , T_w indicate the wall's temperature, T_∞ is intended for the temperature of free stream. The continuity equation is identically fulfilled after applying the similarity transformations, whereas the form of the momentum and energy

equations is as follows:

$$\frac{\frac{\mu_{nf}}{\rho_{nf}}}{\rho_f} p'''' + p''(p+q) - 2p'(p'+q') + 4\gamma q' = 0, \quad (4.11)$$

$$\frac{\frac{\mu_{nf}}{\rho_{nf}}}{\rho_f} q'''' + q''(p+q) - 2q'(p'+q') - 4\gamma p' = 0, \quad (4.12)$$

$$\left(\frac{1}{Pr}\right) \left(\frac{\frac{k_{nf}}{k_f}}{(\rho C_p)_{nf}}\right) \theta'' - A(p'+q')\theta + (p+q)\theta' = 0, \quad (4.13)$$

while the boundary conditions are

$$\left. \begin{aligned} p(0) = 0, \quad p'(0) = 1, \quad q(0) = 0, \quad q'(0) = \alpha, \\ \theta'(0) = -N_c \left(\frac{1}{\frac{k_{nf}}{k_f}}\right) (1 - \theta(0)) \quad \text{at } \eta = 0 \\ p' \rightarrow 0, \quad q' \rightarrow 0, \quad \theta \rightarrow 0 \quad \text{as } \eta \rightarrow \infty \end{aligned} \right\}. \quad (4.14)$$

Here $\gamma = \frac{L\omega}{\mu_0}$ is the rotation parameter, $Pr = \frac{(\mu C_p)_f}{k_f}$ indicates Prandtl number, $\alpha = \frac{v_0}{u_0}$ is denoted

for stretching ratio parameter, $N_c = \frac{h_f}{K_f} \sqrt{\frac{2\nu_f L}{u_0}} e^{-\left(\frac{x+y}{2L}\right)}$ is represented for convective parameter,

μ_{nf} stands for dynamic viscosity, ρ_{nf} shows density, a_{nf} indicates thermal diffusivity, k_{nf} stands for thermal conductivity, $(\rho C_p)_{nf}$ is heat ability of nanofluid.

The Nusselt number and Skin friction coefficient have been calculated as

$$C_{fx} = \frac{\tau_{wx}}{\frac{1}{2}\rho_f(u_w)^2}, \quad (4.15)$$

$$C_{fy} = \frac{\tau_{wy}}{\frac{1}{2}\rho_f(u_w)^2}, \quad (4.16)$$

$$Nu_x = \frac{xq_w}{k_f(T_w - T_\infty)}. \quad (4.17)$$

The wall shear stresses τ_{wx} , τ_{wy} and heat flux q_w are defined as

$$\tau_{wx} = \mu_{nf} \left(\frac{\partial u}{\partial z} \right)_{z=0}, \quad (4.18)$$

$$\tau_{wy} = \mu_{nf} \left(\frac{\partial v}{\partial z} \right)_{z=0}, \quad (4.19)$$

$$q_w = -k_{nf} \left(\frac{\partial T}{\partial z} \right)_{z=0}. \quad (4.20)$$

Applying equation (4.10) and (4.18 - 4.20) in (4.15 - 4.17) now, the following expressions are obtained

$$\frac{1}{\sqrt{2}} C_{fx} (Re_x)^{\frac{1}{2}} = \frac{1}{(1-\phi)^{2.5}} p''(0), \quad (4.21)$$

$$\frac{1}{\sqrt{2}} C_{fy} (Re_x)^{\frac{1}{2}} = \frac{1}{(1-\phi)^{2.5}} q''(0), \quad (4.22)$$

$$\sqrt{2} \frac{L}{x} Nu_x (Re_x)^{-\frac{1}{2}} = -\frac{k_{nf}}{k_f} \theta'(\eta). \quad (4.23)$$

4.2 Numerical Algorithm

The bvp4c technique is applied considering the equations (4.11 - 4.14) in order to achieve a numerical solution. The first order system of equations is illustrated as

$$\left. \begin{array}{l} y_1 = p \\ y_2 = p' \\ y_3 = p'' \\ y_4 = q \\ y_5 = q' \\ y_6 = q'' \\ y_7 = \theta \\ y_8 = \theta' \end{array} \right\}. \quad (4.24)$$

Thus, the system of equations achieve the following forms.

$$y_3' = \frac{\frac{\rho_{nf}}{\mu_{nf}}}{\mu_f} (-y_3(y_1 + y_4) + 2y_2(y_2 + y_5) - 4\gamma y_5), \quad (4.25)$$

$$y_6' = \frac{\frac{\rho_{nf}}{\mu_{nf}}}{\mu_f} (-y_6(y_1 + y_4) + 2y_5(y_2 + y_5) + 4\gamma y_2), \quad (4.26)$$

$$y_8' = \text{Pr} \frac{\frac{(\rho c_p)_{nf}}{(\rho c_p)_f}}{\frac{k_{nf}}{k_f}} [-(y_1 + y_4)y_8 + A(y_2 + y_5)y_7]. \quad (4.27)$$

With conditions

$$\left. \begin{aligned} y_1(a) = 0, \quad y_2(a) = 1, \quad y_4(a) = 0, \quad y_5(a) = \alpha, \quad y_8(a) = -Nc \frac{1}{\frac{k_{nf}}{k_f}} (1 - y_7(0)) \\ y_2(b) = 0, \quad y_5(b) = 0, \quad y_7(b) = 0. \end{aligned} \right\} \quad (4.28)$$

Table 4.1: Important thermal feature of TiO_2 & CuO . (Hussain *et al.* [73])

Properties	Nanofluids
Density	$\rho_{nf} = \rho_f(1 - \phi) + \phi\rho_s$
Specific Heat	$(\rho c_p)_{nf} = (\rho c_p)_f(1 - \phi) + \phi(\rho c_p)_s$
Dynamic Viscosity	$\mu_{nf} = \frac{\mu_f}{(1 - \phi)^{2.5}}$
Kinematic Viscosity	$\nu_{nf} = \frac{\mu_{nf}}{\rho_{nf}}$
Thermal Conductivity	$\frac{k_{nf}}{k_f} = \frac{k_s + 2k_f - 2\phi(k_f - k_s)}{k_s + 2k_f + \phi(k_f - k_s)}$

Table 4.2: Thermo-physical characteristics of considered nanoparticles and hybrid base fluid. (Hussain *et al.* [73])

Physical Properties	$\rho \left(\frac{kg}{m^3} \right)$	$C_p \left(\frac{J}{kg.K} \right)$	$k \left(\frac{W}{m.K} \right)$
$C_2H_6O_2-H_2O$	1063.8	3630	0.387
CuO	6500	540	18
TiO_2	4250	686.2	8.9538

Table 4.3: Comparison with the literature of heat transfer rate for pure fluid with $\alpha = \phi = \gamma = 0$ and $Nc \rightarrow \infty$.

$\theta'(0)$ for CuO -hybrid base fluid					
Pr	A	Magyari and Keller [81]	Liu <i>et al.</i> [82]	Nadeem <i>et al.</i> [83]	Present results
1	-1.5	0.37741	0.37741256	0.377412	0.377407
	0	-0.549643	-0.54964375	-0.549646	-0.549645
	1	-0.954782	-0.95478270	-0.954786	-0.954783
	3	-1.560294	-1.56029540	-1.560295	-1.560296
5	-1.5	1.353240	1.35324050	1.3532405	1.3532405
	0	-1.521243	-1.52123900	-1.521240	-1.521239
	1	-2.500135	-2.500135157	-2.500135	-2.500131
	3	-3.886555	-3.88655510	-3.886555	-3.886555
10	-1.5	2.200000	2.20002816	2.2000282	2.2000281
	0	-2.257429	-2.25742372	-2.257424	-2.257424
	1	-3.660379	-3.66037218	-3.660372	-3.660371
	3	-5.635369	-5.62819631	-5.628196	-5.628196

4.3 Discussion for the Graphical Results:

The nanofluid flow over a rotating surface stretching exponentially is analyzed. Table 4.1, 4.2 & 4.3 presents the required properties for the considered fluid and Table. 4.4 shows the comparative study for Nusselt number in case of *CuO* nanoparticles. The results obtained from the present analysis almost matches with the previous studies.

This section mainly addresses the effects of certain pertinent factors such as stretching ratio parameter α , rotation parameter γ and temperature exponent A on velocity distributions $p'(\eta)$, $q'(\eta)$ and temperature distribution $\theta(\eta)$ for *CuO* and *TiO₂* nanoparticles. The visual findings are obtained in sequence to determine the influence of nanoparticles on different profiles. To achieve the goal, Figures 4.2 - 4.15 are shown. The implications of the stretching ratio parameter α on the velocity profile $p'(\eta)$ for *CuO* and *TiO₂* hybrid base fluid is depicted in Figures 4.2 & 4.3 by assuming $Nc = 3.0$, $Pr = 25.33$, $\phi = 0.1$, $R = 0.5$, $\gamma = 0.1$, $A = 0.2$ for *CuO* and $Nc = 3.0$, $Pr = 25.33$, $\phi = 0.1$, $R = 0.5$, $\gamma = 0.2$, $A = 0.3$ for *TiO₂*. The figure shows that *CuO* and *TiO₂* hybrid base fluids experience a drop in velocity when the stretching ratio α is increased. The impact of rotation parameter γ on the velocity profile $p'(\eta)$ is observed in Figures 4.4 & 4.5 with *CuO*, $Nc = 3.0$, $Pr = 25.33$, $\phi = 0.1$, $R = 0.5$, $\alpha = 0.8$, $A = 3.5$ and for *TiO₂*, $Nc = 3.0$, $Pr = 25.33$, $\phi = 0.1$, $R = 0.5$, $\alpha = 0.6$, $A = 3.0$. In a comparable manner as seen in Figure 4.4 & 4.5, the velocity $p'(\eta)$ in both kinds of nanoparticles decreases when the rotation parameter γ grows. It has been established that for *CuO* and *TiO₂* hybrid base fluids, the horizontal velocity field exhibits a lowering mode when the amounts of α and γ expand respectively. The influences of stretching ratio parameter α on the vertical component $q'(\eta)$ for the hybrid base fluid of *CuO* and *TiO₂* are illustrated in Figures 4.6 & 4.7 for *CuO*, $Nc = 3.0$, $Pr = 25.33$, $\phi = 0.1$, $R = 0.5$, $\gamma = 0.1$, $A = 2.0$ and *TiO₂*, $Nc = 3.0$, $Pr = 25.33$, $\phi = 0.1$, $R = 0.5$, $\gamma = 0.1$, $A = 1.0$. It is observed that when stretching ratio parameter α rises the velocity profile improves for both kind of nanoparticles. Figures 4.8 & 4.9 show the velocity profile $q'(\eta)$ under the influence of rotation parameter γ and a decreasing impact is obvious for a considered values of γ while $Nc = 3.0$, $Pr = 25.33$, $\phi = 0.1$, $R = 0.5$, $\alpha = 3.0$, $A = 0.2$ for *CuO* and $Nc = 3.0$, $Pr = 25.33$, $\phi = 0.1$, $R = 0.5$, $\alpha = 3.0$, $A = 2.5$ for *TiO₂*. Figure 4.10 - 4.15 depict the variances in the temperature distribution $\theta(\eta)$ for both forms of nanostructures with respect to α , γ and A . As the value of α climbs for both types of nanoparticles, it is obvious from Figure 4.10 & 4.11 that the temperature profile $\theta(\eta)$ decreases for both *CuO* and *TiO₂* hybrid base fluid and $Nc = 3.0$, $Pr = 25.33$, $\phi = 0.1$, $R = 0.5$, $\gamma = 1.0$, $A = 0.7$ for *CuO* and $Nc = 3.0$, $Pr =$

25.33, $\phi = 0.1$, $R = 0.5$, $\gamma = 1.0$, $A = 6.0$ for TiO_2 . The deteriorating performance of the temperature profile for higher values of A for the CuO -hybrid base fluid and the TiO_2 hybrid base fluid is displayed through Figures 4.12 & 4.13 for $Nc = 3.0$, $Pr = 25.33$, $\phi = 0.1$, $R = 0.5$, $\alpha = 3.0$, $\gamma = 7.0$ in case of CuO nanoparticles and $Nc = 3.0$, $Pr = 25.33$, $\phi = 0.1$, $R = 0.5$, $\alpha = 2.0$, $\gamma = 5.0$ in case of TiO_2 nanoparticles. The influence of rotation parameter γ on the temperature profile is clarified in Figures 4.14 & 4.15 with CuO nanoparticles for $Nc = 3.0$, $Pr = 25.33$, $\phi = 0.1$, $R = 0.5$, $\alpha = 0.1$, $A = 0.2$ and TiO_2 nanoparticles for $Nc = 3.0$, $Pr = 25.33$, $\phi = 0.1$, $R = 0.5$, $\alpha = 0.2$, $A = 0.2$. This indicates that the temperature profile $\theta(\eta)$ for CuO and TiO_2 hybrid base fluid increases when the value of γ rises.

The consequences of various parameters on the skin friction coefficients (C_{fx} , C_{fy}) and the Nusselt number (Nu_x) for both CuO and TiO_2 hybrid base fluids are examined using Figures 4.16 - 4.21. The association of the skin friction coefficient (along x -axis) with a stretching ratio α and volume fraction ϕ for both kinds of nanoparticles is outlined thoroughly in Figures 4.16 & 4.17 for $Nc = 3.0$, $Pr = 25.33$, $R = 0.5$, $\gamma = 0.1$, $A = 0.2$. Here, as α grows, the skin friction coefficient decreases for CuO and TiO_2 hybrid base fluids and same behavior is noticed for variation of ϕ . Figure 4.18 & 4.19 are sketched to find out the behavior of skin friction coefficient along the y -axis under the stretching ratio α and the figures exhibit a drop in skin friction along the y -axis and the similar pattern is encountered by variation of ϕ by keeping $Nc = 3.0$, $Pr = 25.33$, $R = 0.5$, $\gamma = 0.1$, $A = 0.2$. Thus the force that assists an hindrance to the fluid's flow is lowered due to the reduction in skin friction coefficients (C_{fx} , C_{fy}). The fluctuations of ϕ and the stretching ratio α on the Nusselt number are shown in Figures 4.20 & 4.21 for $Nc = 3.0$, $Pr = 25.33$, $R = 0.5$, $\gamma = 0.1$, $A = 0.2$. Here, it is apparent that for CuO and TiO_2 hybrid base fluids, the rate of heat transfer upsurge as α and ϕ rise.

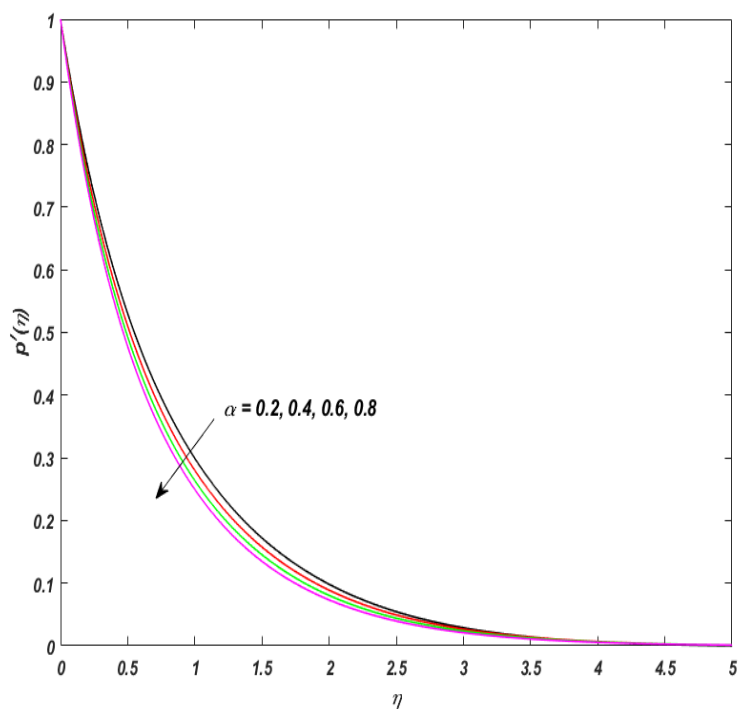


Figure 4.2. Velocity distribution $p'(\eta)$ for α with CuO -hybrid base fluid.

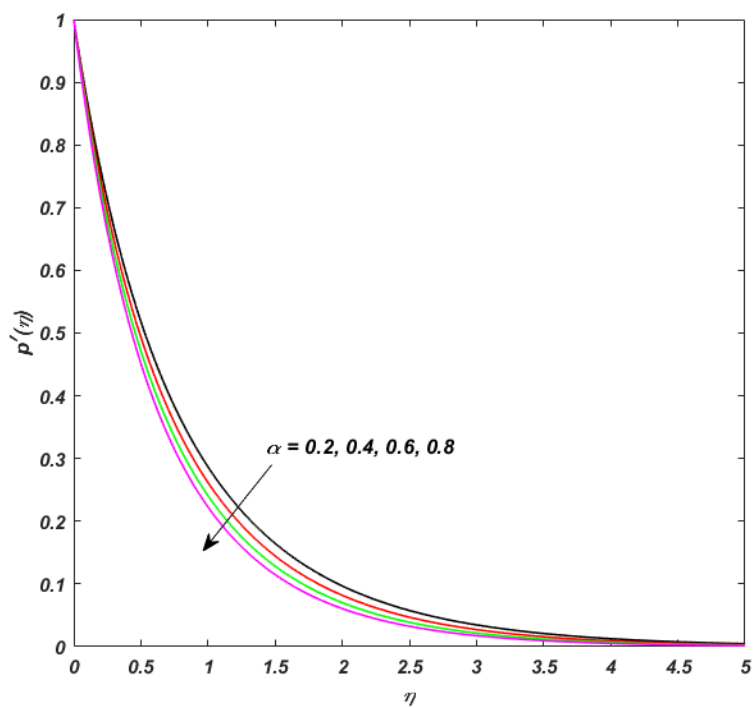


Figure 4.3. Velocity distribution $p'(\eta)$ for α with TiO_2 -hybrid base fluid.

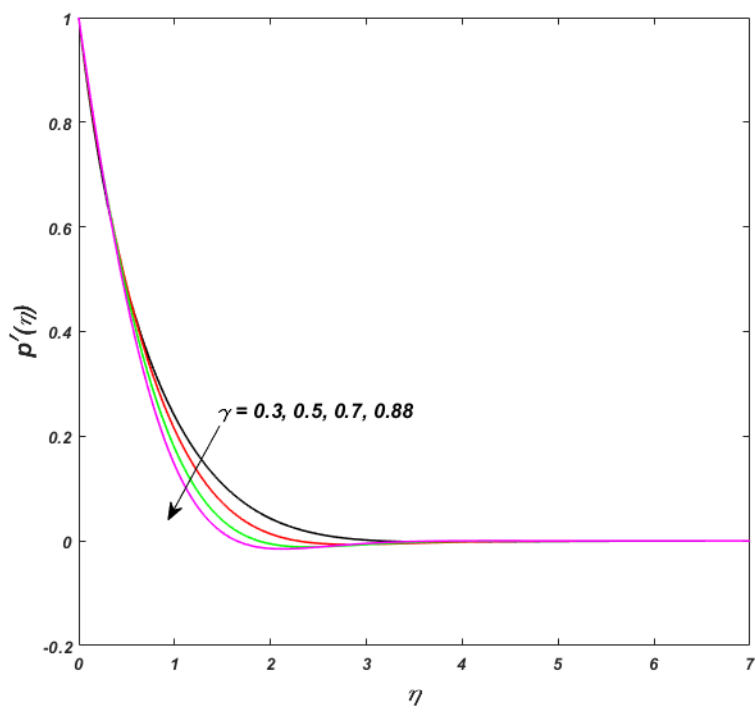


Figure 4.4. Velocity distribution $p'(\eta)$ for γ with CuO–hybrid base fluid.

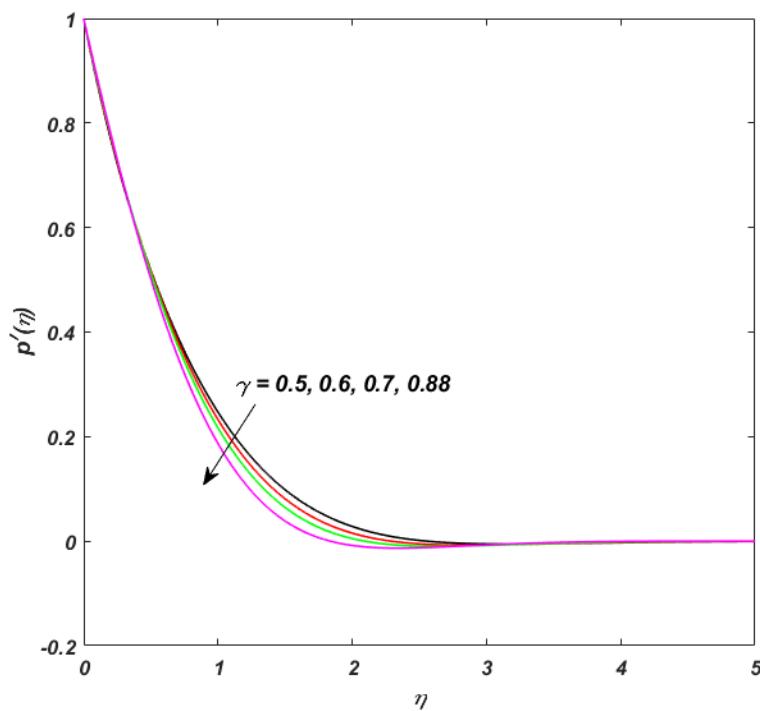


Figure 4.5. Velocity distribution $p'(\eta)$ for γ with TiO₂–hybrid base fluid.

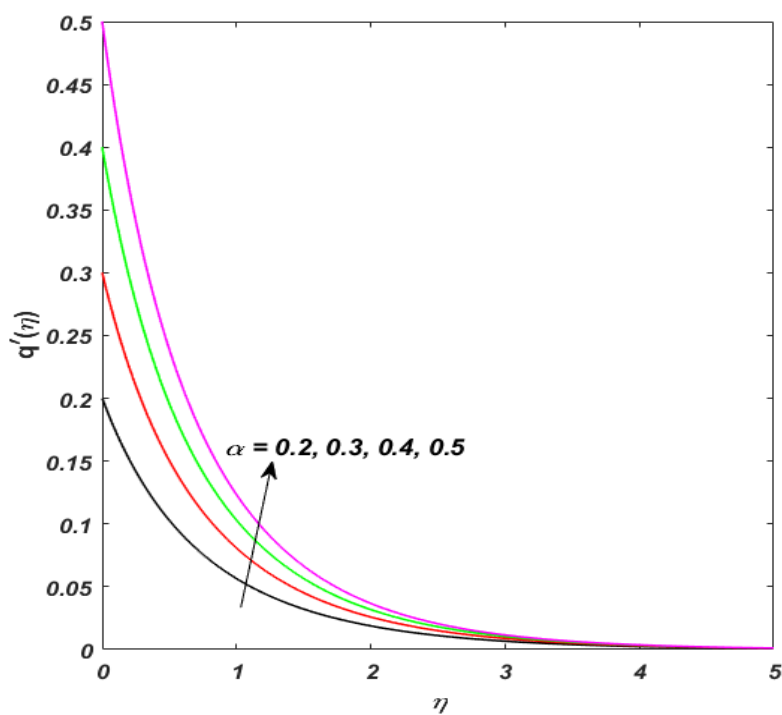


Figure 4.6. Velocity distribution $q'(\eta)$ for α with CuO–hybrid base fluid.

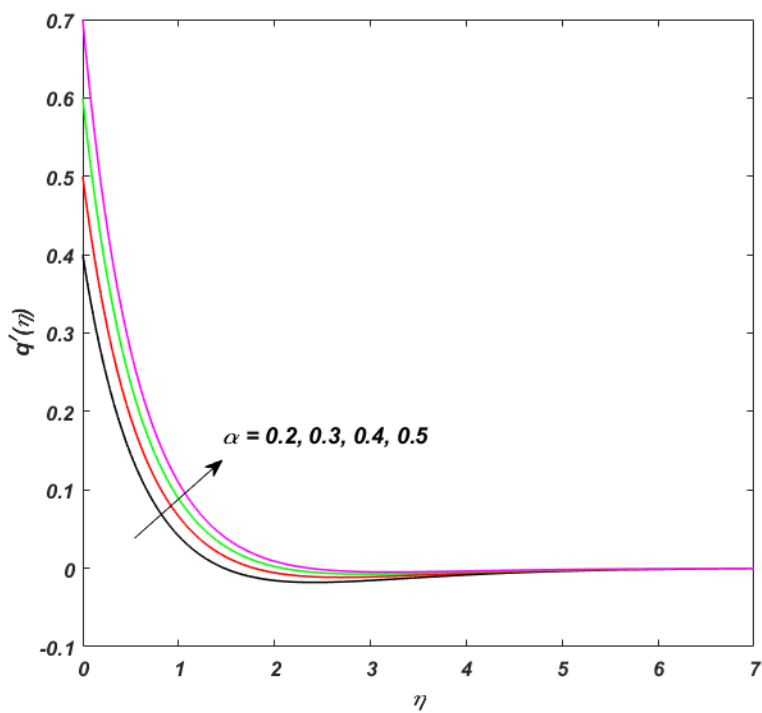


Figure 4.7. Velocity distribution $q'(\eta)$ for α with TiO_2 –hybrid base fluid.

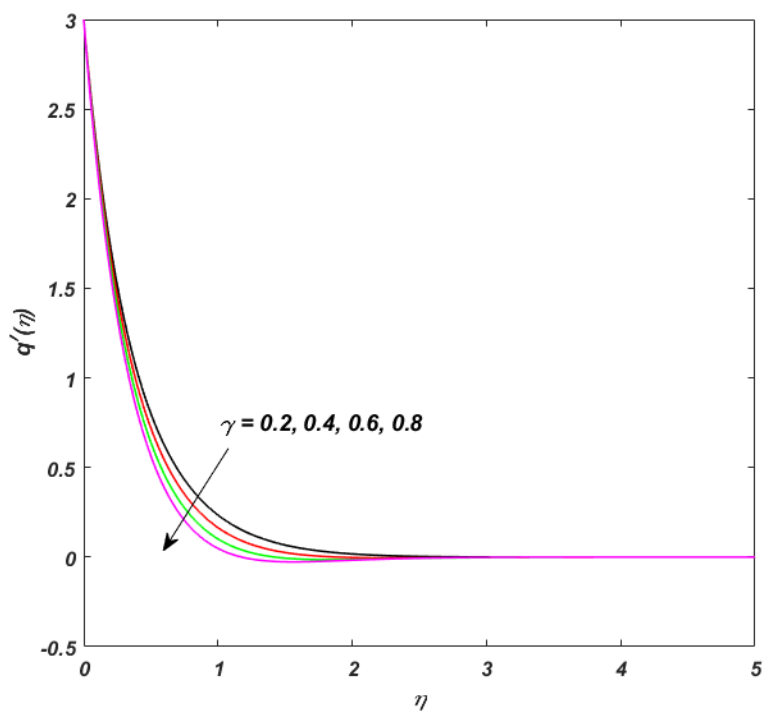


Figure 4.8. Velocity distribution $q'(\eta)$ for γ with CuO–hybrid base fluid.

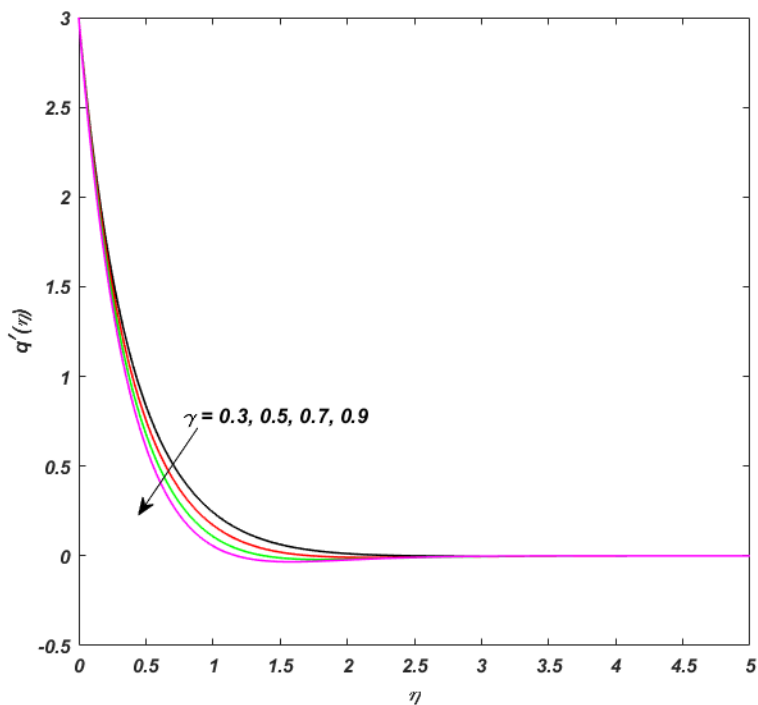


Figure 4.9. Velocity distribution $q'(\eta)$ for γ with TiO_2 –hybrid base fluid.

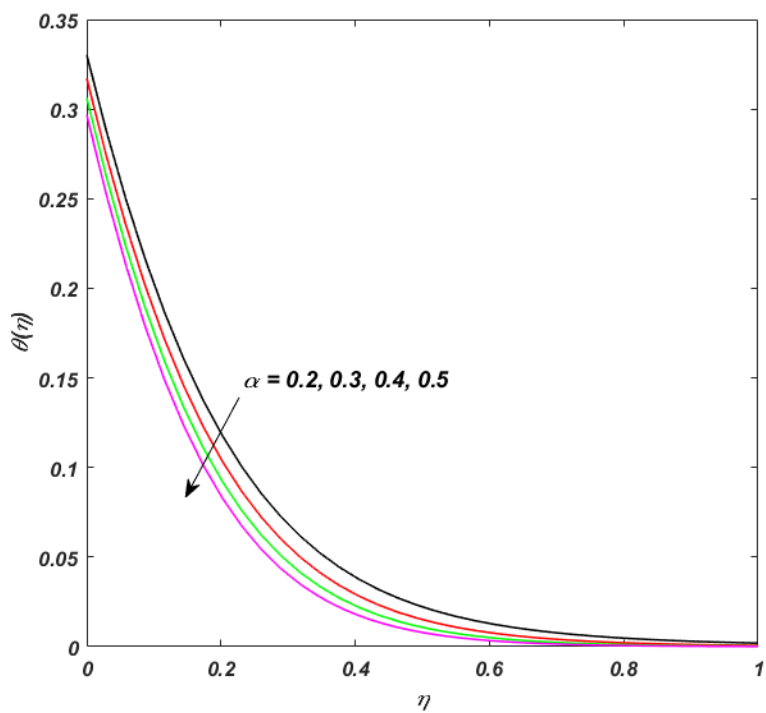


Figure 4.10. Temperature distribution $\theta(\eta)$ for α with CuO -hybrid base fluid.

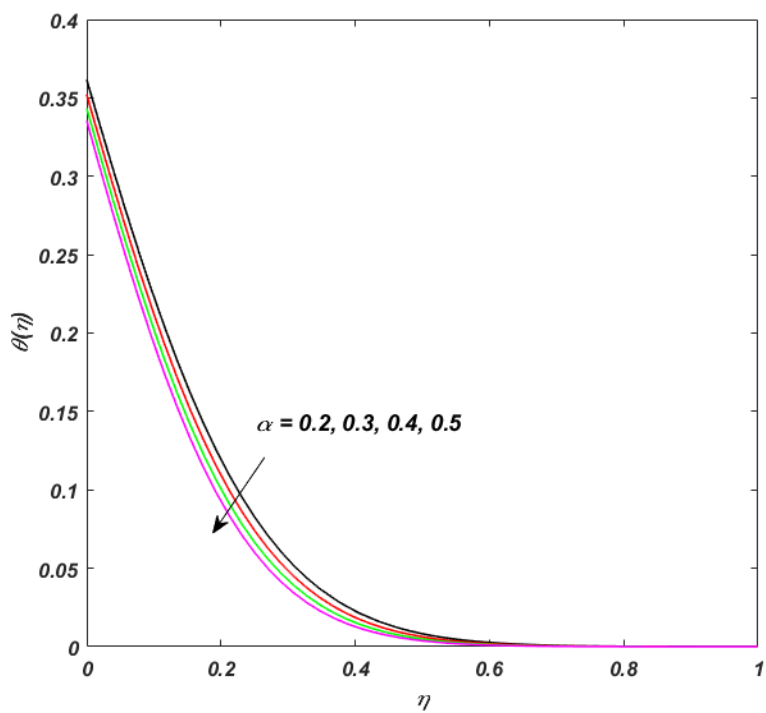


Figure 4.11. Temperature distribution $\theta(\eta)$ for α with TiO_2 -hybrid base fluid.

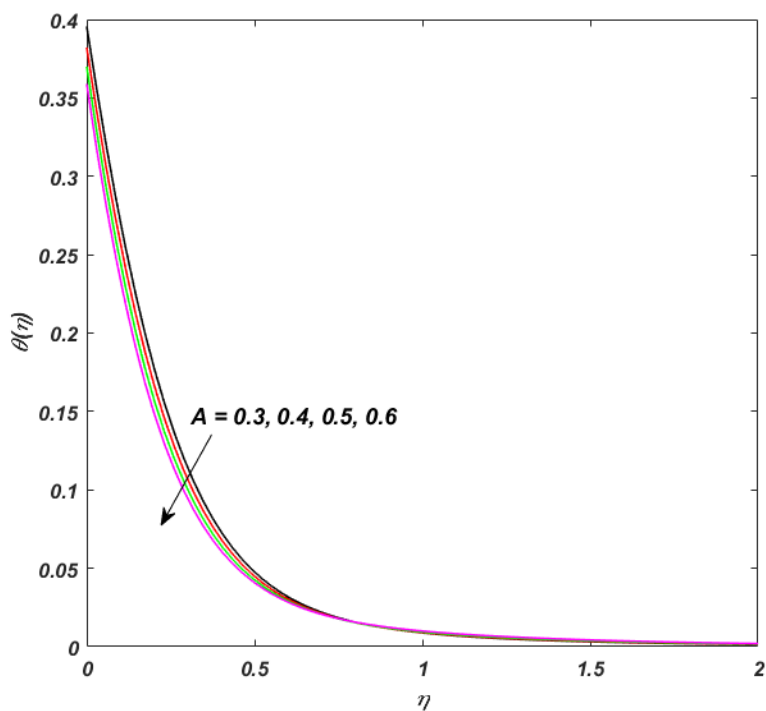


Figure 4.12. Temperature distribution $\theta(\eta)$ for A with CuO–hybrid base fluid.

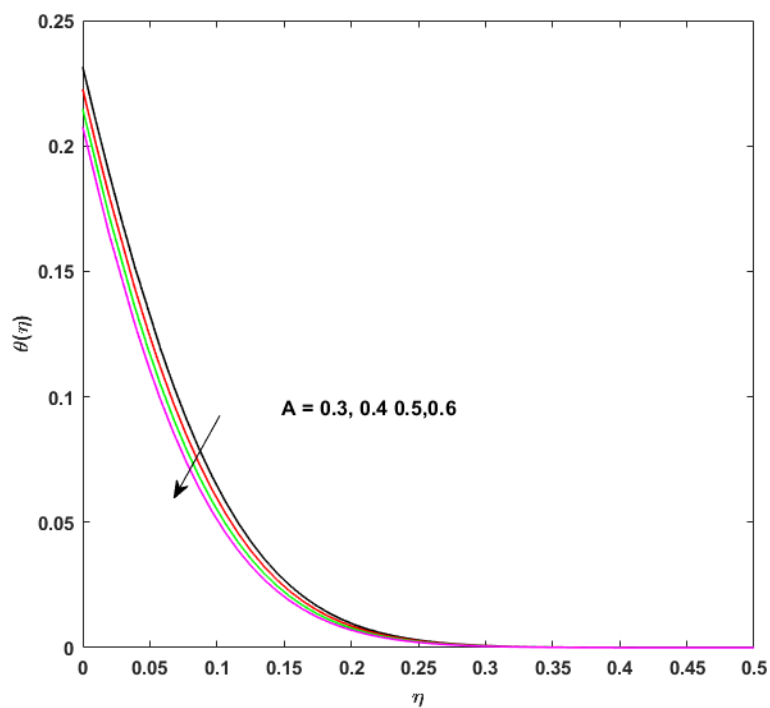


Figure 4.13. Temperature distribution $\theta(\eta)$ for A with TiO_2 –hybrid base fluid.

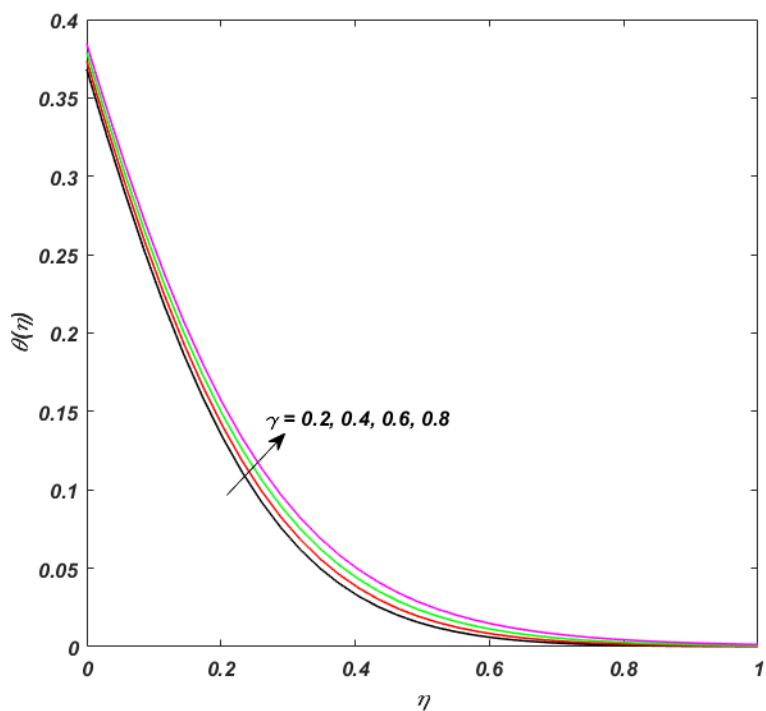


Figure 4.14. Temperature distribution $\theta(\eta)$ for γ with CuO–hybrid base fluid.

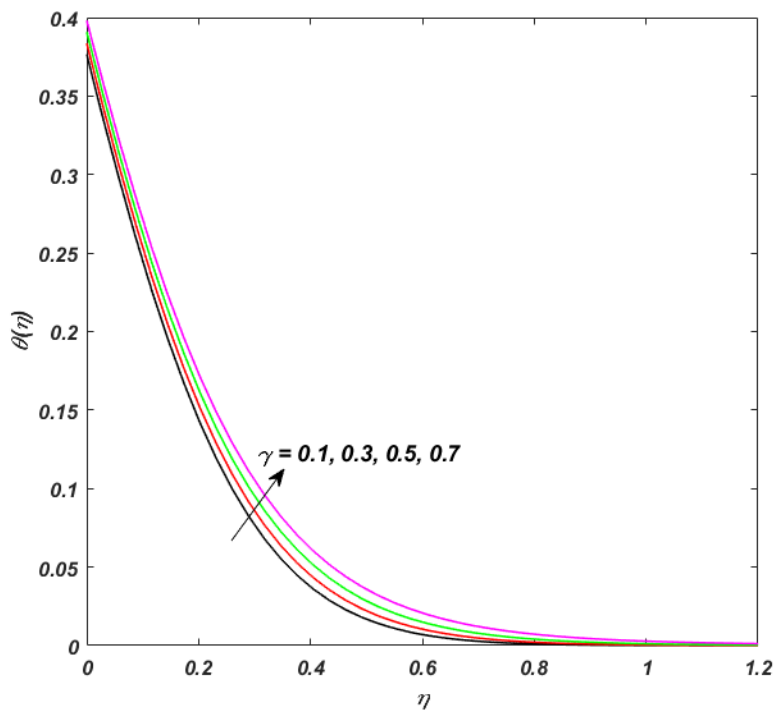


Figure 4.15. Temperature distribution $\theta(\eta)$ for γ with TiO_2 –hybrid base fluid.

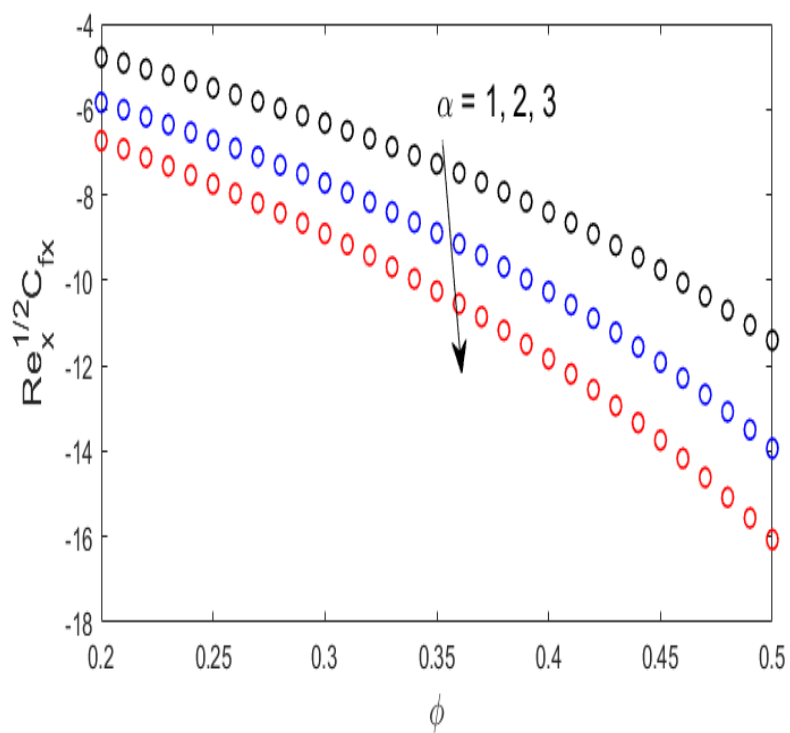


Figure 4.16. Skin friction coefficient along x -axis for α and ϕ with CuO -hybrid base fluid.

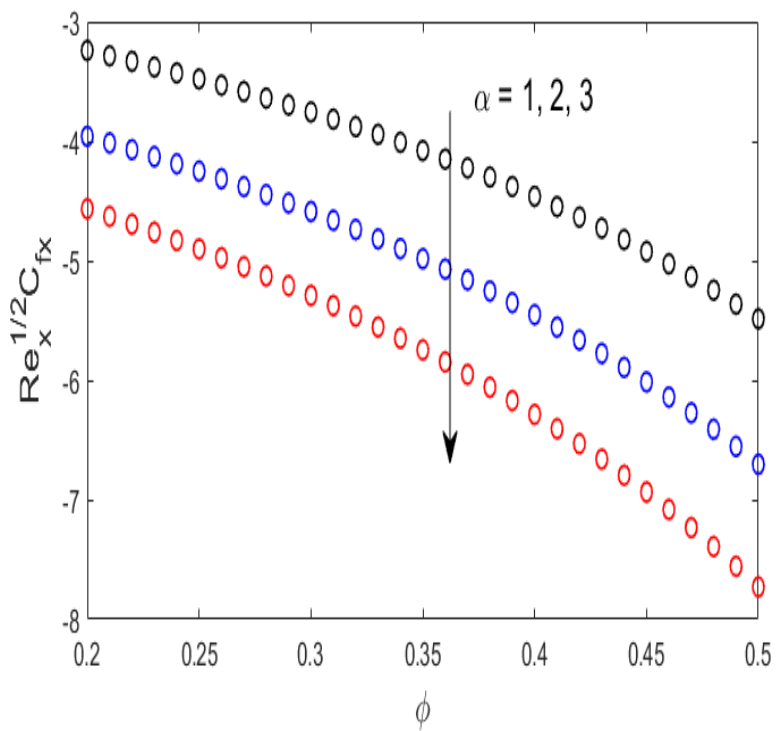


Figure 4.17. Skin friction coefficient along x -axis for α and ϕ with TiO_2 -hybrid base fluid.

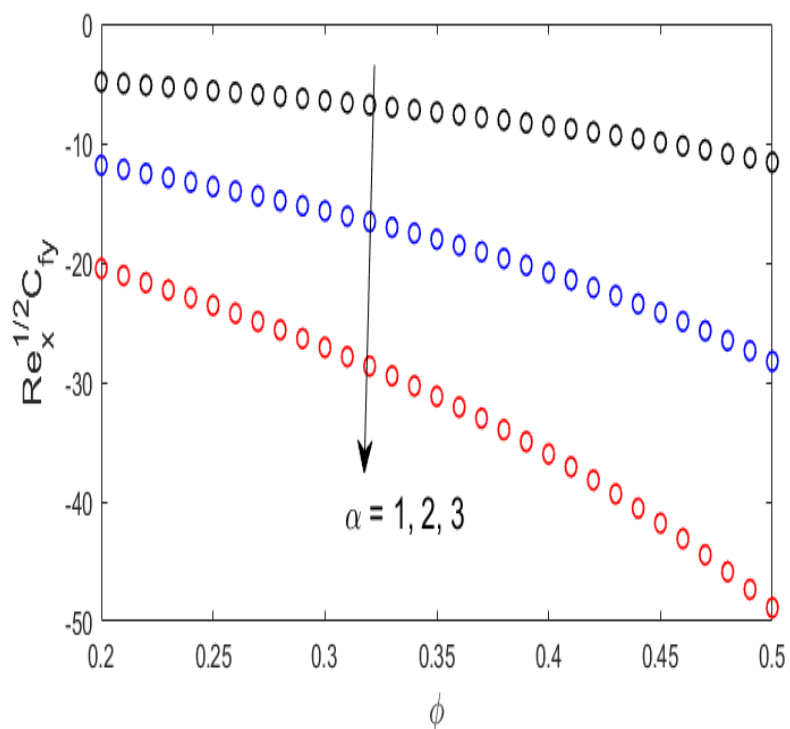


Figure 4.18. Skin friction coefficient along y-axis for α and ϕ with CuO -hybrid base fluid.

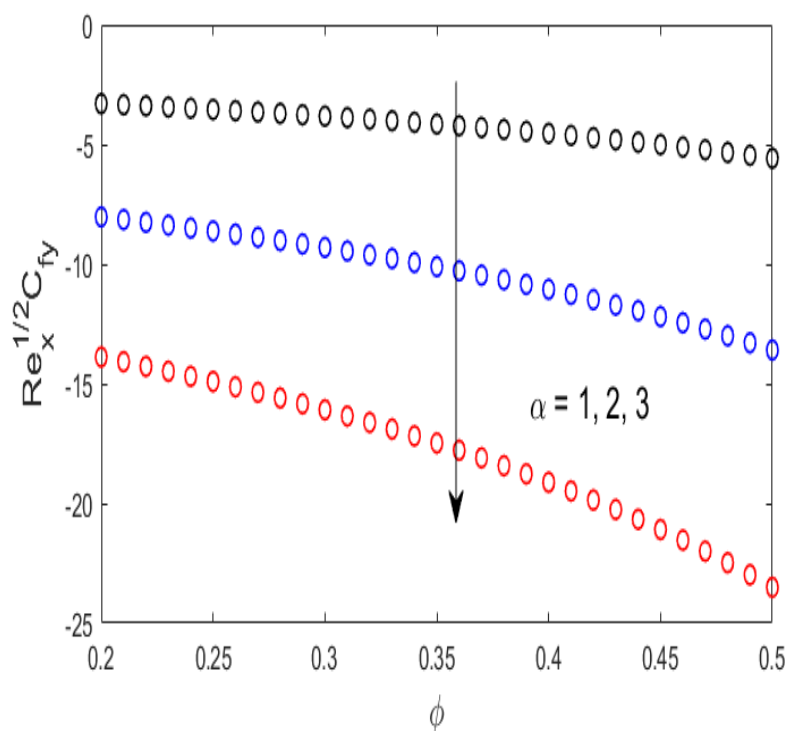


Figure 4.19. Skin friction coefficient along y-axis for α and ϕ with TiO_2 -hybrid base fluid.

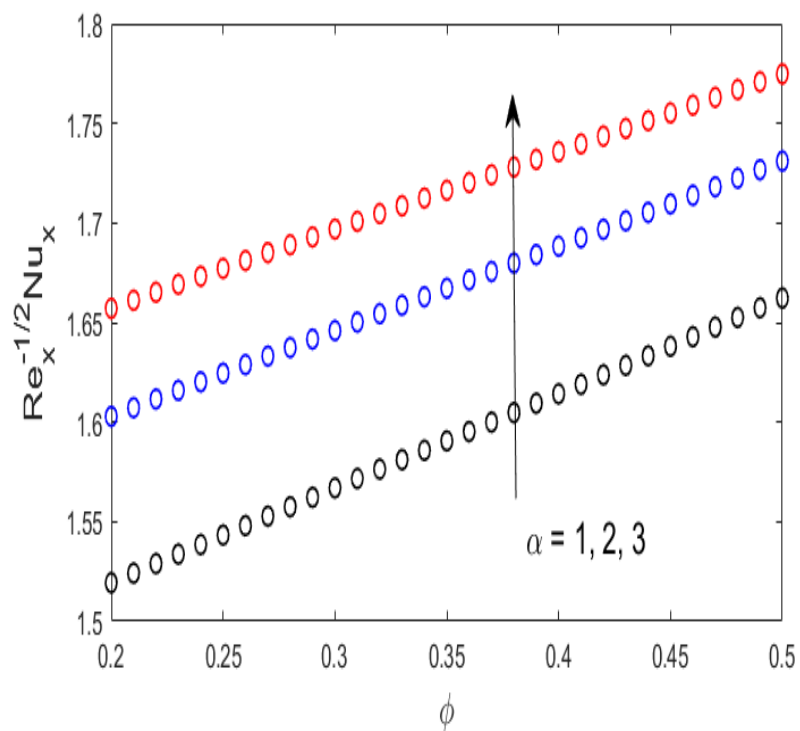


Figure 4.20. Nusselt number for α and ϕ with CuO –hybrid base fluid.

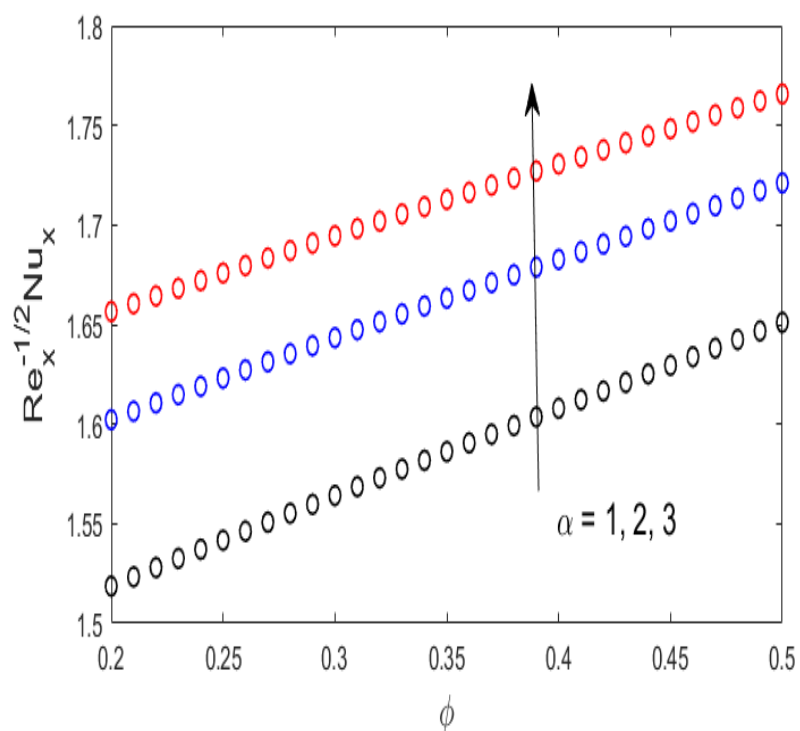


Figure 4.21. Nusselt number $\theta'(0)$ for α and ϕ with TiO_2 –hybrid base fluid.

Chapter 5

The Unsteady Hybrid Nanofluids Flow over an Exponentially Stretching Surface in the Presence of Velocity Slip

5.1 Introduction

This analysis is performed for the unsteady, rotating and three dimensional flow of hybrid nanofluids over an exponentially stretching surface. The fluid flow is also influenced by important effects of mixed convection and velocity slip. A system of complex partial differential equations is needed to model the considered fluid problem. As the system is highly complex, so similarity transformation are used to convert the system into a less complex system of differential equations. The system is solved with a numerical methodology via `bvp4c` function in MALTAB software and the graphical results for velocity, temperature, as well as Skin friction and Nusselt number are achieved. A comparative study is also done which shows that the currents results are in accord with the already published results.

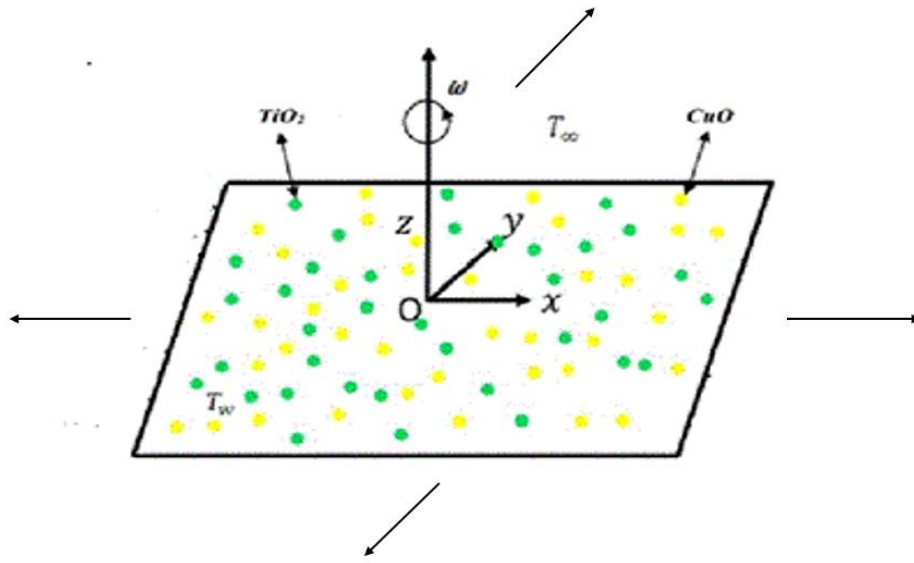


Figure 5.1. Geometry of the problem.

5.2 Formulation of the problem

The present study is based on three-dimensional, incompressible and unsteady flow of a hybrid nanofluid in the considered region $z \geq 0$. The fluid is flowing over an exponentially stretching surface with stretching velocities along x and y axes. The surface is also rotating around the z -axis with an angular velocity ω . T_∞ is the ambient temperature while T_w is denoted for temperature of the sheet. The phenomenon of mixed convection and slip velocity is considered in the current model. The considered nanoparticles are CuO and TiO_2 and the base fluid is the mixture of ethylene glycol and water. The flow model is based on continuity equation, momentum equation and energy equation as

$$\frac{\partial \rho}{\partial t} + \nabla \cdot (\rho \mathbf{V}) = 0, \quad (5.1)$$

$$\rho \frac{\partial \mathbf{V}}{\partial t} + (\mathbf{V} \cdot \nabla) \mathbf{V} = \nabla \cdot \boldsymbol{\tau} + \rho \mathbf{b}, \quad (5.2)$$

$$\frac{\partial T}{\partial t} + (\mathbf{V} \cdot \nabla) T = \alpha_f \nabla^2 T, \quad (5.3)$$

where ρ denotes the density, \mathbf{V} stands for velocity field, $\boldsymbol{\tau}$ is represent stress tensor, \mathbf{b} is for body force, T denotes the temperature and α_f is the thermal diffusivity.

After imposing boundary layer theory on the system, the flow model is shown as a system of partial differential equations. Thus the necessary equations become.

The Continuity equation

$$\frac{\partial u}{\partial x} + \frac{\partial v}{\partial y} + \frac{\partial w}{\partial z} = 0. \quad (5.4)$$

The Momentum equation

$$\frac{\partial u}{\partial t} + u \frac{\partial u}{\partial x} + v \frac{\partial u}{\partial y} + w \frac{\partial u}{\partial z} - 2\omega v = \frac{\mu_{hnf}}{\rho_{hnf}} \frac{\partial^2 u}{\partial z^2} + g \frac{(\rho\beta)_{hnf}}{\rho_{hnf}} (T - T_\infty), \quad (5.5)$$

$$\frac{\partial v}{\partial t} + u \frac{\partial v}{\partial x} + v \frac{\partial v}{\partial y} + w \frac{\partial v}{\partial z} + 2\omega v = \frac{\mu_{hnf}}{\rho_{hnf}} \frac{\partial^2 v}{\partial z^2}. \quad (5.6)$$

The Energy equation

$$\frac{\partial T}{\partial t} + u \frac{\partial T}{\partial x} + v \frac{\partial T}{\partial y} + w \frac{\partial T}{\partial z} = \frac{K_{hnf}}{(\rho C_p)_{hnf}} \frac{\partial^2 T}{\partial z^2}. \quad (5.7)$$

The boundary conditions are

$$\left. \begin{aligned} u &= u_w + h_1 \frac{\partial u}{\partial z}, \quad v = v_w + h_2 \frac{\partial v}{\partial z}, \quad w = 0, \quad T = T_w \quad \text{at } z = 0 \\ u &\rightarrow 0, \quad v \rightarrow 0, \quad T \rightarrow T_\infty \quad \text{as } z \rightarrow \infty \end{aligned} \right\}. \quad (5.8)$$

The expressions of velocities at the surface and wall temperature are

$$u_w = \frac{u_0}{1-bt} e^{\frac{x+y}{L}}, \quad v_w = \frac{v_0}{1-bt} e^{\frac{x+y}{L}}, \quad T_w = T_\infty + \frac{T_0}{1-bt} e^{\frac{A(x+y)}{2L}}. \quad (5.9)$$

The similarity transformation required for the system are

$$\left. \begin{aligned} u &= \frac{u_0}{1-bt} e^{\frac{x+y}{L}} p'(\eta), \quad v = \frac{u_0}{1-bt} e^{\frac{x+y}{L}} q'(\eta), \quad \eta = \left(\frac{u_0}{2\nu L(1-bt)} \right)^{\frac{1}{2}} e^{\frac{x+y}{2L}} z \\ w &= - \left(\frac{\nu u_0}{2L(1-bt)} \right)^{\frac{1}{2}} e^{\frac{x+y}{2L}} \{p + \eta p' + q + \eta q'\}, \quad \theta(\eta) = \frac{T-T_\infty}{T_w-T_\infty} \end{aligned} \right\} \quad (5.10)$$

The equation of continuity is identically satisfied through these transformations while momentum and energy equations take on the following forms

$$\begin{aligned} \frac{\mu_{hnf}}{\rho_f} p'''' - A_0(\eta p'' + 2p') + p''(p + q) - 2p'(p' + q') + 4\gamma q' + \\ 2 \left(\frac{(\rho\beta)_{hnf}}{\rho_f} \right) \lambda \theta = 0, \end{aligned} \quad (5.11)$$

$$\frac{\mu_{hnf}}{\rho_f} q'''' - A_0(\eta q'' + 2q') + q''(p + q) - 2q'(p' + q') - 4\gamma p' = 0, \quad (5.12)$$

$$\frac{1}{Pr} \left(\frac{K_{hnf}}{K_f} \right) \theta'' - A_0(\eta \theta' + 2\theta) - A(p' + q')\theta + (p + q)\theta' = 0, \quad (5.13)$$

In this case, the boundary conditions are modified as

$$\left. \begin{aligned} p(0) = 0, \quad p'(0) = 1 + Gp''(0), \quad q(0) = 0, \quad q'(0) = \alpha + Gq''(0), \\ \theta(0) = 1 \quad \text{at } \eta = 0, \\ p' \rightarrow 0, \quad q' \rightarrow 0, \quad \theta \rightarrow 0 \quad \text{as } \eta \rightarrow \infty \end{aligned} \right\} \quad (5.14)$$

Here $Pr = \frac{(\mu C_p)_f}{K_f}$ is the Prandtl number, $A_0 = \frac{\beta L}{u_0} e^{-\left(\frac{x+y}{L}\right)}$ the unsteadiness parameter, $\lambda = \frac{Gr}{Re_x^2}$

the mixed convection parameter, $Gr = \frac{gB(T_w-T_\infty)}{\nu^2} L^3$ the local Grashof number, $Re = \frac{Lu_w}{\nu}$ the

local Reynolds number, $\gamma = \frac{wL}{u_w}$ the rotating parameter. $\alpha = \frac{v_0}{u_0}$ the stretching ratio parameter,

$G = h_1 \left(\frac{u_0}{2\nu L(1-bt)} \right)^{\frac{1}{2}} e^{\frac{x+y}{2L}}$ the slip velocity parameter.

The Skin friction coefficient and the Nusselt number have been mentioned as

$$C_{fx} = \frac{\tau_{wx}}{\frac{1}{2}\rho_f(u_w)^2}, \quad (5.15)$$

$$C_{fy} = \frac{\tau_{wy}}{\frac{1}{2}\rho_f(u_w)^2}, \quad (5.16)$$

$$Nu_x = \frac{xq_w}{k_f(T_w - T_\infty)}. \quad (5.17)$$

The wall shear stresses and the heat flux are

$$\tau_{wx} = \mu_{hnf} \left(\frac{\partial u}{\partial z} \right)_{z=0}, \quad (5.18)$$

$$\tau_{wy} = \mu_{hnf} \left(\frac{\partial v}{\partial z} \right)_{z=0}, \quad (5.19)$$

$$q_w = -k_{hnf} \left(\frac{\partial T}{\partial z} \right)_{z=0}. \quad (5.20)$$

Applying equation (5.10), (5.18 - 5.20) in (5.15-5.17) now, the following equations are acquired

$$\frac{1}{\sqrt{2}} C_{fx} (Re_x)^{\frac{1}{2}} = \frac{\mu_{hnf}}{\mu_f} p''(\eta), \quad (5.21)$$

$$\frac{1}{\sqrt{2}} C_{fy} (Re_x)^{\frac{1}{2}} = \frac{\mu_{hnf}}{\mu_f} q''(\eta), \quad (5.22)$$

$$\sqrt{2} \frac{L}{x} Nu_x (Re_x)^{-\frac{1}{2}} = -\frac{k_{hnf}}{k_f} \theta'(\eta). \quad (5.23)$$

5.3 Numerical Algorithm

The considered system of equations is solve using the bvp4c methodology. The following are the first order differential equations required for the method.

$$\left. \begin{aligned} y_1 &= p \\ y_2 &= p' \\ y_3 &= p'' \\ y_4 &= q \\ y_5 &= q' \\ y_6 &= q'' \\ y_7 &= \theta \\ y_8 &= \theta' \end{aligned} \right\}, \quad (5.24)$$

$$p''' = \frac{\frac{\rho_{hnf}}{\rho_f}}{\frac{\mu_{hnf}}{\mu_f}} \left[\begin{array}{c} 2y_2 (y_2 + y_5) - y_3 (y_1 + y_4) - 4\gamma y_5 + A_0(\eta y_3 + 2y_2) \\ -2 \frac{\frac{(\rho\beta)_{hnf}}{(\rho\beta)_f}}{\frac{\rho_{hnf}}{\rho_f}} \lambda y_7 \end{array} \right], \quad (5.25)$$

$$q''' = \frac{\frac{\rho_{hnf}}{\rho_f}}{\frac{\mu_{hnf}}{\mu_f}} [2y_5 (y_2 + y_5) - y_6 (y_1 + y_4) + 4\gamma y_2 + A_0(\eta y_6 + 2y_5)], \quad (5.26)$$

$$\theta'' = \text{Pr} \frac{\frac{(\rho c_p)_{hnf}}{(\rho c_p)_f}}{\frac{K_{hnf}}{K_f}} [A_0(\eta y_8 + 2y_7) + A(y_2 + y_5)y_7 - (y_1 + y_4)y_8], \quad (5.27)$$

$$\left. \begin{aligned} y_1(a) &= 0, \quad y_2(a) = 1 + Gy_3(a), \quad y_4(a) = 0, \\ y_5(a) &= \alpha + Gy_6(a), \quad y_7(a) + 1 \text{ at } \eta = 0, \\ y_2(b) &\rightarrow 0, \quad y_5(b) \rightarrow 0, \quad y_7(b) \rightarrow 0 \text{ as } \eta \rightarrow \infty \end{aligned} \right\}. \quad (5.28)$$

Table 5.1: Properties of considered hybrid base fluid with nanoparticles in terms of thermo-physical aspects. (Ghadikolaie *et al.* [74])

Properties	Nano fluids
Density	$\rho_{nf} = \rho_f(1 - \phi_1) + \phi_1\rho_{s1}$
Specific Heat	$(\rho c_p)_{nf} = (\rho c_p)_f(1 - \phi_1) + \phi_1(\rho c_p)_{s1}$
Thermal expansion	$(\rho\beta)_{nf} = (\rho\beta)_f(1 - \phi_1) + \phi_1(\rho\beta)_{s1}$
Dynamic Viscosity	$\mu_{nf} = \frac{\mu_f}{(1 - \phi_1)^{2.5}}$
Kinematic Viscosity	$v_{nf} = \frac{\mu_{nf}}{\rho_{nf}}$
Thermal Conductivity	$\frac{k_{nf}}{k_f} = \frac{k_{s1} + 2k_f - 2\phi_1(k_f - k_{s1})}{k_{s1} + 2k_f + \phi_1(k_f - k_{s1})}$

Table 5.2: Thermo-physical properties for considered hybrid base fluid with nanoparticles. (Ghadikolaie *et al.* [74])

Properties	Hybrid Nano fluids
Density	$\rho_{hnf} = \rho_{nf}(1 - \phi_2) + \phi_2\rho_{s2}$
Specific Heat	$(\rho c_p)_{hnf} = (\rho c_p)_{nf}(1 - \phi_2) + \phi_2(\rho c_p)_{s2}$
Thermal expansion	$(\rho\beta)_{hnf} = (\rho\beta)_{nf}(1 - \phi_2) + \phi_2(\rho\beta)_{s2}$
Dynamic Viscosity	$\mu_{hnf} = \frac{\mu_{nf}}{(1 - \phi_1)^{2.5}(1 - \phi_2)^{2.5}}$
Kinematic Viscosity	$v_{hnf} = \frac{\mu_{hnf}}{\rho_{hnf}}$
Thermal Conductivity	$\frac{k_{hnf}}{k_f} = \frac{k_{s2} + 2k_{nf} - 2\phi_2(k_{nf} - k_{s2})}{k_{s2} + 2k_{nf} + \phi_2(k_{nf} - k_{s2})}$

Table 5.3: Thermo-physical properties of hybrid base fluid and nanoparticles. (Rasool *et al.* [75], Ghadikolaei *et al.* [76], Usman *et al.* [77])

Physical properties	ρ	$c_p \left(\frac{J}{kg \cdot K} \right)$	$k \left(\frac{W}{m \cdot K} \right)$	β	Pr
$C_2H_6O_2-H_2O$	1063.8	3630	0.387	$5.8 \times (10)^{-4}$	25.33
CuO	6500	540	18	$8.5 \times (10)^{-6}$	
TiO_2	4250	686.22	8.9538	$9 \times (10)^{-6}$	

Table 5.4: Comparison with the literature for heat transfer rate with $\alpha = \phi_1 = \phi_2 = \gamma = \lambda = G = A_0 = 0$.

$\theta'(0)$					
Pr	A	Magyari and Keller [81]	Liu <i>et al.</i> [82]	Nadeem <i>et al.</i> [83]	Present results
1	-1.5	0.37741	0.37741256	0.377412	0.377407
	0	-0.549643	-0.54964375	-0.549646	-0.549645
	1	-0.954782	-0.95478270	-0.954786	-0.954783
	3	-1.560294	-1.56029540	-1.560295	-1.560296
5	-1.5	1.353240	1.35324050	1.3532405	1.3532405
	0	-1.521243	-1.52123900	-1.521240	-1.521239
	1	-2.500135	-2.500135157	-2.500135	-2.500131
	3	-3.886555	-3.88655510	-3.886555	-3.886555
10	-1.5	2.200000	2.20002816	2.2000282	2.2000281
	0	-2.257429	-2.25742372	-2.257424	-2.257424
	1	-3.660379	-3.66037218	-3.660372	-3.660371
	3	-5.635369	-5.62819631	-5.628196	-5.628196

5.4 Discussion for the Graphical Results

The mixed convection flow of hybrid nanofluid flowing over an exponentially stretched surface in the presence of mixed convection and velocity slip has been explored. Table. 5.1, 5.2, 5.3 are displayed to mention the thermophysical properties needed for the problem and Table. 5.4 is a comparative table and represents the comparison between the already existing analyses done on the fluid and the current analysis and the results are in good agreement.

The graphical depictions of the results obtained after solving the considered fluid model are presented in the form of two velocity profiles $p'(\eta)$ and $q'(\eta)$, temperature distribution $\theta(\eta)$, skin friction, and Nusselt number. These are obtained in relation to a number of variables, including the stretching ratio parameter α , rotating parameter γ , temperature exponent parameter A , unsteady parameter A_0 , mixed convection parameter λ and slip velocity parameter G . The graphical depictions of the results obtained after solving the considered fluid model are presented in the form of two velocity profiles $p'(\eta)$ and $q'(\eta)$, temperature distribution $\theta(\eta)$, skin friction and Nusselt number. These are obtained in relation to a number of variables, including the stretching ratio parameter α , rotating parameter γ , temperature exponent parameter A , unsteady parameter A_0 , mixed convection parameter λ , slip velocity parameter G , CuO nanoparticle volume fraction ϕ_1 and TiO_2 nanoparticle volume fraction ϕ_2 .

The effects of the stretching ratio parameter α , temperature exponent parameter A , velocity slip parameter G , mixed convection parameter λ , unsteadiness parameter A_0 , nanoparticle volume fractions ϕ_1 and ϕ_2 on the velocity profile $p'(\eta)$ are shown in Figures 5.2 - 5.8. As the stretching ratio α increases, velocity $p'(\eta)$ decreases, with the specified values $\phi_1 = 0.1$, $\phi_2 = 0.1$, $G = 0.1$, $A_0 = 0.1$, $\gamma = 0.1$ and $\lambda = 1$. The velocity profile $p'(\eta)$ drops down as a result of growing temperature exponent A for the values mentioned to be $\alpha = 0.1$, $\gamma = 0.1$, $A_0 = 0.1$, $\lambda = 1$, $\phi_1 = 0.1$, $\phi_2 = 0.1$ and $G = 0.1$, as presented in Figure 5.3. Figure 5.4 is plotted to see how the velocity slip parameter G affects the velocity distribution $p'(\eta)$. This figure shows that the velocity distribution $p'(\eta)$ significantly decrease with increasing velocity slip parameter G concurrently with the adjustment of certain parameters like $\alpha = 1$, $\gamma = 0.1$, $A_0 = 0.1$, $\lambda = 1$, $A = 0.1$, $\phi_1 = 0.1$ and $\phi_2 = 0.1$. This is due to the fact that the fluid's near surface velocity and the stretched surface velocity cease to exist within the slip's field of view. As a result, the liquid velocity decreases since the stretched surface deformation can only be transferred to the fluid when there is slip. From figure 5.5, it is observed that the velocity $p'(\eta)$

increases by the elevated mixed convection parameter λ for $\alpha = 1$, $\gamma = 0.1$, $A_0 = 0.1$, $A = 0.1$, $\phi_1 = 0.1$, $\phi_2 = 0.1$, and $G = 0.1$. The relationship between buoyancy and inertial forces is known as mixed convection. The buoyancy forces outweigh the inertial forces as λ grows, increasing the velocity profile. Figure 5.6 illustrates the impact of unsteadiness parameter A_0 on the velocity profile $p'(\eta)$. The observations reveal that the fluid velocity for $\alpha = 1$, $\gamma = 0.1$, $\lambda = 1$, $\phi_1 = 0.1$, $\phi_2 = 0.1$ and $G = 0.1$ shows an increasing tendency when the values of A_0 rise. Figure 5.7 exemplifies the impact of ϕ_1 for the fluid velocity $p'(\eta)$ with $\alpha = 1$, $\gamma = 0.1$, $A = 0.1$, $A_0 = 0.1$, $\lambda = 1$, $\phi_2 = 0.1$ and $G = 0.1$ and depicts an aggregate tendency when the values of ϕ_1 grow. Figure 5.8 explains the impact of ϕ_2 on the fluid velocity with $\alpha = 1$, $\gamma = 0.1$, $A = 0.1$, $A_0 = 0.1$, $\lambda = 1$, $\phi_1 = 0.1$ and $G = 0.1$ and points towards a rise in profile when the values of ϕ_2 upsurge.

The Figures 5.9 - 5.15 demonstrate the impact of stretching ratio parameter α , temperature exponent parameter A , velocity slip parameter G , mixed convection parameter λ , unsteadiness parameter A_0 , nanoparticle volume fractions ϕ_1 and ϕ_2 on the velocity component $q'(\eta)$. It can be shown from Figure 5.9 that when stretching ratio parameter α rises, the velocity $q'(\eta)$ also rises. The values of the parameters are $G = 0.1$, $\lambda = 1$, $A_0 = 0.1$, $\gamma = 0.1$, $\lambda = 1$, $\phi_1 = 0.1$, $\phi_2 = 0.1$ and $A = 0.1$. The velocity profile findings for A are shown in Figure 5.10. As A increases, the velocity distribution shows an increasing trend. for $\alpha = 1$, $\gamma = 0.1$, $A_0 = 0.1$, $\lambda = 1$, $\phi_1 = 0.1$, $\phi_2 = 0.1$ and $G = 0.1$. By enhancing the value of velocity slip parameter G , the velocity $q'(\eta)$ decreases as seen in Figure 5.11. Furthermore, the particular values of the are $\alpha = 1$, $\gamma = 0.1$, $A_0 = 0.1$, $\lambda = 1$, $\phi_1 = 0.1$, $\phi_2 = 0.1$ and $A = 0.1$. Figure 5.12 shows the effect of the mixed convection parameter λ on $q'(\eta)$. It has been noted that when λ increases, $q'(\eta)$ decreases for the values $\alpha = 1$, $\gamma = 0.1$, $A_0 = 0.1$, $G = 0.1$, $\phi_1 = 0.1$, $\phi_2 = 0.1$ and $A = 0.1$. Figure 5.13 shows how the velocity component $q'(\eta)$ is affected by the unsteadiness parameter A_0 . It is shown that with increasing values of A_0 , $q'(\eta)$ increases for $\alpha = 1$, $\gamma = 0.1$, $G = 0.1$, $\lambda = 1$, $\phi_1 = 0.1$, and $\phi_2 = 0.1$. Figure 5.14 manifests the velocity component $q'(\eta)$ for increasing ϕ_1 . It is revealed that with emergent values of ϕ_1 , $q'(\eta)$ upsurges with the values $\alpha = 1$, $\gamma = 0.1$, $A_0 = 0.1$, $G = 0.1$, $\phi_2 = 0.1$, $G = 0.1$ and $A = 0.1$. Figure 5.15 depicts the velocity component $q'(\eta)$ for ϕ_2 . It is displayed that with growing values of ϕ_2 , $q'(\eta)$ rises for $\alpha = 1$, $\gamma = 0.1$, $\lambda = 1$, $A_0 = 0.1$, $G = 0.1$, $G = 0.1$, $\phi_1 = 0.1$ and $A = 0.1$.

The temperature profiles $\theta(\eta)$ for various significant parameters are presented through Figures 5.16 - 5.22. Figure 5.16 indicates that the temperature profile decreases when the values

of α are augmented. In addition the values of the parameters are chosen to be $G = 0.1$, $\lambda = 1$, $A_0 = 0.1$, $A = 0.1$, $\gamma = 0.1$, $\phi_1 = 0.1$ and $\phi_2 = 0.1$. Figure 5.17 shows how the temperature exponent parameter A affects the temperature profile. Increase in A decelerates the temperature profile $\theta(\eta)$ for $G = 0.1$, $\alpha = 1$, $\lambda = 1$, $A_0 = 0.1$, $\gamma = 0.1$, $\phi_1 = 0.1$ and $\phi_2 = 0.1$. Figure 5.18 is sketched to show the impact of rotating parameter γ and it is seen that the temperature profile enhances with increased γ for $G = 0.1$, $\alpha = 1$, $\lambda = 1$, $A_0 = 0.1$, $A = 0.1$, $\phi_1 = 0.1$, and $\phi_2 = 0.1$. From Figure 5.19, it is evident that the temperature distribution $\theta(\eta)$ for the hybrid nanofluid decreases as the mixed convection parameter λ is raised for $G = 0.1$, $\alpha = 1$, $\gamma = 0.1$, $A_0 = 0.1$, $A = 0.1$, $\phi_1 = 0.1$ and $\phi_2 = 0.1$. The effect of the unsteadiness parameter A_0 on temperature distribution $\theta(\eta)$ is presented in Figure 5.20. It indicates that temperature distribution $\theta(\eta)$ increases with increase in unsteady parameter A_0 . Likewise, the particular parameters of the hybrid base fluids are adjusted to be $G = 0.1$, $\alpha = 1$, $\gamma = 0.1$, $\lambda = 0.1$, $A = 0.1$, $\phi_1 = 0.1$ and $\phi_2 = 0.1$. The impact of the ϕ_1 on temperature distribution $\theta(\eta)$ is presented in Figure 5.21. It indicates that temperature distribution $\theta(\eta)$ increases with increasing in ϕ_1 for $G = 0.1$, $\alpha = 1$, $\gamma = 0.1$, $\lambda = 0.1$, $A = 0.1$, $A_0 = 0.1$ and $\phi_2 = 0.1$. The outcome of the raised ϕ_2 for temperature distribution $\theta(\eta)$ is displayed in Figure 5.22. It shows that temperature distribution $\theta(\eta)$ rises with increase in ϕ_2 with the values specified as $G = 0.1$, $\alpha = 1$, $\gamma = 0.1$, $\lambda = 0.1$, $A = 0.1$, $A_0 = 0.1$ and $\phi_1 = 0.1$.

The behavior of the drag force components $p''(0)$ and $q''(0)$ are explored for λ and ϕ_2 , while the results are based on experimental values set as $\phi_1 = 0.1$, $\alpha = 1$, $A = 0.1$, $\gamma = 0.1$, $\text{Pr} = 25.33$, and $A_0 = 0.1$. It is worth noting that as G values expand, the drag force along x -axis enhances while it is opposite for ϕ_2 as seen in Figure 5.23. Figure 5.24 is presented to demonstrate the effect of A_0 and ϕ_2 for $\phi_1 = 0.1$, $\alpha = 1$, $A = 0.1$, $\gamma = 0.1$, $\text{Pr} = 25.33$, $A_0 = 0.1$, $G = 0.1$. The skin friction coefficient increase for increasing A_0 but this is not the case for ϕ_2 . Figure 5.25 explores that for both G and ϕ_2 increasing values, the drag force $q''(0)$ points towards opposite trend. The same behavior is depicted for rising A_0 and ϕ_2 on the drag force $q''(0)$ as seen in Figure 5.26 for $\phi_1 = 0.1$, $\alpha = 1$, $A = 0.1$, $\gamma = 0.1$, $\text{Pr} = 25.33$, $A_0 = 0.1$, $G = 0.1$. The impacts of ϕ_2 and λ on the Nusselt number value $\theta'(0)$ can be observed in Figure 5.27. The parameters are configured as $\phi_1 = 0.1$, $\alpha = 0.1$, $A = 0.1$, $\gamma = 0.1$, $\lambda = 1$, $A_0 = 0.1$ and $G = 0.1$. It is noted that when ϕ_2 and λ grow, the Nusselt value $\theta'(0)$ increases. Figure 5.28 shows the effects of A and ϕ_2 on the Nusselt number $\theta'(0)$. The arrangement of the parameters is as $A = 0.1$, $\gamma = 0.1$, $A_0 = 0.1$, $G = 0.1$, $\phi_1 = 0.1$ and $\lambda = 1$. It is seen that the Nusselt value $\theta'(0)$ grows as ϕ_2 and A climbs up.

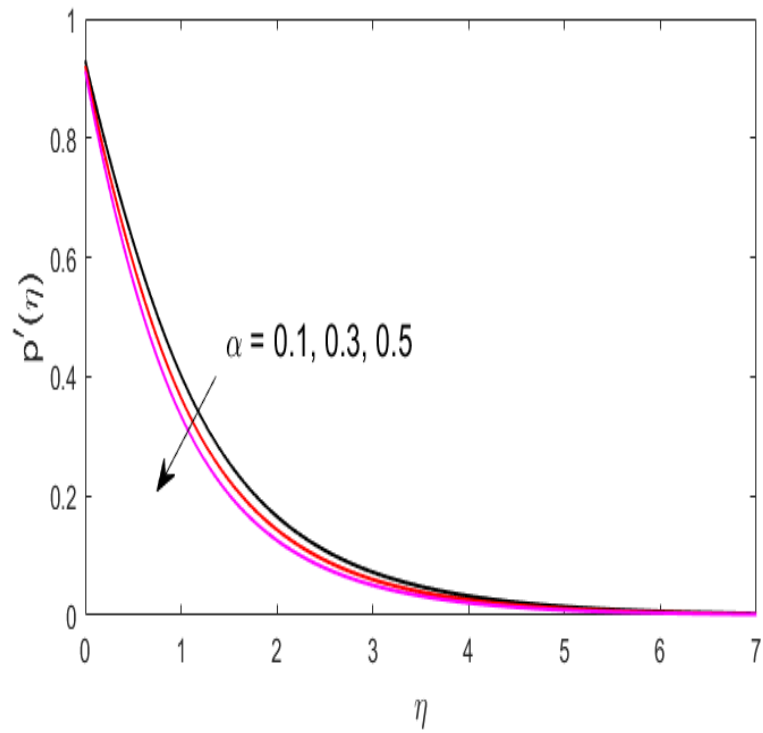


Figure 5.2. Velocity distribution $p'(\eta)$ for α .

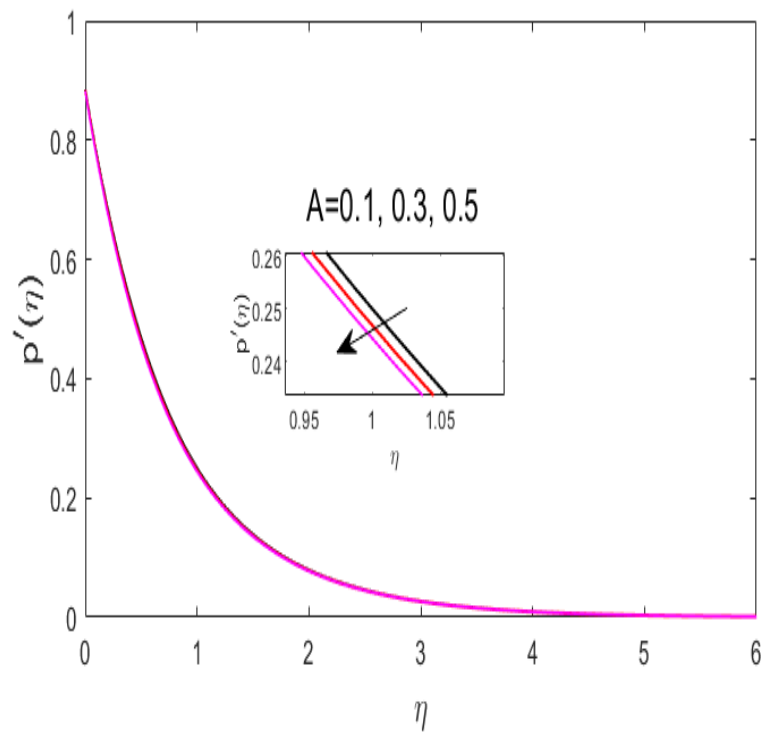


Figure 5.3. Velocity distribution $p'(\eta)$ for A .

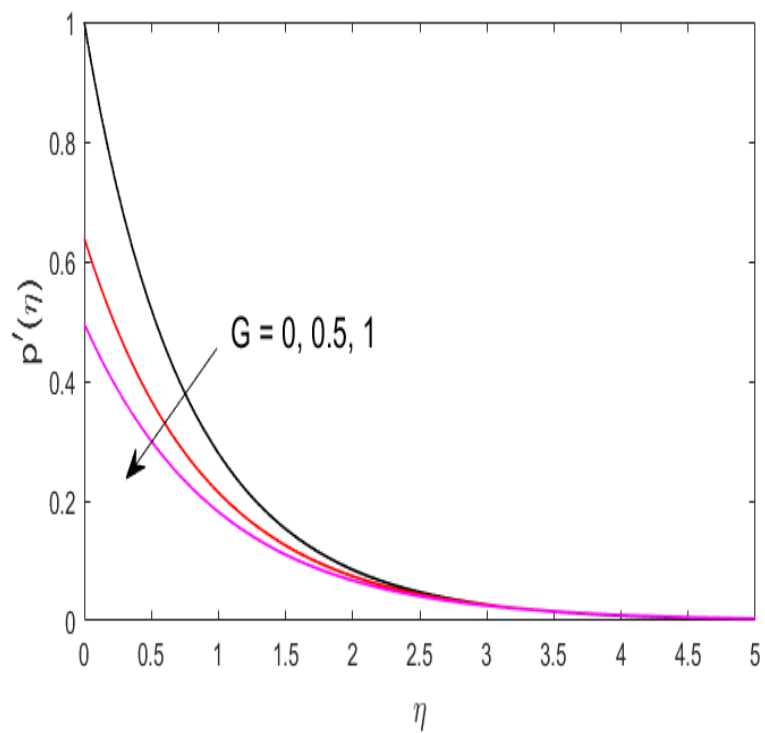


Figure 5.4. Velocity distribution $p'(\eta)$ for G .

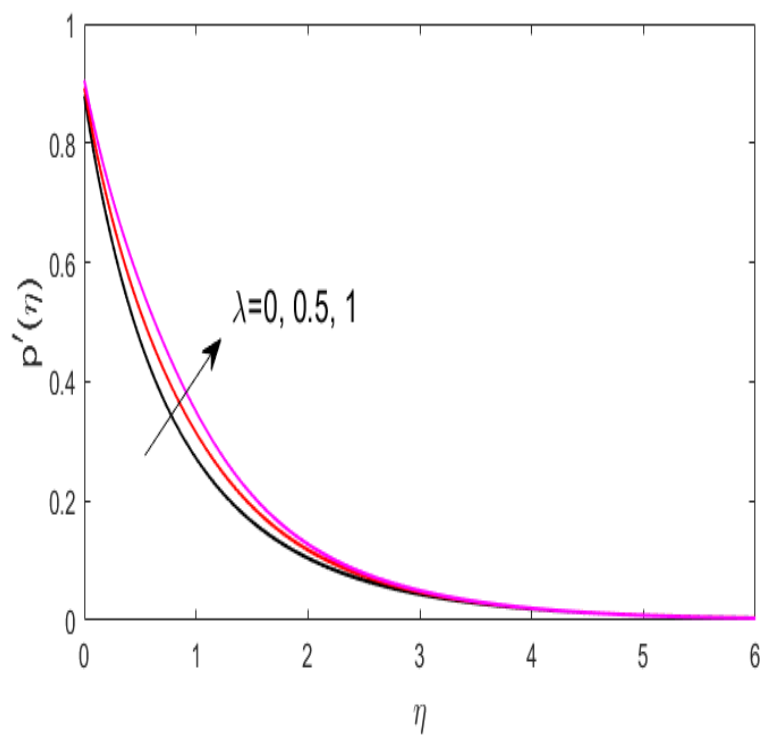


Figure 5.5. Velocity distribution $p'(\eta)$ for λ .

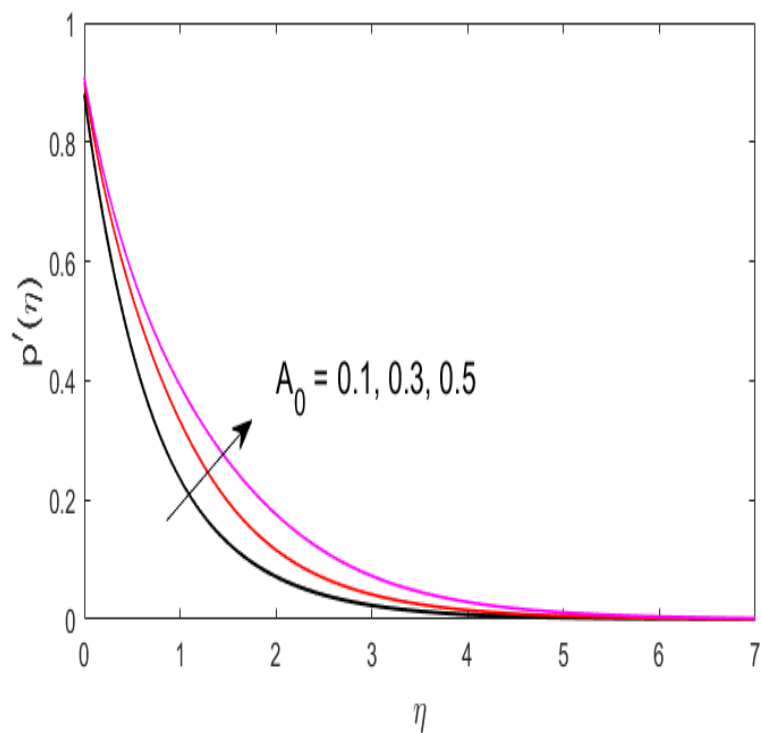


Figure 5.6. Velocity distribution $p'(\eta)$ for A_0 .

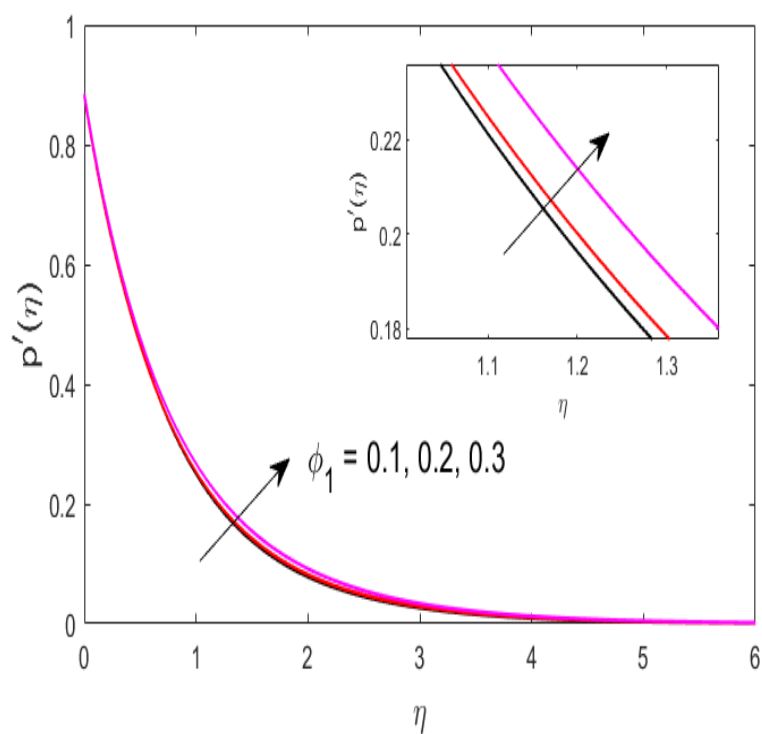


Figure 5.7. Velocity distribution $p'(\eta)$ for ϕ_1 .

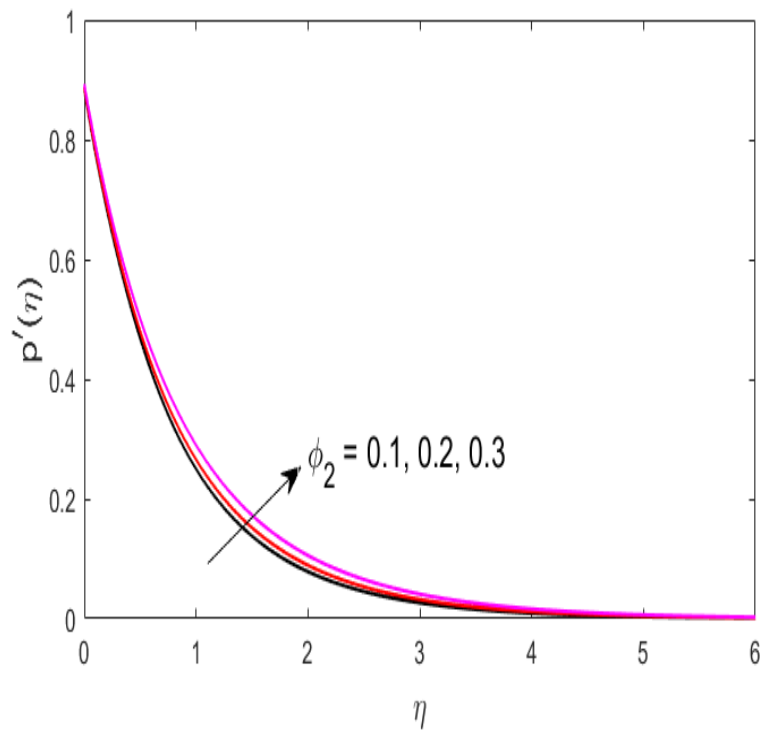


Figure 5.8. Velocity distribution $p'(\eta)$ for ϕ_2 .

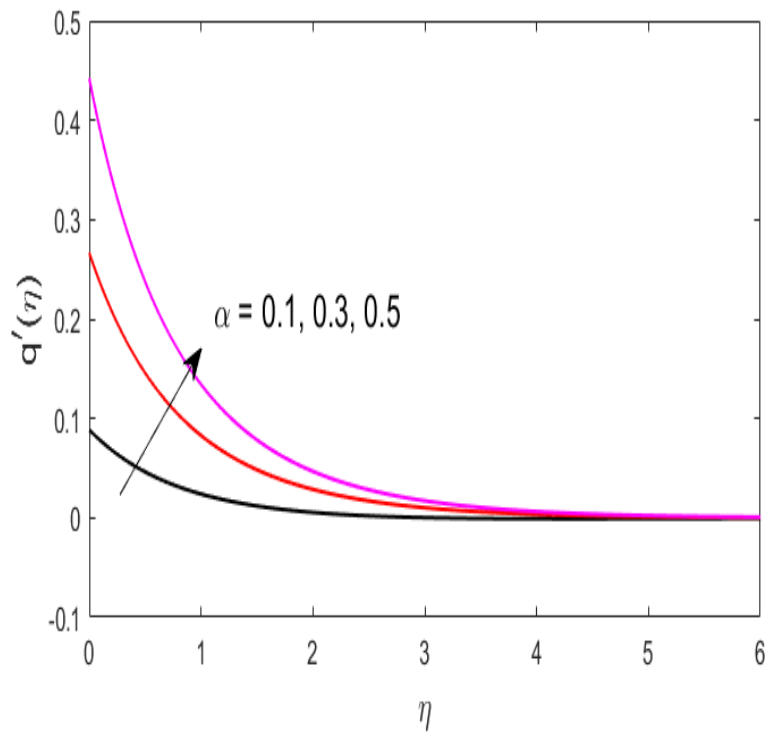


Figure 5.9. Velocity distribution $q'(\eta)$ for α .

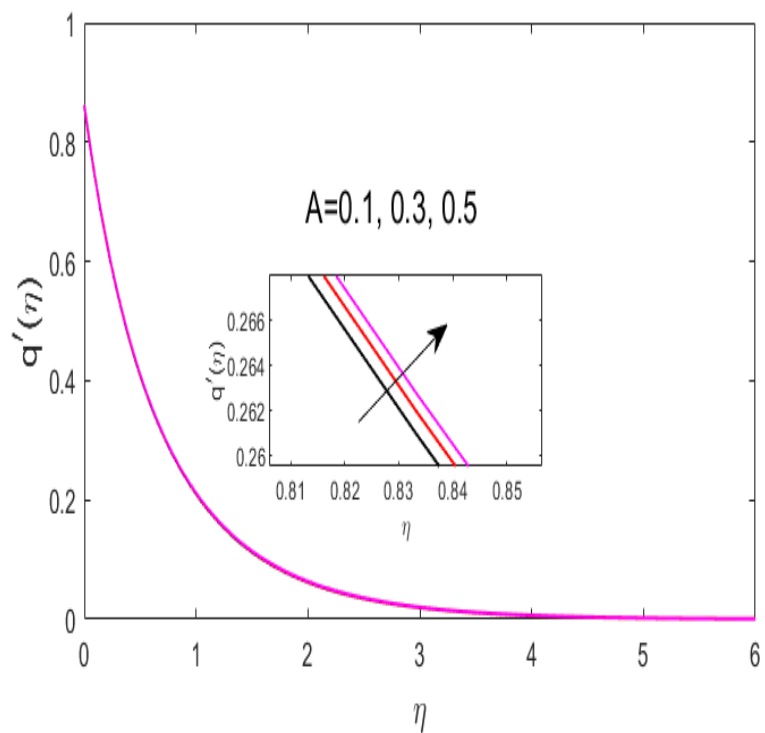


Figure 5.10. Velocity distribution $q'(\eta)$ for A .

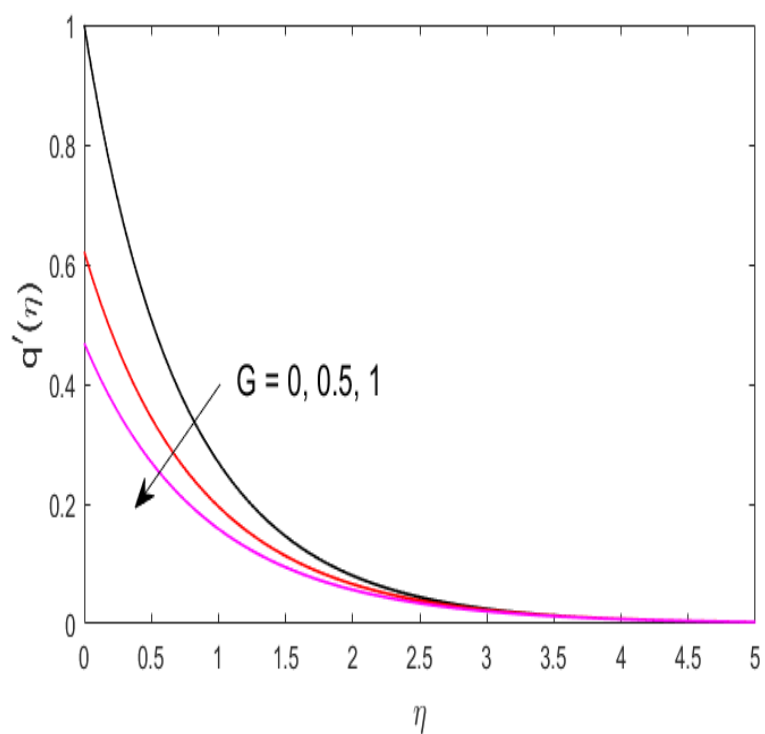


Figure 5.11. Velocity distribution $q'(\eta)$ for G .

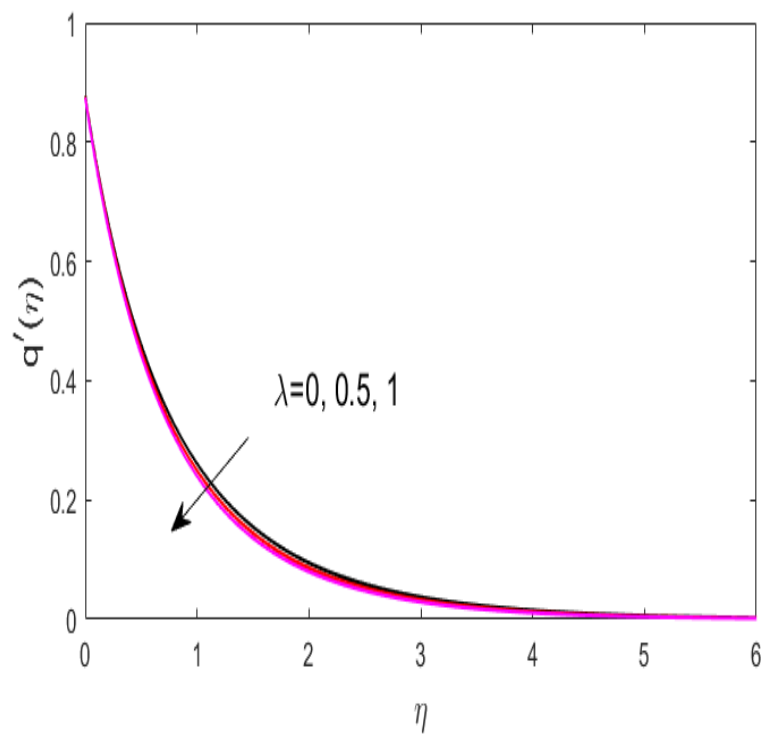


Figure 5.12. Velocity distribution $q'(\eta)$ for λ .

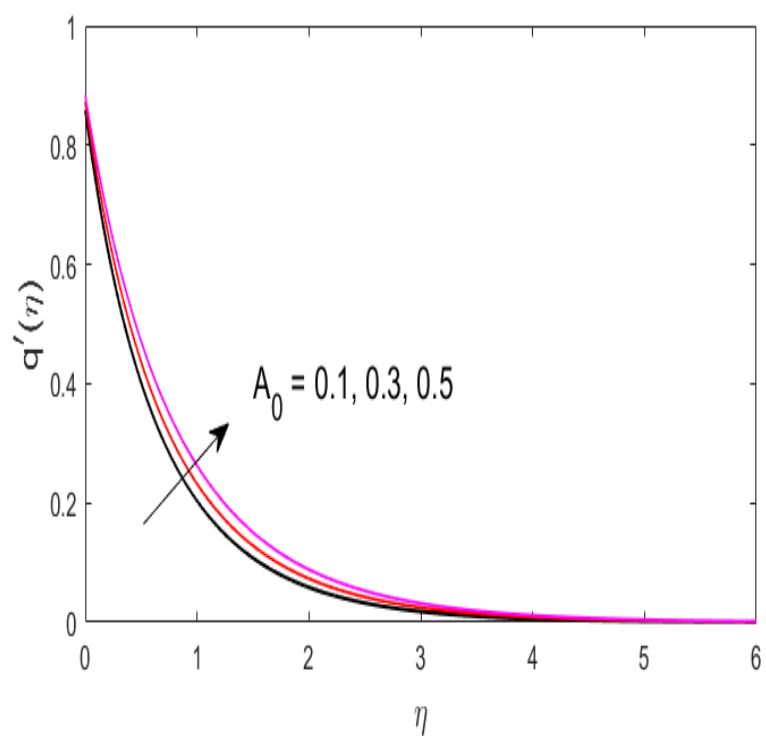


Figure 5.13. Velocity distribution $q'(\eta)$ for A_0 .

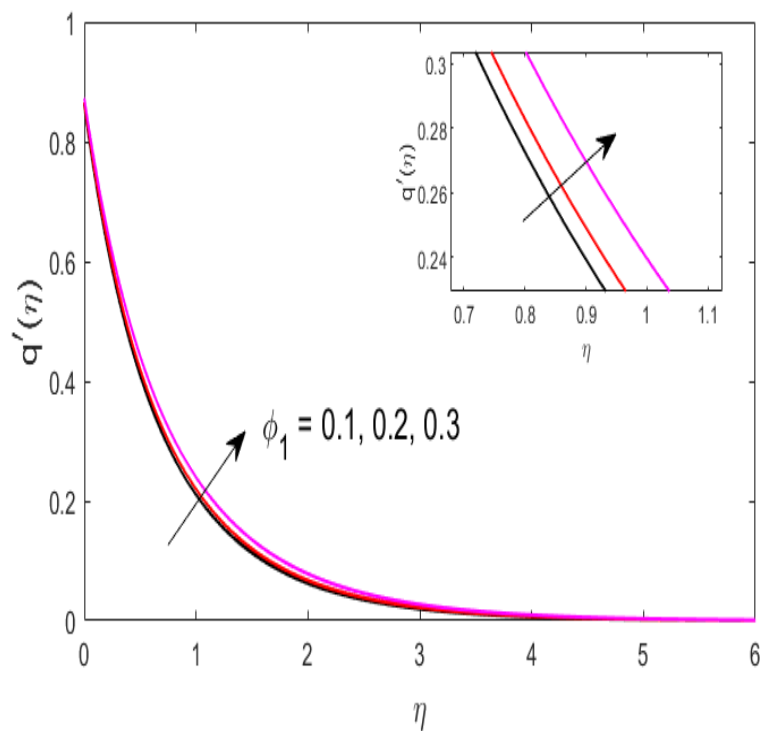


Figure 5.14. Velocity distribution $q'(\eta)$ for ϕ_1 .

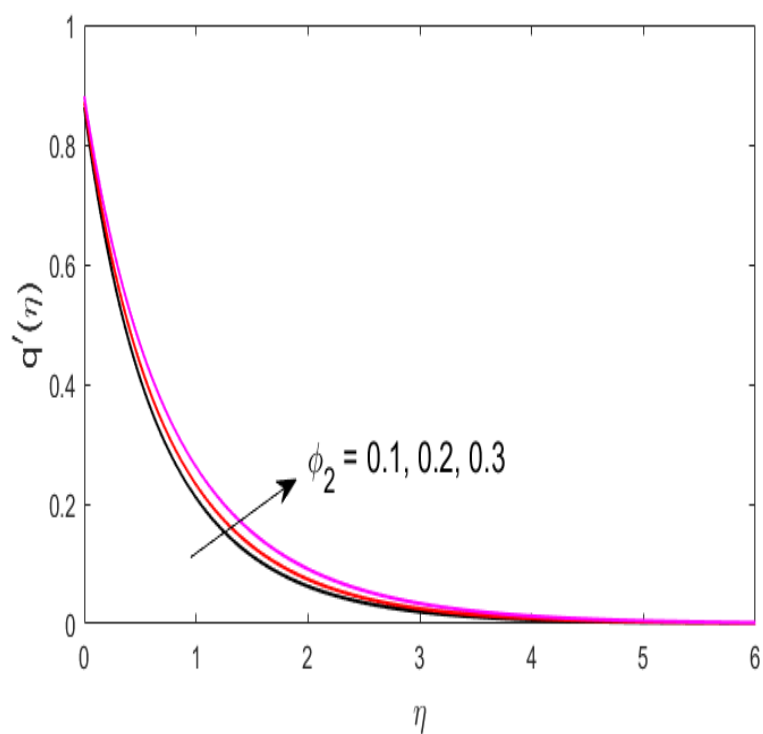


Figure 5.15. Velocity distribution $q'(\eta)$ for ϕ_2 .

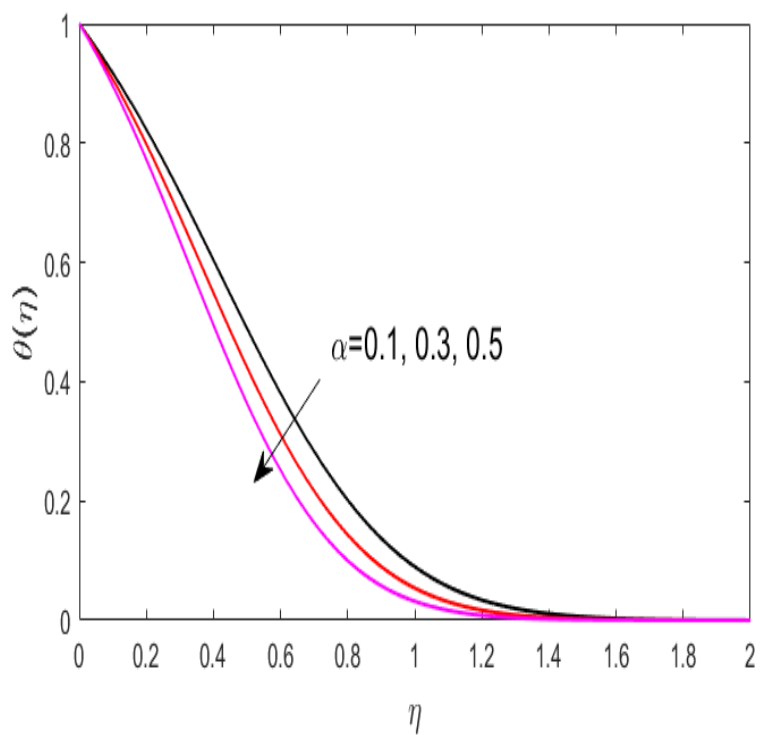


Figure 5.16. Temperature distribution $\theta(\eta)$ for α .

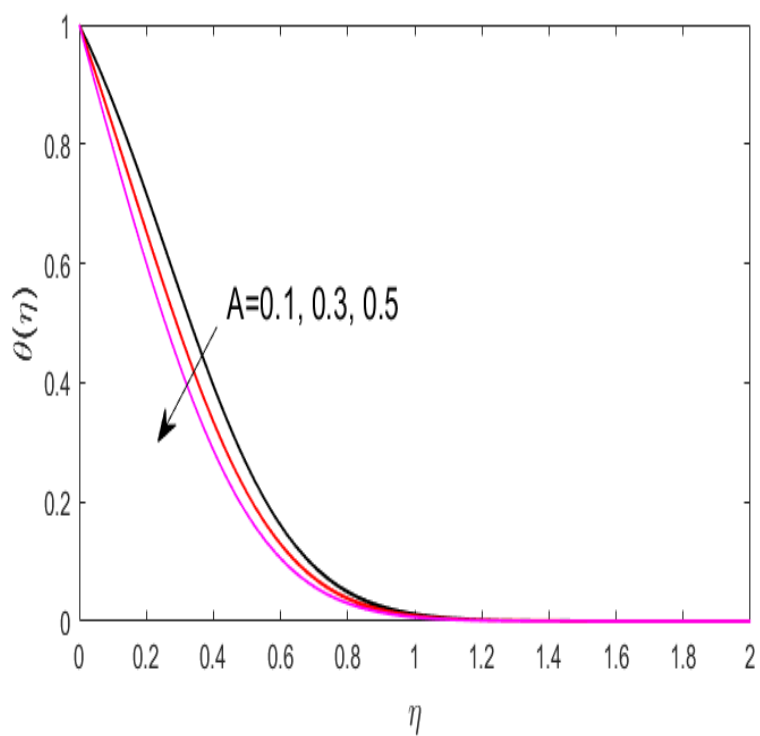


Figure 5.17. Temperature distribution $\theta(\eta)$ for A .

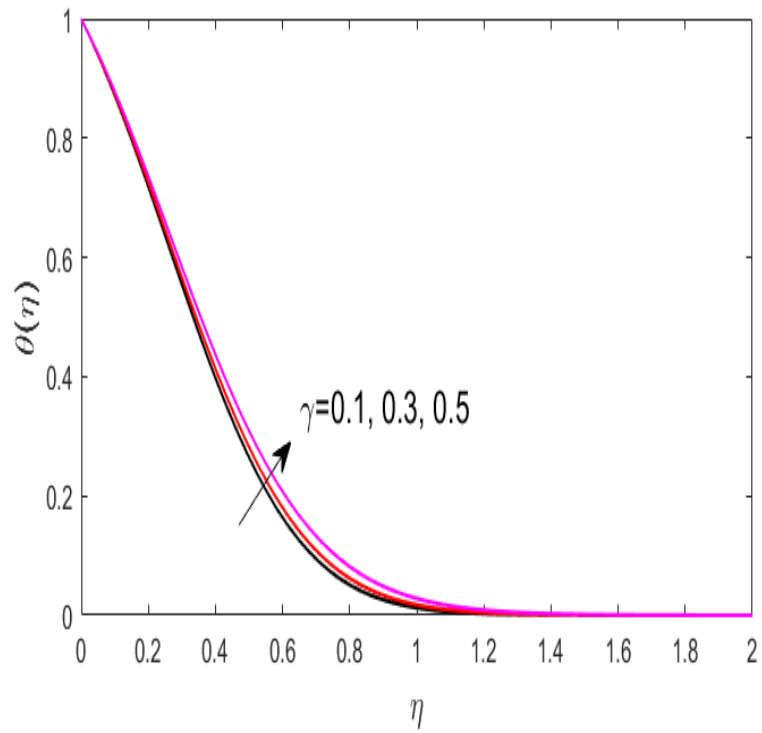


Figure 5.18. Temperature distribution $\theta(\eta)$ for γ .

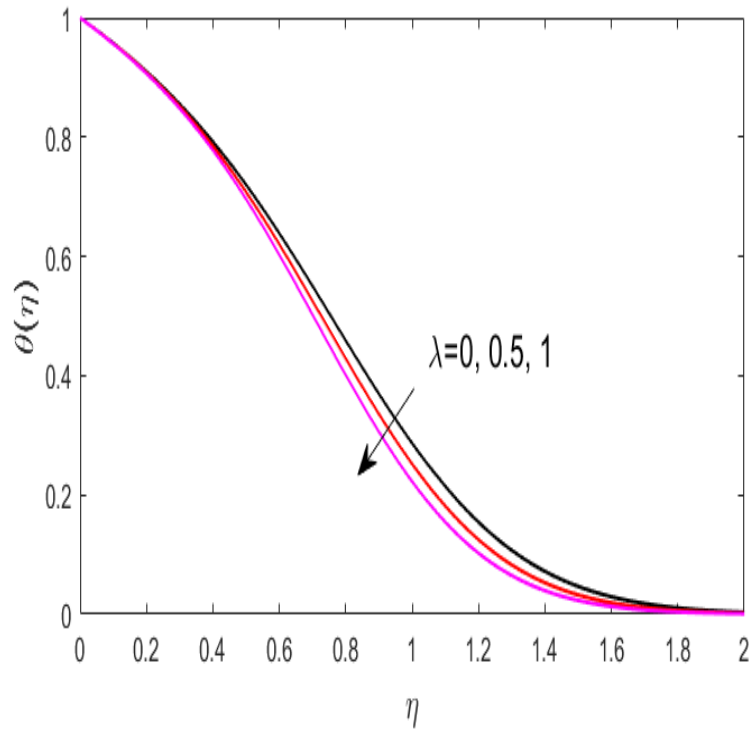


Figure 5.19. Temperature distribution $\theta(\eta)$ for λ .

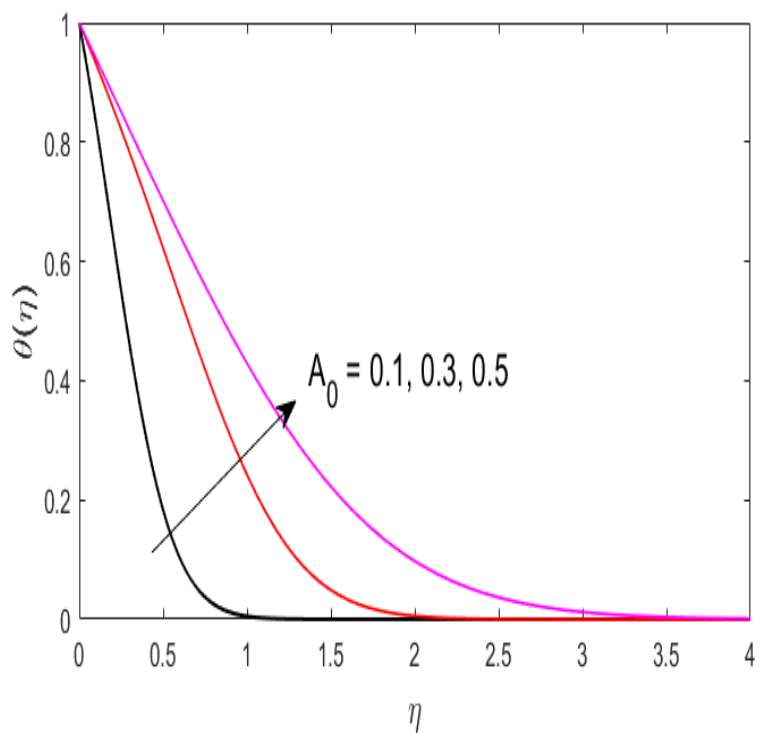


Figure 5.20. Temperature distribution $\theta(\eta)$ for A_0 .

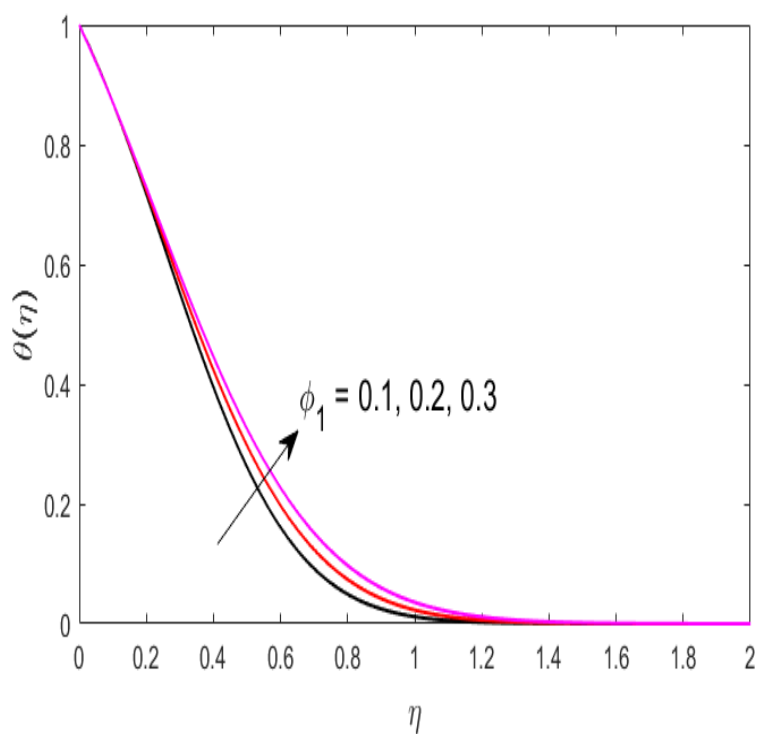


Figure 5.21. Temperature distribution $\theta(\eta)$ for ϕ_1 .

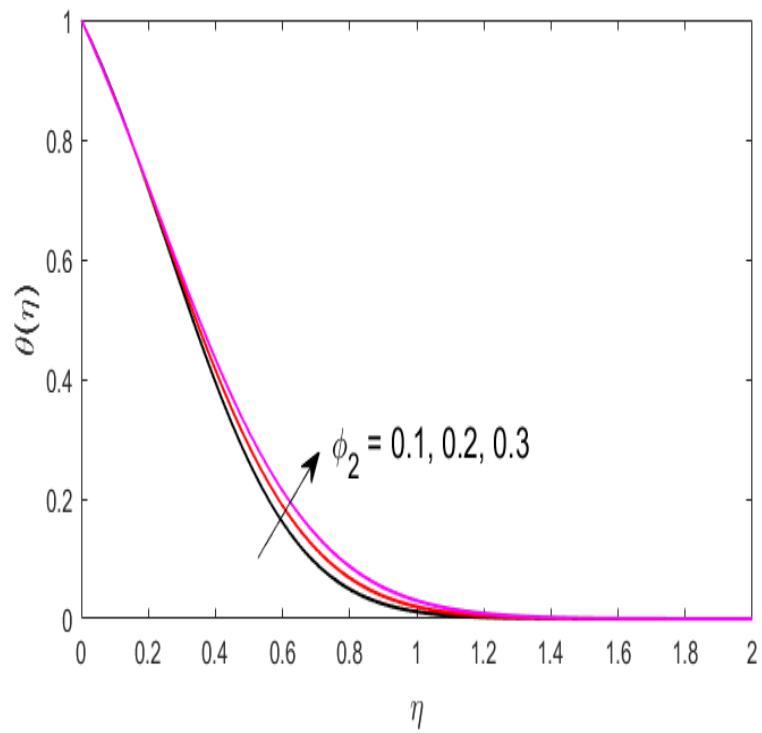


Figure 5.22. Temperature distribution $\theta(\eta)$ for ϕ_2 .

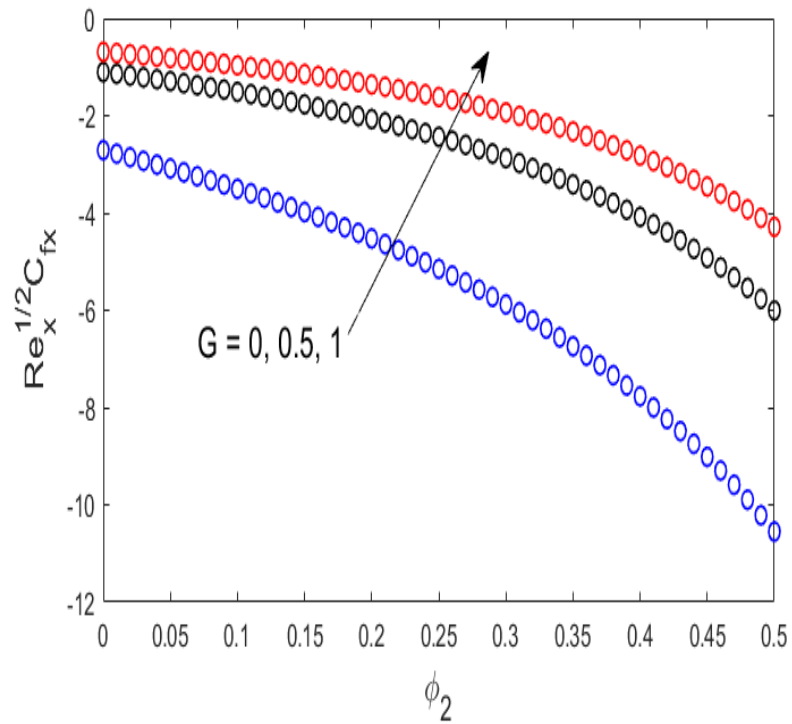


Figure 5.23. Skin friction coefficient along x -axis for G and ϕ_2 .

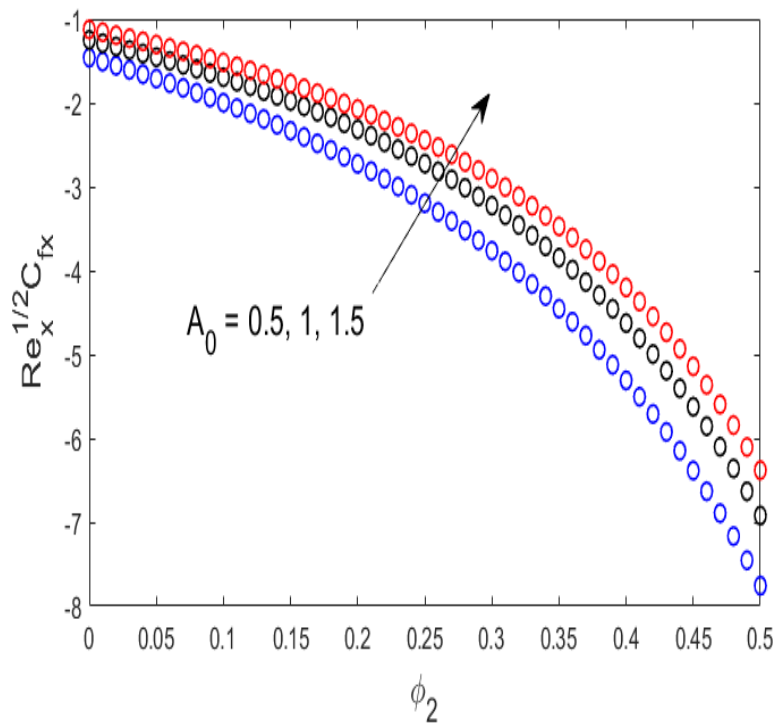


Figure 5.24. Skin friction coefficient along x -axis for A_0 and ϕ_2 .

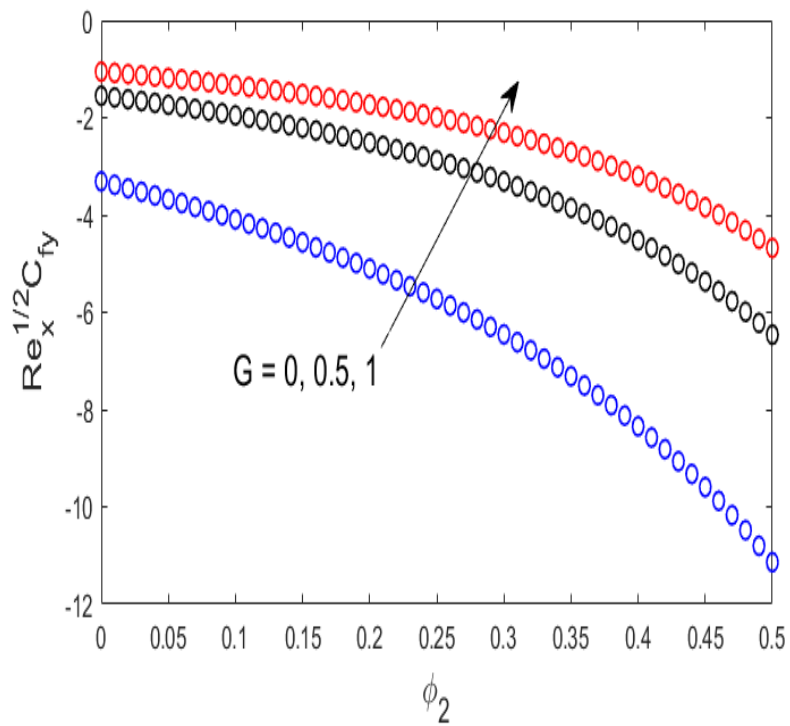


Figure 5.25. Skin friction coefficient along y -axis for G and ϕ_2 .

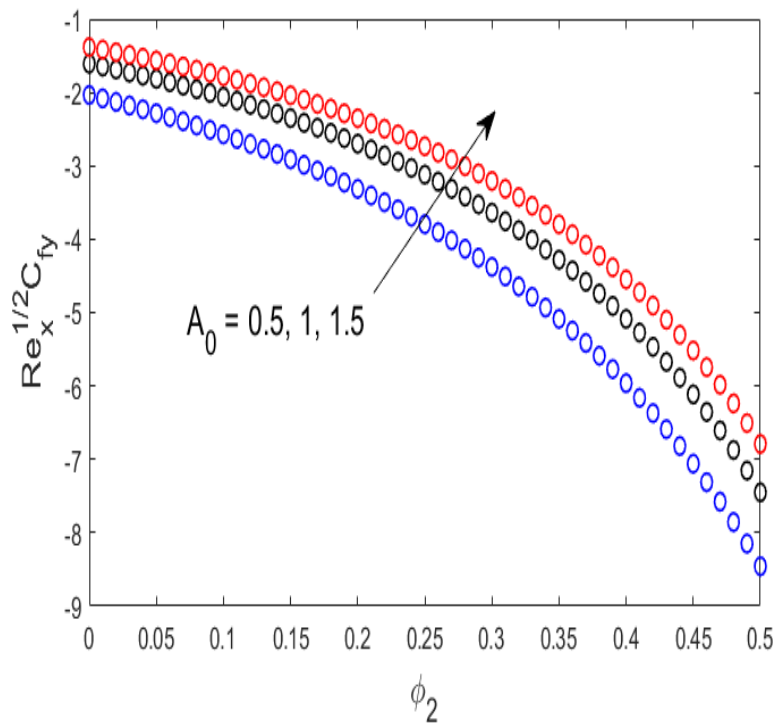


Figure 5.26. Skin friction coefficient along y-axis for A_0 and ϕ_2 .

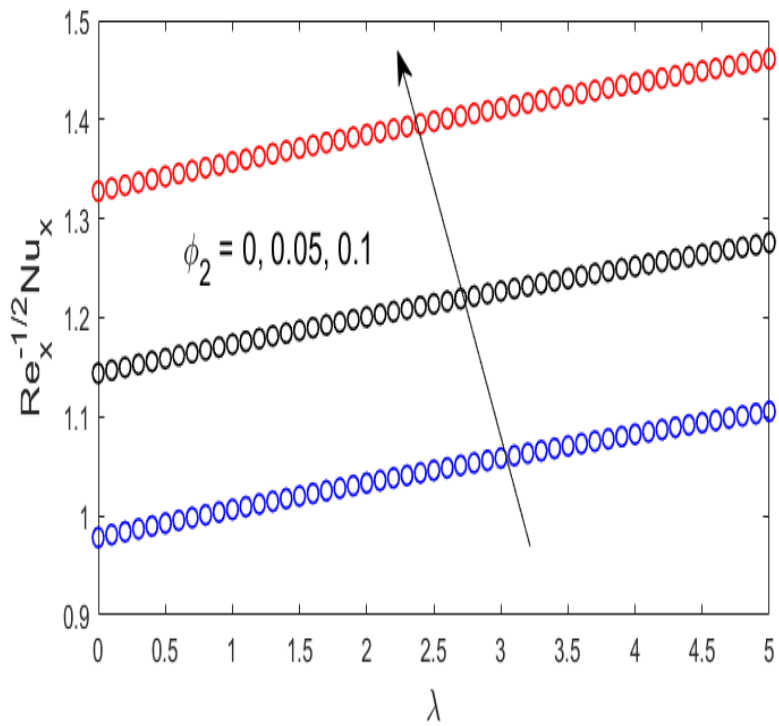


Figure 5.27. Nusselt number for ϕ_2 and λ .

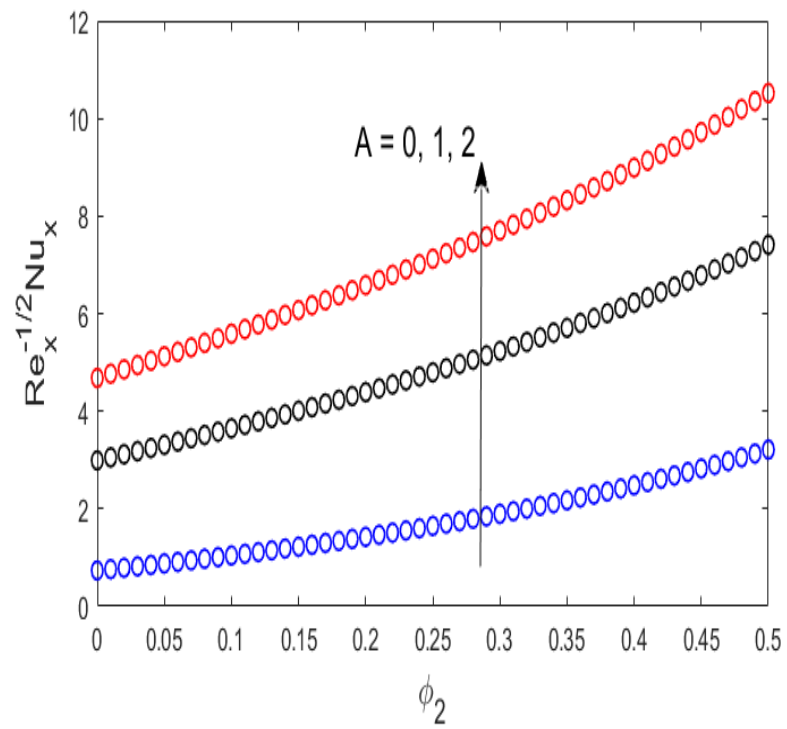


Figure 5.28. Nusselt number for A and ϕ_2 .

Chapter 6

Conclusion and Future Projects

6.1 Conclusions from the Study

The goal of the current investigation is to analyze the fluid flow and heat transfer characteristics of the unsteady hybrid nanofluid flow over an exponentially stretching and rotating surface. The phenomenon of mixed convection and velocity slip has been considered in the current model. CuO and TiO_2 are taken as nanoparticles and the base fluid is 50% ethylene glycol and 50% water. The system of partial differential equations is reduced using appropriate similarity transformations to a system of ordinary differential equations. With the use of the MATLAB built-in solver `bvp4c` function, the resultant system was numerically solved. The flow analysis has been carried out through the graphical behavior for velocity and temperature profiles, Nusselt number and skin friction. When the stretching ratio parameter α for the hybrid nanofluid is increased, the velocity profile $p'(\eta)$ and temperature profile $\theta(\eta)$ exhibit a declining trend. Larger values of the stretching parameter α leads to an increasing trend in velocity profile $q'(\eta)$. The velocity profiles $p'(\eta)$ and $q'(\eta)$ as well as temperature profile $\theta(\eta)$ grows when the unsteadiness parameter A_0 is raised. With a higher value of the mixed convection parameter λ , the temperature profile and velocity $q'(\eta)$ drop. When the mixed convection parameter is raised, the velocity $p'(\eta)$ exhibits increasing behavior. The velocity profiles $p'(\eta)$, $q'(\eta)$ declines as the velocity slip parameter G increases. Both the velocity profile $p'(\eta)$ and the temperature profile $\theta(\eta)$ drops when the value of temperature

exponent parameter A increases. The fluctuation in the flow parameters that are taken into consideration affects both the drag force and the Nusselt number. It is essential to note that the drag forces along both the axes increase when both G and A_0 values grow. It is suggested that when ϕ_2 increase, the drag force coefficients decline. It is noticeable that when ϕ_2 climbs up, the Nusselt number value increases. The improved behavior of Nusselt number is also examined for increasing λ . It has been shown that when A and ϕ_2 boosts, the Nusselt value also show an enhancement.

6.2 Potential Projects

The unsteady hybrid nanofluid flow over an exponentially stretched surface is investigated in this work. Nevertheless there remains opportunity to enhance the current problem to and inquire more research works. Some interesting possible research that might be conducted in the future are listed.

- The stagnation point flow of ternary hybrid nanofluid using the Cattaneo-Christov heat flux model.
- Analyzing the three-dimensional magnetohydrodynamic flow over a stretched with temperature jump.
- Three-dimensional non-Newtonian hybrid nanofluid flow on a stretched sheet in the presence of thermal radiation and viscous dissipation.

References

1. Choi, S. U. S. (1995). Enhancing thermal conductivity of fluids with nanoparticles. *Developments and Applications of Non-Newtonian Flows*, 231, 99– 105.
2. Sarkar, J., Ghosh, P., & Adil, A. (2015). A review on hybrid nanofluids: recent research, development and applications. *Renewable and Sustainable Energy Reviews*, 43, 164-177.
3. Al-Kouz, W., Abderrahmane, A., Shamsuddin, M. D., Younis, O., Mohammed, S., Bég, O. A., & Toghraie, D. (2021). Heat transfer and entropy generation analysis of water-Fe₃O₄/CNT hybrid magnetic nanofluid flow in a trapezoidal wavy enclosure containing porous media with the Galerkin finite element method. *The European Physical Journal Plus*, 136(11), 1184.
4. Nayak, M. K., Pandey, V. S., Shaw, S., Makinde, O. D., Ramadan, K. M., Henda, M. B., & Tlili, I. (2021). Thermo-fluidic significance of non-Newtonian fluid with hybrid nanostructures. *Case Studies in Thermal Engineering*, 26, 101092
5. Zubair, M., Jawad, M., Bonyah, E., & Jan, R. (2021). MHD analysis of couple stress hybrid nanofluid free stream over a spinning Darcy-Forchheimer porous disc under the effect of thermal radiation. *Journal of Applied Mathematics*, 2021, 1-18.
6. Maraj, E. N., Akbar, N. S., Iqbal, Z., & Azhar, E. (2017). Framing the MHD mixed convective performance of CNTs in rotating vertical channel inspired by thermal deposition: closed form solutions. *Journal of Molecular Liquids*, 233, 334-343.
7. Zainal, N. A., Nazar, R., Naganthran, K., & Pop, I. (2020). MHD mixed convection stagnation point flow of a hybrid nanofluid past a vertical flat plate with convective boundary condition. *Chinese Journal of Physics*, 66, 630-644.
8. Bouslimi, J., Abdelhafez, M. A., Abd-Alla, A. M., Abo-Dahab, S. M., & Mahmoud, K. H. (2021). MHD mixed convection nanofluid flow over convectively heated nonlinear due to an extending surface with Soret effect. *Complexity*, 2021, 1-20.

9. Varun K., R. S., Alhadhrami, A., Punith Gowda, R. J., Naveen Kumar, R., & Prasannakumara, B. C. (2021). Exploration of Arrhenius activation energy on hybrid nanofluid flow over a curved stretchable surface. *ZAMM-Journal of Applied Mathematics and Mechanics/Zeitschrift für Angewandte Mathematik und Mechanik*, *101*(12), e202100035.
10. Naidu, K. K., Babu, D. H., Reddy, S. H., & Narayana, P. V. (2021). Radiation and partial slip effects on magnetohydrodynamic Jeffrey nanofluid containing gyrotactic microorganisms over a stretching surface. *Journal of Thermal Science and Engineering Applications*, *13*(3).
11. Ramzan, M., Dawar, A., Saeed, A., Kumam, P., Watthayu, W., & Kumam, W. (2021). Heat transfer analysis of the mixed convective flow of magnetohydrodynamic hybrid nanofluid past a stretching sheet with velocity and thermal slip conditions. *Plos one*, *16*(12), e0260854.
12. Sajid, T., Jamshed, W., Shahzad, F., Aiyashi, M. A., Eid, M. R., Nisar, K. S., & Shukla, A. (2021). Impact of Maxwell velocity slip and Smoluchowski temperature slip on CNTs with modified Fourier theory: Reiner-Philippoff model. *Plos one*, *16*(10), 0258367.
13. Nandi, S., Kumbhakar, B., & Seth, G. S., (2022). Quadratic regression analysis of unsteady MHD free convective and radiative–dissipative stagnation flow of hybrid nanofluid over an exponentially stretching surface under porous medium. *Chinese Journal of Physics*, *77*, 2090-2105.
14. Zainal, N. A., Nazar, R., Naganthran, K., & Pop, I., (2021). Unsteady MHD stagnation point flow induced by exponentially permeable stretching/shrinking sheet of hybrid nanofluid. *Engineering Science and Technology, an International Journal*, *24*, 1202-1210.
15. Ahmad, F., Abdal, S., Ayed, H., Hussain, S., Salim, S., & Almatroud, A. O., (2021). The improved thermal efficiency of Maxwell hybrid nanofluid comprising of graphene oxide plus silver/kerosene oil over stretching sheet. *Case Studies in Thermal Engineering*, *27*, 101257.
16. Rehman, A., & Salleh, Z. (2021). Approximate analytical analysis of unsteady MHD mixed flow of non-Newtonian hybrid nanofluid over a stretching surface. *Fluids*, *6*(4), 138.
17. Nabwey, H. A., Rashad, A. M., Reddy, P. B. A., Jakeer, S., Mansourf, M. A., & Salah, T., (2022). Radiative effects on unsteady MHD natural convection flow in an inclined

- wavy porous cavity using hybrid nanofluid containing a square obstacle. *Alexandria Engineering Journal*.
18. Khashi'ie, N. S., Waini, I., Wahid, N. S., MdArifin, N., & Pop, I., (2022). Unsteady separated stagnation point flow due to an EMHD Riga plate with heat generation in hybrid nanofluid. *Chinese Journal of Physics*,
 19. Arshad, M., Hussain, A., Hassan, A., Haider, Q., Ibrahim, A. H., Alqurashi, M. S., & Abdussattar, A. (2021). Thermophoresis and brownian effect for chemically reacting magneto-hydrodynamic nanofluid flow across an exponentially stretching sheet. *Energies*, 15(1), 143.
 20. Hussain, A., Arshad, M., Rehman, A., Hassan, A., Elagan, S. K., Ahmad, H., & Ishan, A. (2021). Three-dimensional water-based magneto-hydrodynamic rotating nanofluid flow over a linear extending sheet and heat transport analysis: A numerical approach. *Energies*, 14(16), 5133.
 21. Mabood, F., & Akinshilo, A. T. (2021). Stability analysis and heat transfer of hybrid Cu-Al₂O₃/H₂O nanofluids transport over a stretching surface. *International Communications in Heat and Mass Transfer*, 123, 105215.
 22. Khan, A. A., Khan, M. N., Ahsan, N., Khan, M. I., Muhammad, T., & Rehman, A. (2022). Heat and mass transfer features of transient second-grade fluid flow through an exponentially stretching surface. *Pramana*, 96(2), 58.
 23. Hameed, N., Noeiaghdam, S., Khan, W., Pimpunchat, B., Fernandez-Gamiz, U., Khan, M. S., & Rehman, A. (2022). Analytical analysis of the magnetic field, heat generation and absorption, viscous dissipation on couple stress casson hybrid nano fluid over a nonlinear stretching surface. *Results in Engineering*, 16, 100601.
 24. Yasir, M., Hafeez, A., & Khan, M. (2022). Thermal conductivity performance in hybrid (SWCNTs-CuO/Ethylene glycol) nanofluid flow: Dual solutions. *Ain Shams Engineering Journal*, 13(5), 101703.
 25. Rauf, A., Mushtaq, A., Shah, N. A., & Botmart, T. (2022). Heat transfer and hybrid ferrofluid flow over a nonlinearly stretchable rotating disk under the influence of an alternating magnetic field. *Scientific Reports*, 12(1), 17548.
 26. Alhowaity, A., Hamam, H., Bilal, M., & Ali, A. (2022). Numerical study of Williamson hybrid nanofluid flow with thermal characteristics past over an extending surface. *Heat transfer*, 51(7), 6641-6655.
 27. Nanda, P., Sandeep, N., Sulochana, C., & Ashwinkumar, G. P. (2023). Enhanced heat transmission in methanol-based AA7072/AA7075 tangent hyperbolic hybrid

- nanofluid flow along a nonlinear expandable surface. *Numerical Heat Transfer, Part A: Applications*, 83(7), 711-725.
28. Ramesh, G. K., Madhukesh, J. K., Khan, U., Hussain, S. M., & Galal, A. M. (2023). Inspection of hybrid nanoparticles flow across a nonlinear/linear stretching surface when heat sink/source and thermophoresis particle deposition impacts are significant. *International Journal of Modern Physics B*, 37(01), 2350008.
 29. Yasir, M., Khan, M., Alqahtani, A. S., & Malik, M. Y. (2023). Numerical study of axisymmetric hybrid nanofluid MgO-Ag/H₂O flow with non-uniform heat source/sink. *Alexandria Engineering Journal*, 75, 439-446.
 30. Sulochana, C., Savita, & Ashwinkumar, G. P. (2023). Joule heating effect on the MHD flow of tangent hyperbolic mixed nanofluid embedded with MgO and CuO nanoparticles. *International Journal of Ambient Energy*, 1-10.
 31. Asghar, A., Vranceanu, N., Ying, T. Y., Lund, L. A., Shah, Z., & Tirth, V. (2023). Dual solutions of convective rotating flow of three-dimensional hybrid nanofluid across the linear stretching/shrinking sheet. *Alexandria Engineering Journal*, 75, 297-312.
 32. Mahmood, Z., Alhazmi, S. E., Alhowaity, A., Marzouki, R., Al-Ansari, N., & Khan, U. (2022). MHD mixed convective stagnation point flow of nanofluid past a permeable stretching sheet with nanoparticles aggregation and thermal stratification. *Scientific Reports*, 12(1), 16020.
 33. Khan, U., Zaib, A., Madhukesh, J. K., Elattar, S., Eldin, S. M., Ishak, A., & Waini, I. (2022). Features of radiative mixed convective heat transfer on the slip flow of nanofluid past a stretching bended sheet with activation energy and binary reaction. *Energies*, 15(20), 7613.
 34. Waqas, H., Farooq, U., Liu, D., Abid, M., Imran, M., & Muhammad, T. (2022). Heat transfer analysis of hybrid nanofluid flow with thermal radiation through a stretching sheet: A comparative study. *International Communications in Heat and Mass Transfer*, 138, 106303.
 35. Habib, U., Abdal, S., Siddique, I., & Ali, R. (2022). A comparative study on micropolar, Williamson, Maxwell nanofluids flow due to a stretching surface in the presence of bioconvection, double diffusion and activation energy. *International Communications in Heat and Mass Transfer*, 127, 105551.
 36. Verma, A. K., Rajput, S., Bhattacharyya, K., & Chamkha, A. J. (2022). Nanoparticles radius effect on unsteady mixed convective copper-water nanofluid flow over an

- expanding sheet in porous medium with boundary slip. *Chemical Engineering Journal Advances*, 12, 100366.
37. Khan, U., Zaib, A., Sakhinah, A. B., & Ishak, A. (2022). Hybrid nanofluid flow with quadratic velocity and thermal slip over a permeable stretching/shrinking surface. *Waves in Random and Complex Media*, 1-18.
 38. Ashraf, S., Mushtaq, M., Jabeen, K., Farid, S., & Muntazir, R. M. A. (2023). Heat and mass transfer of unsteady mixed convection flow of Casson fluid within the porous media under the influence of magnetic field over a nonlinear stretching sheet. *Proceedings of the Institution of Mechanical Engineers, Part C: Journal of Mechanical Engineering Science*, 237(1), 20-38.
 39. Mahato, R., Das, M., Sen, S. S. S., & Nandkeolyar, R. (2023). Hydromagnetic mixed convection unsteady radiative Casson fluid flow towards a stagnation-point with chemical reaction, induced magnetic field, Soret effect, and convective boundary conditions. *Heat Transfer*, 52(2), 1142-1160.
 40. Zainodin, S., Jamaludin, A., Nazar, R., & Pop, I. (2023). MHD Mixed Convection Flow of Hybrid Ferrofluid through Stagnation-Point over the Nonlinearly Moving Surface with Convective Boundary Condition, Viscous Dissipation, and Joule Heating Effects. *Symmetry*, 15(4), 878.
 41. Ali, B., Mishra, N. K., Rafique, K., Jubair, S., Mahmood, Z., & Eldin, S. M. (2023). Mixed convective flow of hybrid nanofluid over a heated stretching disk with zero-mass flux using the modified Buongiorno model. *Alexandria Engineering Journal*, 72, 83-96.
 42. Asghar, A., Chandio, A. F., Shah, Z., Vrinceanu, N., Deebani, W., Shutaywi, M., & Lund, L. A. (2023). Magnetized mixed convection hybrid nanofluid with effect of heat generation/absorption and velocity slip condition. *Heliyon*, 9(2).
 43. Tlili, I., Nabwey, H. A., Ashwinkumar, G. P., & Sandeep, N. (2020). 3-D magnetohydrodynamic AA7072-AA7075/methanol hybrid nanofluid flow above an uneven thickness surface with slip effect. *Scientific reports*, 10(1), 4265.
 44. Anuar, N. S., Bachok, N., & Pop, I. (2021). Numerical computation of dusty hybrid nanofluid flow and heat transfer over a deformable sheet with slip effect. *Mathematics*, 9(6), 643.
 45. Usafzai, W. K., Aly, E. H., Alshomrani, A. S., & Ullah, M. Z. (2022). Multiple solutions for nanofluids flow and heat transfer in porous medium with velocity slip and temperature jump. *International Communications in Heat and Mass*

- Transfer*, 131, 105831.
46. Eid, M. R., & Nafe, M. A. (2022). Thermal conductivity variation and heat generation effects on magneto-hybrid nanofluid flow in a porous medium with slip condition. *Waves in Random and Complex Media*, 32(3), 1103-1127.
 47. Manigandan, A., & Satya Narayana, P. V. (2023). Influence of variable thermal conductivity and mixed convection on hybrid nanofluid (SWCNT+ MWCNT/H₂O) flow over an exponentially elongated sheet with slip conditions. *Indian Journal of Physics*, 1-14.
 48. Nasir, S., Berrouk, A. S., Aamir, A., & Shah, Z. (2023). Entropy optimization and heat flux analysis of Maxwell nanofluid configured by an exponentially stretching surface with velocity slip. *Scientific Reports*, 13(1), 2006.
 49. Aly, E. H., Mahabaleshwar, U. S., Anusha, T., & Pop, I. (2023). Exact solutions for MHD and radiative wall jet hybrid nanofluid flow over a permeable surface with velocity slip and convective boundary conditions. *ZAMM-Journal of Applied Mathematics and Mechanics/Zeitschrift für Angewandte Mathematik und Mechanik*, 103(1), e202100261.
 50. Kumbhakar, B., & Nandi, S. (2022). Unsteady MHD radiative-dissipative flow of Cu-Al₂O₃/H₂O hybrid nanofluid past a stretching sheet with slip and convective conditions: A regression analysis. *Mathematics and Computers in Simulation*, 194, 563-587.
 51. Mohd Sohut, N. F. H., Soid, S. K., Abu Bakar, S., & Ishak, A. (2022). Unsteady Three-Dimensional Flow in a Rotating Hybrid Nanofluid over a Stretching Sheet. *Mathematics*, 10(3), 348.
 52. Lone, S. A., Ali, F., Saeed, A., & Bognár, G. (2023). Irreversibility analysis with hybrid cross nanofluid of stagnation point and radiative flow (TiO₂+CuO) based on engine oil past a stretchable sheet. *Heliyon*, 9(4).
 53. Mohana, C. M., & Rushi Kumar, B. (2023). Shape effects of Darcy–Forchheimer unsteady three-dimensional CdTe-C/H₂O hybrid nanofluid flow over a stretching sheet with convective heat transfer. *Physics of Fluids*, 35(9)
 54. Nadeem, M., Siddique, I., Riaz, Z., Makhdoum, B. M., Zulqarnain, R. M., & Sallah, M. (2023). Numerical study of unsteady tangent hyperbolic fuzzy hybrid nanofluid over an exponentially stretching surface. *Scientific Reports*, 13(1), 15551.
 55. Qayyum, M., Afzal, S., Ali, M. R., Sohail, M., Imran, N., & Chambashi, G. (2023). Unsteady hybrid nanofluid (UO₂, MWCNTs/blood) flow between two rotating

- stretchable disks with chemical reaction and activation energy under the influence of convective boundaries. *Scientific Reports*, 13(1), 6151.
56. Triveni, B., & Venkata Subba Rao, M. (2023). Unsteady flow of magnetohydrodynamic hybrid nanofluid over a stretching/shrinking sheet: Multiple solutions. *Proceedings of the Institution of Mechanical Engineers, Part E: Journal of Process Mechanical Engineering*, 237(4), 1224-1234.
 57. Yasir, M., Ahmed, A., Khan, M., Alzahrani, A. K., Malik, Z. U., & Alshehri, A. M. (2023). Mathematical modelling of unsteady Oldroyd-B fluid flow due to stretchable cylindrical surface with energy transport. *Ain Shams Engineering Journal*, 14(1), 101825.
 58. Chu, Y. M., Bashir, S., Ramzan, M., & Malik, M. Y. (2023). Model-based comparative study of magnetohydrodynamics unsteady hybrid nanofluid flow between two infinite parallel plates with particle shape effects. *Mathematical Methods in the Applied Sciences*, 46(10), 11568-11582.
 59. Mathews, J., & Hymavathi, T. (2023). Magnetohydrodynamic stagnation point flow and heat transfer effects of Al₂O₃-Cu/water hybrid nanofluid over a porous stretching surface. *Proceedings of the Institution of Mechanical Engineers, Part E: Journal of Process Mechanical Engineering*, 237(3), 1064-1072.
 60. Kumar, V., R. S., Alhadhrami, A., Punith Gowda, R. J., Naveen Kumar, R., & Prasannakumara, B. C. (2021). Exploration of Arrhenius activation energy on hybrid nanofluid flow over a curved stretchable surface. *ZAMM-Journal of Applied Mathematics and Mechanics/Zeitschrift für Angewandte Mathematik und Mechanik*, 101(12), e202100035.
 61. Sahu, S. K., Shaw, S., Thatoi, D. N., & Nayak, M. K. (2022). A thermal management of Darcy-Forchheimer SWCNT–MWCNT cross hybrid nanofluid flow due to vertical stretched cylinder with and without inertia effects. *Waves in Random and Complex Media*, 1-27.
 62. Elattar, S., Helmi, M. M., Elkotb, M. A., El-Shorbagy, M. A., Abdelrahman, A., Bilal, M., & Ali, A. (2022). Computational assessment of hybrid nanofluid flow with the influence of hall current and chemical reaction over a slender stretching surface. *Alexandria Engineering Journal*, 61(12), 10319-10331.
 63. Manjunatha, S., Puneeth, V., Giresha, B. J., & Chamkha, A. (2022). Theoretical study of convective heat transfer in ternarynanofluid flowing past a stretching .sheet *Journal of Applied and Computational Mechanics*, 8(4), 1279-1286.

64. Animasaun, I. L., Shah, N. A., Wakif, A., Mahanthesh, B., Sivaraj, R., & Koriko, O. K. (2022). *Ratio of momentum diffusivity to thermal diffusivity: introduction, meta-analysis, and scrutinization*. CRC Press
65. Sarfraz, M., & Khan, M. (2023). Thermodynamic irreversibility analysis of water conveying argentine and titania nanoparticles subject to inclined stretching surface. *Physica Scripta*, 98(2), 025205.
66. Farooq, U., Waqas, H., Aldhabani, M. S., Fatima, N., Alhushaybari, A., Ali, M. R., & Muhammad, T. (2023). Modeling and computational framework of radiative hybrid nanofluid configured by a stretching surface subject to entropy generation: Using Keller box scheme. *Arabian Journal of Chemistry*, 16(4), 104628.
67. Alqahtani, A. M., Bilal, M., Usman, M., Alsenani, T. R., Ali, A., & Mahmood, S. R. (2023). Heat and mass transfer through MHD Darcy Forchheimer Casson hybrid nanofluid flow across an exponential stretching sheet. *ZAMM-Journal of Applied Mathematics and Mechanics/Zeitschrift für Angewandte Mathematik und Mechanik*, e202200213.
68. Alqahtani, A. M., Bilal, M., Usman, M., Alsenani, T. R., Ali, A., & Mahmood, S. R. (2023). Heat and mass transfer through MHD Darcy Forchheimer Casson hybrid nanofluid flow across an exponential stretching sheet. *ZAMM-Journal of Applied Mathematics and Mechanics/Zeitschrift für Angewandte Mathematik und Mechanik*, e202200213.
69. Whitaker, S. (1977). *Fundamental Principles of Heat Transfer*. 1st United Kingdom. Elsevier Science and Technology Books.
70. Venkateswarlu, B., Chavan, S., Narayana, P. V. S., & Joo, S. W. (2023). A numerical investigation of cross-diffusion on magnetohydrodynamic Cu-Al₂O₃/H₂O hybrid nanofluid flow over a stretching sheet with chemical reaction. *Asia-Pacific Journal of Chemical Engineering*, e2985.
71. McDonald, A. T., Fox, R.W., and Pritchard, P. J. (2009). *Introduction to fluid mechanics (8th Ed.) India*. Wiley
72. Musharafa (2021). Lie group study of some non-newtonian fluid flow with heat transfer analysis. MS Thesis pages 30-34, *University of Engineering and Technology, Lahore*.
73. Hussain, A., Alshbool, M. H., Abdussattar, A., Rehman, A., Ahmad, H., Nofal, T. A., & Khan, M. R. (2021). A computational model for hybrid nanofluid flow on a rotating surface in the existence of convective condition. *Case Studies in Thermal*

- Engineering*, 26, 101089.
74. Ghadikolaie, S. S., Yassari, M., Sadeghi, H., Hosseinzadeh, K., & Ganji, D. D. (2017). Investigation on thermophysical properties of TiO₂-Cu/H₂O hybrid nanofluid transport dependent on shape factor in MHD stagnation point flow. *Powder technology*, 322, 428-438.
 75. Rasool, G., Wakif, A., Wang, X., Alshehri, A., & Saeed, A. M. (2023). Falkner-Skan aspects of a radiating (50% ethylene glycol+ 50% water)-based hybrid nanofluid when Joule heating as well as Darcy-Forchheimer and Lorentz forces affect significantly. *Propulsion and Power Research*, 12(3), 428-442.
 76. Ghadikolaie, S. S., Hosseinzadeh, K., & Ganji, D. D. (2018). Investigation on ethylene glycol-water mixture fluid suspend by hybrid nanoparticles (TiO₂-CuO) over rotating cone with considering nanoparticles shape factor. *Journal of Molecular Liquids*, 272, 226-236.
 77. Usman, Ghaffari, A., Muhammad, T., & Mustafa, I. (2022). Heat transfer enhancement in a power-law nanofluid flow between two rotating stretchable disks. *Pramana*, 96(1), 40.
 78. Magyari, E., & Keller, B. (1999). Heat and mass transfer in the boundary layers on an exponentially stretching continuous surface. *Journal of Physics D: Applied Physics*, 32(5), 577.
 79. Liu, I.-C., Wang, H.-H., & Peng, Y.-F. (2013). Flow and heat transfer for three-dimensional flow over an exponentially stretching surface. *Chemical Engineering Communications*, 200(2), 253-268.
 80. Nadeem, S., Haq, R. U., & Khan, Z. H. (2014). Heat transfer analysis of water-based nanofluid over an exponentially stretching sheet. *Alexandria Engineering Journal*, 53(1), 219-224.
 81. Magyari, E., & Keller, B. (1999). Heat and mass transfer in the boundary layers on an exponentially stretching continuous surface. *Journal of Physics D: Applied Physics*, 32(5), 577.
 82. Liu, I. C., Wang, H. H., & Peng, Y. F. (2013). Flow and heat transfer for three-dimensional flow over an exponentially stretching surface. *Chemical Engineering Communications*, 200(2), 253-268.
 83. Nadeem, S., Haq, R. U., & Khan, Z. H. (2014). Heat transfer analysis of water-based nanofluid over an exponentially stretching sheet. *Alexandria Engineering Journal*, 53(1), 219-224.